CLM-R 112

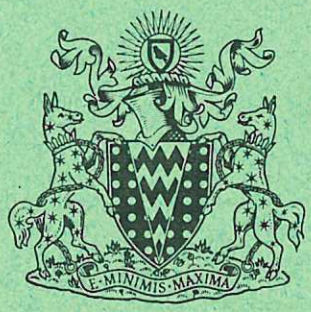

CLM-R 112

UKAEA RESEARCH GROUP

Report

NEUTRAL INJECTION HEATING OF TOROIDAL REACTORS

A report from the Culham Study Group

CULHAM LABORATORY
Abingdon Berkshire
1971

Available from H. M. Stationery Office

C.18

£2.50

SBN 85311 003 4
UDC 621.039.64.026

CLM-R 112

NEUTRAL INJECTION HEATING OF TOROIDAL REACTORS

A report from the Culham Study Group, 1970

MEMBERS:

D. R. SWEETMAN (Chairman)
A. C. RIVIERE (Secretary)
H. C. COLE
D. P. HAMMOND
M. F. A. HARRISON
J. HUGILL
F. A. JULIAN
F. B. MARCUS
G. M. McCRACKEN
E. THOMPSON
C. J. H. WATSON

U.K.A.E.A. Research Group
Culham Laboratory
Abingdon
Berks.

July 1971

CONTENTS

FOREWORD

The work of the Study Group ceased, and the first draft of this report was written, in February 1971. The report therefore represents the state of the art at that time. Substantial developments in ion sources have occurred over the last few months that are not included. These are likely to lead to the achievement of 10-20 amps from one unit (albeit at low energy) within a year or two.

In view of this, some of the discussion of possible ion source developments is somewhat outdated. Nevertheless we feel that it is worth publishing the report since much of the information contained therein is not obtainable elsewhere.

1. INTRODUCTION

In this report we summarise the conclusions of a Study Group on Neutral Injection into Toroidal Systems. The study grew out of a working party which was set up to investigate the feasibility of neutral injection into mirror systems taking into account the large recirculating power. In February 1970, however, as a result of the work for the Heating and Injection Study Group at Culham, the terms of reference were changed and effort was concentrated on establishing the feasibility of neutral (or ion) injection as a means of start-up for toroidal reactors.

The parameter range of reactors based on Stellarator/Tokamak systems is open to much debate at the moment. In order to sidestep these rather complex issues, for the purposes of much of this study we assume a toroidal system of the general type discussed by Carruthers, Davenport and Mitchell[1] though expanded somewhat in major radius to allow for additional windings that may be necessary.

Thus as a starting point the following parameters are taken for the running reactor conditions:

Minor wall radius	= 175 cm
Mean plasma radius	= 125 cm
Major radius	= 750 cm
Power flux at wall	= 1300 watts/cm^2
Mean power density	= 30 watts/cm^2
Total power output	= 7000 MW(th)
Mean plasma temperature	= 20 keV
Mean plasma density	= $3 \times 10^{14} cm^{-3}$

The work is not however, restricted to this reactor design and where possible calculations have been performed over a wide parameter range.

For much of this report it is assumed that a beam of deuterium atoms is used for injection. All the relevant data on beam penetration have not been assembled for any other mass particle but in several places in the report the differences introduced by the use of a higher atomic mass beam are discussed.

The length of time for which injection is required is likely to range from some tens of seconds for stellarator start-up to quasi-continuous for an injection heated Tokamak. Pulsing with on-times of order seconds does not give any substantial advantage over continuous operation except in the consideration of induced radioactivity (Section 3.8.2), beam dumping (Section 3.5) and overall reliability requirements. The accelerator is assumed to be capable therefore of essentially continuous operation.

The following order of presentation is adopted. In Section 2 of the report the major constraints that decide the basic parameters of injection are discussed and we arrive at a unit size suitable for more detailed design study. In Section 3 the technological constraints that decide the design of such a unit are discussed stage by stage and, where appropriate, attention is drawn to areas requiring further work. Some physical processes in the resulting plasma are then discussed. The conclusions reached in the Study are then enumerated. Much of the detailed discussion is put into the several Appendices. These Appendices were based on papers presented at Study Group meetings and are not therefore necessarily completely consistent, in balance or content, with the main body of the Report.

2. BASIC REQUIREMENTS

In this section we discuss the constraints which define the beam power and energy and the basic neutralisation requirements.

2.1 Beam Power Requirements

Appendix 1 discusses the start-up power requirements following the original analysis of Wort[2]. In this treatment the power requirements were calculated on the assumption that the loss rate from the reactor scales from the 20 keV running requirement either as the Bohm rate ($\propto T$) or as the classical rate ($\propto T^{3/2}$). Thus the diffusion time was assumed to be long during the start-up period and only reached its final value ($\tau_c \sim 0.6$ sec) at the working temperature. The density was assumed to be constant during the build-up phase (necessary to keep the neutral beam penetration roughly the same).

This treatment is not accurate in a number of respects pointed out in the Appendix. More significantly than these is the assumption of the $T^{3/2}$ classical scaling which implies operation in the plateau regime: for temperatures above 2 keV the collisionless regime is more appropriate. To correct these matters a calculation of the actual heat transport as a function of temperature has been made (rather than scaling from the 20 keV value). The results are shown in Fig.1.

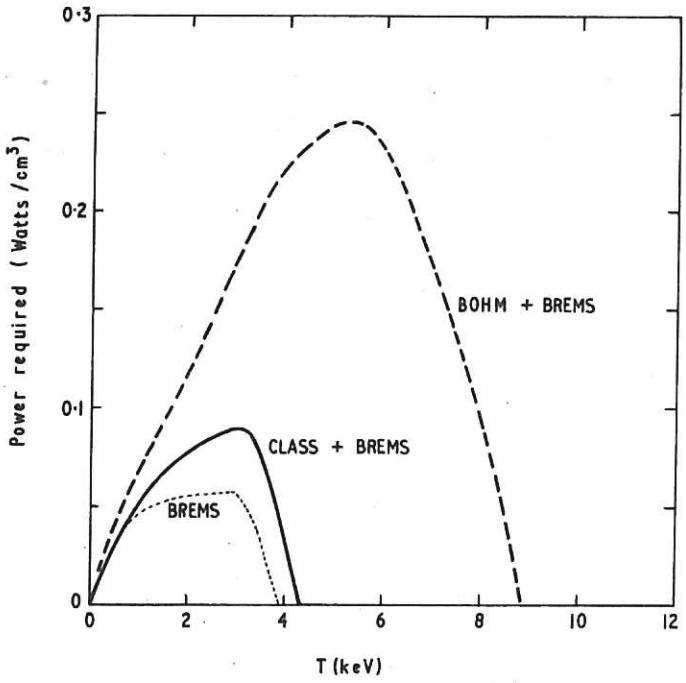

Fig.1 Net power required to overcome losses v. plasma temperature ($T_e = T_i$). In the classical case, the heat transport component of the energy loss rate scales as $T^{\frac{1}{2}}$ in the collisionless regime (> 2 keV) and as $T^{5/2}$ in the plateau regime (< 2 keV). The curve labelled BREMS, calculated assuming only bremsstrahlung loss is operative, is shown for comparison.

The following relationships were used in the two regimes and are derived from transport coefficients given by Hinton[12] and Rutherford[13] respectively:

$$\underline{\text{banana regime}} \qquad P = 1.9 \times 10^{-20} \frac{q^2\, n^2\, T^{\frac{1}{2}}}{r^2\, (r/R)^{3/2}\, B^2} \quad \text{watts/cm}^3$$

$$\underline{\text{plateau regime}} \qquad P = 5.1 \times 10^{-8} \frac{q\, n\, T^{5/2}}{r^2\, R\, B^2} \quad \text{watts/cm}^3$$

where the units are gauss, cm, eV.

In the banana regime the energy loss rate scales in the same way as bremsstrahlung loss and, moreover, for the example chosen the latter is dominant.

It should be noted that on classical assumptions the major loss processes (particle loss and bremsstrahlung) scale as n^2 and the thermonuclear power generation scales in the same way. Thus the ignition temperature is independent of density and in principle, the reactor may be started at arbitrarily low density, the start-up power scaling as n^2. This carries with it the assumption however, that the containment time may be increased as the density is reduced (keeping $n\tau$ fixed): a particle containment time of 7 seconds is already implied at T = 2 keV. Other losses which do not scale as n^2, for example synchrotron radiation, are likely to restrict this line of approach and for the purposes of this report we prefer to keep this as a favourable factor in hand and we assume a fixed density.

The Bohm curve shown for comparison in Fig.1 is calculated on the assumption that the particle loss time is 0.6 sec at the working temperature of 20 keV and scales as T_e^{-1} below that temperature.

As may be seen from the figure the maximum power requirements are estimated to be 0.09 and 0.25 watts/cm^3 for the classical and Bohm assumptions which result in total power requirements for our standard reactor of 20 and 60 MW respectively. In view of the changing state of toroidal diffusion theory at the moment, these should be regarded as only estimates and for the purposes of this report we prefer to regard a total power requirement of 100 MW as our design aim. For general servicing/reliability reasons we have broken this down into 10 × 10 MW units.

2.2 Beam Penetration

Appendix 2 deals with the question of neutral beam penetration into the reacting plasma for reactor conditions appropriate to both mirror and toroidal systems. Fig.11 of that Appendix summarises the situation for toroidal systems where $T_e \simeq T_i$. The plasma thickness for a 1/e attenuation of a D^o beam is calculated for various injection energies: it is essentially independent of

plasma temperature. To achieve a reasonable radial distribution of injected particles and to minimise the loading on the far wall, approximately 2 e-folding distances are required in the plasma radius. Thus for our standard case the plasma thickness for an e-folding distance is required to be $2.10^{16}cm^{-2}$ and with our assumed density of $3 \times 10^{14}cm^{-3}$ that determines a D^0 injection energy of $\sim$ 1 MeV. As will be seen later, this is a reasonably convenient injection energy from the point of view of power supplies and acceleration. As will also be discussed later this choice of D^0 energy implies that heat is transferred initially to the plasma electrons. Since a lower energy would be required to transfer energy directly to the ions, the possibility of relaxing the beam penetration requirements has been considered briefly. Perhaps the most profitable way to achieve this is to reduce the starting density as discussed in the previous section: the energy required for beam penetration scales approximately linearly with density. However, the reservations discussed there prevent this being pushed too far.

As an alternative method Appendix 1 discusses the drifts in simple stellarator geometry and shows that it may be possible to use the natural drifts of energetic ions in the stellarator field to deposit the energy relatively uniformly even though the injection is only at the outside. This possibility may not be open in Tokamak geometry (or in stellarators with the diffusion current included) because of the higher rotational transform near the minor axis. Also if drifts can be invoked to transfer particles to the centre the injection of high energy ion beams is not completely excluded though we do not consider this further here.

If we take then our basic requirement as a 10 MW beam of D^0 at 1 MeV, the equivalent current requirement is 10 amps.

2.3 Energy Transfer Processes

The rate of transfer of energy from a trapped ion to the electrons is given by[14]

$$v_e \gg v_i \quad , \qquad \frac{1}{E_i}\frac{dE_i}{dt} = -3.3 \times 10^{-9} \frac{z^2 \ell n\Lambda\, n}{A\, T_e^{3/2}} \ sec^{-1} \qquad \ldots (1)$$

where A, E_i are the incident ion atomic mass (AMU) and energy (eV) and T_e is the electron temperature (eV).

The rate of transfer of energy to the ions is given approximately by[14]

$$\frac{1}{E_i}\frac{dE_i}{dt} \simeq 1.8 \times 10^{-7} \frac{A^{\frac{1}{2}}}{A_p} \frac{z^2 \ell n\Lambda\, n}{E_i^{3/2}} \quad \text{sec}^{-1} \qquad \ldots (2)$$

where A_p is the mean plasma ion mass (AMU).

Thus the ratio

$$\frac{\text{transfer rate to ions}}{\text{transfer rate to electrons}} = 56 \frac{A^{3/2}}{A_p} \frac{T_e^{3/2}}{E_i^{3/2}} \qquad \ldots (3)$$

and we may set a condition for the energy transfer to be primarily to the ions:

if

$$A_p = 2$$

then

$$E_i < 10\, A\, T_e. \qquad \ldots (4)$$

The above gives the condition for the transfer rates to equate at a given value of E_i. If we integrate the energy drain to the ions and electrons as the injected particles decrease in energy from the injected value E_o then E_o is allowed to be 2.4 times the above values.

One possibility that would enable energy transfer to be primarily to the ions is the use of a high atomic mass beam. In this case the permissible impurity level in the plasma (ε) sets a lower limit to the mass that may be used.

From conservation of energy flux

$$\varepsilon = \frac{T_i + T_e}{E_o} \cdot \frac{\tau_i}{\tau_E} \qquad \ldots (5)$$

where τ_i, τ_E are the lifetimes of the injected ions and the plasma energy containment times respectively.

But from equation (4)

$$E_o < 23\ A\ T_e \qquad \ldots (6)$$

$$\therefore \quad \varepsilon > \frac{T_i + T_e}{23\ AT_e} \cdot \frac{\tau_i}{\tau_e}. \qquad \ldots (7)$$

If $T_i = T_e$ then

$$\varepsilon > \frac{1}{11\ A}\left(\frac{\tau_i}{\tau_e}\right) .$$

Thus if $\tau_i \sim \tau_e$ and the contamination level is to be kept below say 1% then A must be greater than 11. A constraint on the impurity level is set by the need to keep the bremsstrahlung radiation within a factor of about two of that used in estimating the power requirements i.e. $\varepsilon\ z^2 < 1$ (where z is the injected ion atomic charge). Combining this with the condition for energy transfer to the ions gives

$$A < 44\ (\tau_E/\tau_i) .$$

Since τ_e is likely to be greater than τ_i this does not appear to be a serious constraint.

In practice, as we have seen, the injected beam energy is decided by beam penetration requirements. To a first approximation (that the ionization cross section is independent of the beam mass) penetration requirements decide the beam velocity. Thus to this level of approximation penetration requirements decide the ratio of energy transfer to ions and electrons (at a given electron temperature) independently of the atomic mass of the beam. A more detailed study might show advantages in using a specific element other than deuterium.

Another important consideration is the absolute rate at which energy is taken from the injected particles. If $n = 3.10^{14}$, $T_e = 5$ keV, A = 2, equation (1) gives a time constant for loss of injected particle energy of 70 msec. This is to be compared with a plasma lifetime which is greater than 2 seconds. However, as is shown in Appendix 1, the energy loss time may be comparable with typical drift times. For this reason the energy deposition as a function of minor radius can only be determined completely for specific systems where the detailed drifts may be calculated.

2.4 Neutralisation Efficiency

Appendix 3 discusses the problem of beam neutralisation. At an energy of 1 MeV the neutralisation efficiency of gaseous targets using D^+ as the primary beam has dropped to an unacceptably low value (< 0.3%). The practical choice appears to be between D_3^+, D_2^+ and D^- as the primary beam ion. D_3^+ is likely to give a neutralisation efficiency of around 20%, D_2^+ of 10-25% and D^- of 65-90% depending in each case on the degree of ionization of the neutraliser gas. It should be noted here that for D_2^+ and D^- it is an advantage to neutralise on a fully ionized plasma. For D_3^+ the relevant cross sections for an ionized neutraliser are not known. Thus to produce our 10 A 1 MeV D^0 beam we may define the beam requirements at the accelerator stage to be:

(i) 17 Amps of 3 MeV D_3^+

or

(ii) 25 Amps of 2 MeV D_2^+

or

(iii) 12 Amps of 1 MeV D^- .

3. TECHNOLOGICAL FEASIBILITY

In this section we examine the technological feasibility of producing a suitable 10 A D^0 injector unit working at 1 MeV. We also examine some of the associated reactor problems.

3.1 Accelerator Design

A combination of the Child-Langmuir law and geometrical restrictions of a cylindrically symmetrical accelerating gap results in an expression for the maximum ion beam that can be obtained from a single ungridded hole (corresponding) to an equivalent electron perveance of 6×10^{-6} ampere volts$^{-3/2}$). This current is independent of the hole size and is given by

$$I_{max} \approx 1.4 \times 10^{-7} \frac{V^{3/2}}{A^{\frac{1}{2}}} \text{ amperes}$$

where V is the extraction potential in volts and A is the mass in A.M.U.

This is shown in Table I as a function of accelerating potential for the case of D_3^+, D_2^+ and D^- ions.

TABLE I

Extraction Potential (volts)	I_{max} (amperes)		
	D_3^+	D_2^+	D^-
10^4	0.057	0.07	0.1
3.10^4	0.3	0.37	0.53
10^5	1.8	2.2	3.2
3.10^5	9.3	11	16
10^6	57	70	100
3.10^6	300	370	530

Most existing high perveance designs give maximum currents less than this theoretical value (by perhaps a factor two). Thus we see that to achieve our design aims with a single symmetrical extraction system would require an extraction voltage of order 500 kV.

With such a single source, however, working at > 500 kV extraction potential, radial space charge considerations lead to a very large plasma boundary. This is illustrated in Fig.5 of Appendix 4 which traces back the trajectory of a 10 amp beam in a uniform accelerating field. The angle of injection of the ions becomes unacceptably large below some 50 kV potential and, in order to reduce the sensitivity of the initial injection condition to the beam current, it is probably desirable to inject into such a single beam at some 200 keV, the beam being divided into a number of separate beams below this energy.

An additional problem with a single unseparated beam is that the beam profile is adjusted for one operating condition and there is therefore the difficulty of switching the beam on without excessive electrode bombardment.

Also, if the unseparated beam is used a large low density plasma boundary with relatively low gas efficiency is implied. As will be discussed later,

pumping near the plasma boundary is a serious difficulty with such systems. The pumping problem is less severe for a series of separated 200 keV injectors working at relatively high current density at the plasma boundary.

Similar arguments apply to the acceleration of these separated beams below 200 keV where it may be desirable to use an initial further sub-division of the beams for acceleration up to 1 to 50 keV. Thus we arrive at the concept of a series of stages of acceleration the beams being screened from each other within each stage. Of course, cylindrical geometry is not essential to this argument and slit or annular beams might be possible alternatives.

That some such staging as the above is likely to be necessary is now generally recognised and discussion rather centres on the number and energy of the stages.

Conditions on Angular Spread

In the calculations that have been carried out to date, perfectly collimated injection into the final single beam has been assumed. Some idea of the angular tolerance at the injection point can be obtained by examining the trajectory of particles with small deviations from the trajectories assumed in a calculation such as that given in Appendix 4. If a condition is set that the displacement of a typical particle at the beam neck is some fraction (ξ) of the radius (r_o) at that point then, for a given maximum ξ there is a condition on the angular spread (θ_1) at the input energy (E_1)

$$\theta_1 < \xi \frac{r_o}{2d} \left(\frac{E_2}{E_1} \right)^{\frac{1}{2}} \qquad \ldots (8)$$

where E_2 is the final energy and d is the length of the accelerating column (see Fig.2).

In addition we have a condition on the angular spread due to the angular acceptance of the reactor (θ_2)

$$\theta_1 < \theta_2 \left(\frac{E_2}{E_1} \right)^{\frac{1}{2}}. \qquad \ldots (9)$$

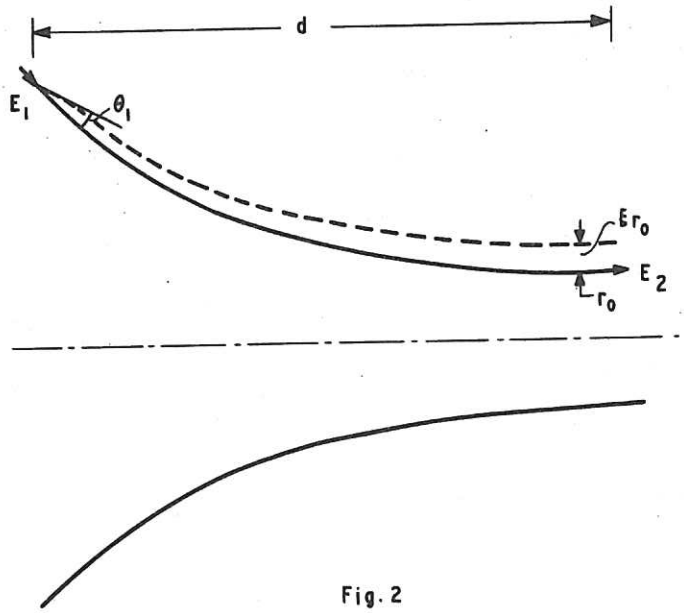

Fig. 2

Alternatively these may be regarded as conditions on the maximum perpendicular energy at the injection point.

From (8)

$$E_{\perp max} < \left(\frac{\xi r_o}{2d} \right)^2 E_2 \qquad \ldots (10)$$

and from (9)

$$E_{\perp max} < \theta_2^2 \, E_2 . \qquad \ldots (11)$$

If we take $\xi = 0.2$, $r_o/d = 0.1$, $\theta_2 = 0.05$ then equation (8) becomes

$$\theta_1 < \frac{1}{100} \left(\frac{E_2}{E_1} \right)^{\frac{1}{2}} \qquad \ldots (12)$$

and equation (9) becomes

$$\theta_1 < \frac{1}{20} \left(\frac{E_2}{E_1} \right)^{\frac{1}{2}} . \qquad \ldots (13)$$

Thus we see that the displacement condition is the most restrictive. If E_2 is taken to be 3 MeV then the acceptable angular spreads for injection at 200 keV, 50 keV, 10 keV and 1 keV are respectively $\pm 2.2^o$, $\pm 4.5^o$, $\pm 10^o$ and $\pm 30^o$ or, alternatively, the maximum perpendicular energy at injection is 300 eV.

These constraints on the beam spread at the injection point into the main combined beam do not appear to be very severe and are well within the performance capability of existing sources (see Table II). Equation (10), however does

emphasize the desirability of short high field gradient accelerators (d/r_o small) to avoid undue constraint on the beam quality in the early stages. Other advantages of high field gradient acceleration are pointed out in Appendix 4 and include reduced electron multiplication effects, reduced gas ionization and reduced space charge problems.

Thus the accelerator problem has been divided into two parts: the production of sub-units of say, 0.5-1 amp at 100-200 keV suitable for injection into the main beam, and the final acceleration of the combined beam.

Some of the practical problems of accelerator design are discussed in Appendices 4 and 7. One of the major problems of existing accelerator designs is back bombardment by electrons resulting in X-ray loading and consequent external current drain. This problem is mentioned in Appendix 7 where it is shown that the power drain may be as much as 20% of the final neutral beam output power. The problems associated with backstreaming electrons although they do not appear to impose a fundamental constraint on the accelerator size, are identifiable as important for study, though little progress can be made until a specific accelerator design has emerged from the other accelerator considerations.

Thus we may summarise the accelerator discussion with the statement that, provided a suitable ion source first stage accelerator system can be devised which produces a beam of 50-200 keV, D_3^+, D_2^+ or preferably D^- ions with current density in the range 10-100 mA/cm^2 and a perpendicular energy of less than 300 eV, then bunching such sources and acceleration to the required energy does not appear to present any in-principle problems. It does, however, represent a substantial extension of existing technology and the back electron bombardment and X-ray problems have not been tackled with any source of the scale required. Also there is the need for further theoretical study of the space charge problems associated with combining beams of this type.

TABLE II

Source Laboratory	Type	Beam	Beam Energy (keV)	Beam ≠ (amps)	Emitting Area (cm^2)	Current/cm^2 (mA/cm^2)	Equivalent ✱ Electron Perveance/hole	Brightness	Beam Power kW
Livermore	331 holes 1.5 mm dia	H^+	1	0.8	32	25	3.3×10^{-6}	5×10^8	0.8
ORNL	48 holes 5 mm dia	H_2^+	50	0.5	20	25	0.2×10^{-6}	1×10^8	87
ORNL	Expanded Plasma Boundary + Central button	H_2^+	50	0.6	19	53	4×10^{-6}	7×10^8	30
Culham	Single hole 6 mm dia	He^+	20	0.15	.28	530	4.5×10^{-6}	4.8×10^8 5×10^8 ≠	.3
Culham	13 holes 3 mm dia	H_3^+	25	0.2	2	100	0.7×10^{-6}	5×10^7	13
		He^+	27	0.35	2	175	0.5×10^{-6}	1.2×10^8	
Kurchatov	Calutron	H^+	25	0.5	60	17		1.2×10^8	25
Sukhumi	Expanded plasma boundary	H_1^+ H_2^+ H_3^+	65	0.85	80	≃ 11	3.3×10^{-6}	2.5×10^9	55
Rutherford	Pulsed Duoplasmatron no lens	H^+	350	0.02	1	20	0.9×10^{-6}	1.5×10^{11} ≠	7
M.P.F. (LASL)	Duoplasmatron	H^+	200	0.02	1	20	0.42×10^{-6}	2.5×10^9 ≠	4
Saclay		H^+	300	0.1			0.8×10^{-6}	1.25×10^{10} ≠	30
Serpukhov		H^+	750	0.3			2.5×10^{-6}	6×10^8 ≠	225
CERN	Pulsed Duoplasmatron gridded	H^+	540	0.5	1	500	7.2×10^{-6}	2.8×10^8 ≠	270
H.V.E.C.	Duoplasmatron	H^+	40	0.2			1.4×10^{-6}	3×10^8 ≠	8
Culham	Hall Accel.		1	1800	60	3×10^4		$\sim 4 \times 10^{10}$ ≠	1800
Berkeley	Calutron	H^-	10	0.005	3	2			

Notes:

✱ Equivalent electron perveance is calculated using the formula $e.e.p = (m_i/m_e)^{\frac{1}{2}} I/V^{3/2}$ where I is the <u>total</u> extracted current in amps and V is the extraction potential in volts.

≠ In these cases the brightness has been calculated using the measured normalised emittance (ε) according to the formula $b = \frac{2\,I\,(mA)}{\pi^2 \varepsilon^2}$, in the other cases the expression given in reference (9) has been used for the beam transmitted through a double stop system. Since in general stop systems are not filled, this latter method gives a lower brightness.

≠ This is the current obtained through a stop system at the brightness indicated. The total extracted current may be larger and is used to calculate the perveance.

3.2 Ion Source and 1st Stage Acceleration

The ion source is required to produce an acceptable current density and have angular spread within the limit discussed above and give a beam suitable for acceleration to ~ 200 keV.

We may take a minimum acceptable average current density of D_3^+, D_2^+ ions at the first acceleration stage to be ~ 10 mA/cm^2, i.e. in the case of our 17 A D_3^+ beam the total area of the first stage would be 1700 cm^2 (a 50 cm diameter circular array for instance). This current density of D_3^+, D_2^+ ions is exceeded by many existing sources (see Table II).

Table II also shows the performance of existing negative ion sources. The best that has been achieved to date is about 2 mA/cm^2. This, if extended to a large array to produce 12 amps of D^- would require a total area of 6000 cm^2 (i.e. a 90 cm diameter array). The negative ion beams obtained to date probably do not represent the best that can be achieved. 0.75 keV H^+ (equivalent to 1.5 keV D^+) incident on Cs vapour has been measured to give an equilibrium yield of 21% H^-[3]: such a capture process might be used with a multihole source which gives a high yield of D^+ at 1.5 keV[11]. Alternative methods of giving high D^- yields include side extraction from a Calutron arc and direct capture of electrons. Further experimental and theoretical study of negative ion sources suitable for large arrays is required.

A normalised measure of the angular spread of ion sources is given by their "brightness". Kelley[4] gives a practical definition in terms of the beam that can be obtained through a double stop system. For circular stops:

$$b = \frac{900\ I\ A}{E_1\ d_1^2\ d_2^2/\ell^2} \qquad \ldots (14)$$

where I is the beam current in mA, A is the mass in AMU, E_1 is the energy in MeV and d_1, d_2 are the diameters of the apertures distance ℓ apart. The brightness of sources for which data is available is given in Table II.

Some idea of the required brightness to match the input of the accelerator can be obtained from our considerations in the previous section. For comparison

purposes we may rewrite the brightness as

$$b = 1.80 \times 10^8 \frac{A\ J}{E_{\perp max}} \qquad \ldots (15)$$

where J is the beam current density (mA/cm^2) and $E_{\perp max}$ is the maximum perpendicular energy as defined by conditions (10) and (11) (in eV).

If we take for example $A = 6$, $E_{\perp max} = 300$ eV and $J = 10\ mA/cm^2$ then the minimum brightness acceptable to the accelerator is

$$\underline{b = 3.6 \times 10^7}\ .$$

This figure is within the capabilities of most of the existing sources listed in Table I.

Thus, if we consider positive ion sources, the choice lies between multihole sources (with 1st stage acceleration to ~ 200 keV, either of the whole beam or the separated beams), single plasma boundary units of the ORNL type, Calutron sources or Hall accelerators.

Hall accelerators have achieved high beam brightness at an energy of a kilo-electron volt or so, but with current density considerably in excess of that which can be handled by the main accelerator. They have $E_\perp$ comparable to the maximum allowable (~ 300 eV). They appear to have no significant advantage over conventional ion sources as a first stage accelerator and are certainly less well understood. Therefore, we regard their primary role as an alternative to the complete accelerators, if by suitable development they could provide 10-100 amps of D_2^+ at 2 MeV: this will be considered later.

Calutron sources also satisfy the beam brightness requirements and achieve suitable current densities at the 90^o deflection point. However, there are problems of stacking them to form a larger array and of developing them to produce high D_3^+ or D_2^+ yields. Progress in solving the latter problem is hampered by the difficulty of obtaining a physical understanding of side-extraction arcs. We conclude that they cannot be dismissed as competitors and that it would be desirable to give further consideration to these problems. Calutrons may have a role as negative ion producers.

Highly developed single expanded plasma boundary sources have produced beams well in excess of the required quality and current density. They are of course limited, by the Child-Langmuir constraints discussed previously, to the currents given in Table I; however, the ORNL button source approaches the theoretical limit for 40 keV extraction potential. It is a subject of debate whether to settle for ~ 0.5 amp at this potential and post-accelerate to ~ 200 keV before merging, or to develop such a system to higher current at higher extraction potential.

Multihole arrays have also achieved brightness and current densities well in excess of the required value and total currents well in excess of the limits given by Table I. Extraction potentials of up to 30 kV have been used. Again it is a subject of debate whether to increase the extraction potential further (thus approaching the concept of a group of expanded plasma sources), or post-accelerate the whole array, or post-accelerate the individual holes. Of course, there is no restriction to arrays of circular holes and linear or annular slits may offer some advantages.

One of the major problems with both multihole sources and expanded plasma boundary sources is the provision of a plasma with suitable enrichment of D_3^+ or D_2^+ ions and uniform density over the required area. For ease of bunching several sources together, compactness is also a consideration. Many existing systems use, for essentially historical reasons, duo-plasmatron plasma sources. Hollow cathode arcs would appear to offer advantages and have been used successfully by Luce and others. In general, there is a need for large area uniform plasma sources and this is an area for further study and development work.

Thus the conclusion of this section is that provision of a basic 0.5-1.0 amp 100-200 keV D_3^+ or D_2^+ injector for the accelerator is a very reasonable extension of existing technology and the most straightforward way of achieving this is simultaneously to develop expanded plasma boundary and multihole sources and suitable techniques of acceleration to 100-200 keV. The decision as to the exact configuration can await further information from these developments.

In addition, for the reasons outlined elsewhere, D^- sources may be capable of achieving the required conditions and would have very considerable technological advantages. Because of the highly resonant charge transfer processes involved, such sources are unlikely to be developed by hit and miss methods and a coordinated experimental and theoretical approach is required.

3.3 The Hall Accelerator as an Alternative Ion Source/Accelerator

In Appendix 5 the possibility of extending the Hall Accelerator to 2-3 MeV as a replacement for the accelerator system is considered. The main advantage of this is that it may be possible to achieve the full output of ~ 100 amps in one relatively cheap unit. Present-day Hall accelerators work at ~ 1 keV and produce ~ 500 amps[5]. The angular divergence is $\pm 30^o$ i.e. $E_\perp \sim 250$ eV which is well within the acceptance limit of the reactor of 7500 eV given by equation (11), provided that further acceleration stages do not introduce much extra perpendicular energy. Some work has been done at 20 kV potential difference but the total current and angular divergence is not known at present.

An extrapolation from the existing devices to ~ 2-3 MeV results in a device of modest dimensions (~ 4 metres long). However, the extrapolation is considerable and does not take into account the extra perpendicular energy acquired due to mismatch in the various stages or the power deposited on the electrodes in the later stages of acceleration. In addition the device would have to be developed for D_2^+ or D_3^+, the survival of which may not be commensurate with the high current densities involved.

Further theoretical and experimental work is required before the usefulness of the Hall accelerator can be properly assessed. It might become competitive if particle drift studies showed that an appreciably lower injection energy than 1 MeV could be used.

3.4 The Neutraliser

As was discussed in Section 2.4 there may be some decided advantage in neutralising on a fully ionized plasma. A total target thickness of order

10^{16} cm^{-2} is required (e.g. a plasma density of $\sim 5 \times 10^{14}$ cm^{-3}, 20 cm long).

Such a density is currently obtained in arcs, and H_2^+ break-up experiments have been carried out on these plasmas in connection with the DCX experiments at ORNL. As far as is known however, no carefully regulated optimum target thickness experiments have been performed. It would be useful to have at least one such practical check on the optimum neutral yield at high impact energy as well as more accurate cross section and equilibrium yield data for H_2^+, H_3^+ impact on ions and electrons.

In our final 10 A unit the necessary plasma conditions might well be obtained by somewhat inhibiting free ion flow from a gas neutraliser. An estimate of the plasma density produced by primary ionization in a field free neutraliser suggests this to be in the range 10^{11} - 10^{12} cm^{-3} (compared with a neutral gas density of $\sim 5 \times 10^{14}$ cm^{-3}). If the plasma is confined for long enough for the electrons to gain appreciable energy by Coulomb collisions with the fast beam ions, then secondary ionization can raise this plasma density appreciably. Under these conditions the plasma in the neutraliser could be maintained essentially fully ionized without any additional source of energy.

The detailed problems of the neutraliser have not been considered in this study. The question of two-stream instabilities needs further investigation. This would appear to be serious if the saturation amplitude of the instability was sufficient to give the fast ions $\gtrsim$ 7·5 keV perpendicular energy (equation (11)) or remove a significant fraction of their parallel energy.

3.5 Dumping the Unwanted Beam

The power efficiencies quoted in Section 2.4 show that, together with the 10 MW of neutral beam, there is emerging from the neutraliser some substantial unwanted charged beam. For the cases of D_3^+, D_2^+ and D^- the powers in the unwanted beams are respectively $\approx$ 40 MW, 30-90 MW and 1-5 MW, the range depending on whether the neutraliser is fully ionized or not.

The possibility of recovering some of this waste power electrically has been considered. However, this is a difficult problem technically and the cost of

converting this to a convenient form for re-injection is not trivial. Therefore, since the power is a small fraction of the station output, required for only a short period and is likely to be available in the form of standby generators, we have considered it hardly worthwhile attempting to recover a large fraction of the energy from all the products of D_3^+ or D_2^+ break-up.

If this energy is not recovered, however, then there is a considerable energy dumping problem. With a conventional solid target the power density at the recovery surface is likely to be limited to ~ 100 watts/cm^2 for quasi-continuous operation. Thus to handle a power level of say 40 MW, an area of 4×10^5 cm^2 would be required. This could conceivably be achieved by clever re-entrant design, but great care would have to be taken to avoid local "hot spots". As will be discussed later, the gas load from such a system is not easy to handle.

An attractive idea is to deposit the beam directly in a liquid lithium target or a lithium spray. To dump 40 MW with a 300^{0}K temperature rise, ~ 60 litres/second of Li metal must be flushed through. This is an order of magnitude smaller than the capacity of a typical pump on a present-day sodium cooled reactor. The system has the additional advantage of greatly easing the vacuum problem (see Section 3.7). Of course, the use of D^- would reduce the loading by more than an order of magnitude.

Thus in summary, it would appear that although beam dumping is not a trivial problem, it can be solved in principle and the use of D^- ions offers a decided advantage in minimising the problem at source.

3.6 Vacuum Problems

Appendix 6 deals with the vacuum problems of neutral injectors. There are two major sources of gas: the ion source itself and the beam dump. Excessive gas pressure near the first region causes unwanted neutralisation in the early stages of acceleration which leads to loss of efficiency and some power drain and deposition. Excessive gas pressure near the beam dump can lead to inefficient neutralisation and excessive power dissipation in unwanted places.

With extended sources of the multihole, or multiple beam type, neutralisation on the ion source gas in the very early stages of acceleration sets a limit on the current density that can be handled (typically ~ 50 mA/cm^2 for a source gas efficiency of 0.5) - from this point of view it is important to develop sources of high gas efficiency. The gas at this stage may be pumped using carefully designed cryogenic panels.

The gas problem in the beam dump region may be greatly eased by using a suitable target which traps ions. Several target materials are available but lithium has the advantage that it may be used in the molten state which facilitates the removal of the beam power (see Section 3.6). The pumping of the untrapped gas again requires substantial cryo-surfaces.

The most important conclusion from this work is that the handling of the ion source gas must be carefully thought out as part of the integrated system or serious beam loss could result.

3.7 Power Supplies

Appendix 7 deals with the power supply question in some detail. Though the voltage (3 MV) is rather higher than that currently used in general power transmission the power requirement (~ 50 MW/unit) is relatively modest.

The Appendix discusses the possible power sources and decided in favour of the transformer-rectifier set where efficiency is of prime importance (for a continuously fed Tokamak for example). The insulating core transformer is a possible competitor for systems where less efficiency can be tolerated (e.g. stellarator start-up).

There do not appear to be any fundamental difficulties in developing either of these systems to the required voltage level. The question of protection in the event of beam collapse is one that would require careful consideration.

3.8 Technological Problems Associated with the Reactor

3.8.1 Blanket penetration

For the purposes of a design study it has been assumed that a roughly cylindrical hole in the blanket structure is allowed. The value of θ_2 inserted

into equation (11) would be consistent with, say, a 60 cm diameter hole 6 metres from the accelerator. A few holes of this diameter through the 2 metre thick blanket would not appear to seriously upset the breeding but may create a radiation shielding problem.

3.8.2 Damage and radioactivity in accelerator due to neutron bombardment

The effect of the neutron flux on the injector materials has been looked at briefly[6]. Depending on the position in the injector the "hard" neutron flux may be in the range 10^{12} - 10^{13} n/sec/cm^2 and the accompanying "soft" flux in the range 10^4 - 10^{13} n/sec/cm^2. These flux levels do not create a serious heating problem, though cooling of the components nearest the reactor will certainly be required. Neutron damage is difficult to assess at the present state of knowledge on the subject and may put constraints on the materials used. Induced radioactivity appears to be the most serious problem and probably excludes the use of iron in constructional materials. If iron is used, the induced Fe^{55} activity (2.6 yr half-life) after one year is estimated to range from 1 to 2 curies/cm^3 at various positions along a typical injection line. Aluminium is a much more reasonable choice - the induced 15.4 hr half-life Na 24 activity level being similar to that for iron but the short half-life would give better access after a cooling off period. It is fairly clear however, that any component continuously exposed to the direct reactor beam will require remote handling techniques for servicing.

The above problems are probably not serious if the injector is used only for start-up and a screening plug is inserted during normal running.

3.8.3 Limitations on gas flow accompanying beam

Gas entering the reactor volume may cause the emission of fast neutral atoms which represent an energy drain and may cause local wall loading. If ε fast atoms are produced (isotropically) per incident gas molecule and the ratio of the power drain to the input beam power is p, then there is a limitation on the input gas flux due to energy drain from the reactor

$$F < \frac{2\ Ip}{\varepsilon} \cdot \frac{E_i}{T_i}$$

where T_i and E_i are the plasma ion energy and beam energy in eV, F and I are the fluxes of gas molecules and beam atoms in particles/second.

Since

$$\varepsilon < 1 \quad , \quad T_i \sim 10^4 \text{ eV} \quad , \quad E_i \sim 10^6 \text{ eV}$$

then for serious power drain not to occur ($p \sim 0.1$) the flux of gas molecules must be < 20 times the beam flux.

Similarly, assuming the vacuum wall is a distance ℓ from the plasma the gas flux is limited by wall loading to

$$F < 7.7 \cdot 10^{19} \frac{\ell^2\ W}{\varepsilon\ T_i}$$

where W is the limiting wall loading (watts/cm^2).

If ℓ = 50 cm, W = 100 watts/cm^2, $\varepsilon < 1$, $T_i = 10^4$ eV

$F < 1.9 \times 10^{21}$ particles/second (i.e. 300 amps current equivalent).

Thus to satisfy the wall loading condition the gas flux must be < 30 times the beam flux.

Since the gas is essentially generated by the beam both of these conditions are easy to satisfy and are considerably less constraint on gas flux than is the vacuum requirement in the accelerator.

3.9 Costs

It is beyond the scope of this report to attempt an accurate estimate of costs. However, some attempt may be made to estimate the constraints on the injector costs.

Our standard reactor has an electrical output power of ~ 3500 MW(e). If we allow that 5% of the total reactor cost of say, £70/kW(e) is available for start-up then the injector system must be built for ~ £12M.

If the neutral beam requirement is 30 MW, D_3^+ is used and the unwanted beam energy thrown to waste, the power requirement is ~ 150 MW. This order of power would be expected to be available for standby in a station of this size. However,

the cost of conversion to a suitable voltage is estimated in Appendix 7 for a 100 MW neutral beam injector. Scaling from those values and allowing for 3 × 55 MW insulating core transformers in action and one standby, the cost of providing the power is ~ £4M. Then approximately £8M is left to be divided between the three 10 MW neutral injectors. At this stage all that can be said is that £2-3M does not seem an unreasonably low sum for the production of a 10 MW accelerator. If however, more than the estimated 30 MW beam power is required then the cost allowance per unit is correspondingly more restricted and the cost of say 100 MW of beam power is likely to be appreciably more than the 5% of the reactor cost.

This gives additional support to the case for negative ion sources with their reduced total power demands.

4. SOME PHYSICAL QUESTIONS ASSOCIATED WITH NEUTRAL INJECTION

4.1 Self-consistent Electric Field and Plasma Currents

Fast ions and electrons created at the same point have a displacement of their guiding centres and this can lead to an electric field. This field has been calculated for a given number of trapped ions injected and, in the plane geometry approximation, it is given by

$$E = 2 \frac{\bar{E}_\perp}{\bar{a}_i} \cdot \frac{A}{zA_p} \cdot \frac{n_i}{n} \quad \text{volt/cm}$$

where $\bar{E}_\perp$ is some average trapped ion energy perpendicular to the field lines (in eV) and $\bar{a}_i$ is the Larmor radius (cm), A and A_p are the injected particle and plasma ion masses, n_i and n are the trapped ion and plasma densities.

It should be noted that this field is essentially a potential equal to the perpendicular injected particle energy dropped across a Larmor radius but reduced by the presence of the reactor plasma.

The above relationship gives essentially the rate of creation of the electric field - the equilibrium value will depend on the processes destroying the electric field. These are not clear at present and are intimately tied up with the toroidal diffusion problem.

The electric field results in an E × B motion of the plasma around the torus. It can be shown that the velocity of this motion is exactly that required to give conservation of momentum. Thus if the ions are injected into trapped orbits or have little velocity parallel to the field lines, essentially all the beam momentum is transferred quickly to the plasma via the electric field. If the beam ions are untrapped and have appreciable momentum along the field lines this part of the momentum remains in the fast ions and is transferred only relatively slowly by collisions.

As we have seen in Section 2.3, the momentum parallel to the field which is transferred to the plasma by collisions, goes primarily to the electrons. This gives rise to a current which is considerably greater than the beam current and which Ohkawa[7] has considered in some detail.

The value of the current depends on the balance of the rate of gain of momentum from the injected ions and loss to the cold ions. Ohkawa takes both of these rates to be the classical electron-ion collision rate (τ_{ie}) and in that case

$$j \approx I_b \frac{\bar{v}_b}{2\pi R} \cdot \tau_{ie}$$

where j and I_b are the electron current and beam current densities, $\bar{v}_b$ is the average beam velocity in the plasma and R is the major radius.

If we take the parameters of our standard reactor: $I_b = 30$ amps, $\bar{v}_b = 5 \times 10^8$ cm/sec, $R = 750$ cm, $\tau_{ie} \sim 0.4$ sec (at $T_e = 10$ keV) then $j \approx 1.4 \times 10^6$ amps, compared with a Kruskal limiting current of $\approx 10^7$ amps. The rate of loss of momentum from the electrons may be greater, and the current consequently smaller, if there is anomalous resistivity or if electron trapping plays a role.

The above current does not include the diffusion current and the derivation is presumably only valid when the latter is small. The ratio of the Ohkawa to the diffusion current for a Tokamak-like field scales as

$$\frac{j_{ohk}}{j_{diff}} \propto \frac{I_b E_i^{\frac{1}{2}} T_e^{\frac{1}{2}} B_\theta}{n^2 R (\frac{r}{R})^{\frac{1}{2}} \frac{1}{n} \frac{dn}{dr}} .$$

Thus the Ohkawa current may be important at low density or if B_θ is high.

The self-consistent electric field and the effect of plasma currents are subjects of intensive study at the moment and will not be considered further here. It should however, be noted that by choosing to inject into trapped or untrapped orbits and with or without net canonical angular momentum, extra degrees of freedom are provided which might be useful during a critical start-up phase.

4.2 Instabilities

Instabilities can arise due to the energy distribution of the injected ions and due to their anisotropy.

Some work has been carried out on the isotropic case aimed at the problem of instabilities caused by reaction products in reactor plasmas.

Kolnesnichenko and Oraevsky[9] and Oliphant[10] have calculated the hot ion energy distribution function over a range of plasma parameters appropriate for reaction products and the former authors[8] have catalogued some possible modes with their thresholds and growth rates. At low β the double hump cyclotron mode is important and electromagnetic modes become important when

$$\beta_c \frac{T_{ih}}{T_{ic}} > 1$$

where β_c is the ratio of plasma pressures to the vacuum field for the cold plasma and T_{ih}, T_{ic} are the respective hot and cold "temperatures".

If this condition is exceeded then there are two Alfven modes and one ion sound mode which must be considered. All these modes rely on the double humped nature of the ion velocity distribution. The distributions appropriate for the neutral injection case have not been calculated during the time dependent plasma build-up and until this is investigated in detail it will not be possible to make categorical statements about the stability or otherwise of the above modes.

The anisotropy of the injected ions depends very much on the geometry of injection and the details of the confinement system. Broadly speaking, however,

if the beam is injected perpendicular to the field lines then there is the whole spectrum of Harris-like modes to be considered. At low β and if we are prepared to assume a quasi-Maxwellian distribution of ion energy, the Harris modes should be stable if $T_{\parallel}/T_{\perp} > \frac{1}{2}$. If on the other hand, the beam is injected along the field lines then two stream modes may occur depending on the shape of the energy distribution function. The effect of finite β on these modes is under investigation.

More definitive statements as to the likely presence or otherwise of micro-instabilities must await more specific, time-dependent, calculations of the injected ion energy distribution functions. Meanwhile it is appropriate to list some possible consequences of micro-instabilities:

(i) they are likely to increase the transfer rate of energy from the fast ions to the plasma. This to some extent, is self-compensating since the increased transfer rate reduces the density of fast ions;

(ii) the Ohkawa current will be modified;

(iii) micro-turbulence might change the effective resistivity of the plasma and this could have consequences for the equilibrium of some systems;

(iv) micro-turbulence could lead to diffusion.

The first toroidal experiments using neutral injection should throw some light on these problems.

5. CONCLUSIONS

We may summarise the conclusions of the Study Group as follows.

1. On the assumption of a classical, or Bohm, dependence of loss rate on T_e the beam power requirements may be estimated to be $\lesssim$ 60 MW for our standard 7000 MW(th) reactor.

2. To penetrate the reactor plasma a deuterium energy of about 1 MeV is required. This implies that the major transfer of energy is to the electrons. The use of high atomic mass beam will increase the energy transfer to the ions but the effect on penetration is not fully known. In certain systems suitable ion drifts may relax the beam penetration requirements. A somewhat lower starting density would reduce both the energy and the power requirements.

3. If the discussion is limited to deuteron injection, then neutraliser efficiency considerations lead to the production of the beam from accelerated beams of D_3^+, D_2^+ or D^-. The neutralisation efficiency using D_3^+ or D_2^+ is low (~ 20%) whereas for D^- it is much higher (80-90%).

4. A useful basic unit size for the purposes of study is 10 MW, i.e. a 10 A, 1 MeV D^0 injector. The feasibility study of this sized unit shows no in-principle objections, it does however, represent a substantial extension of existing technology.

5. Acceleration in two or more stages is likely to be necessary, the beams being separated in the early stages and combined only in the final stage. The choice of 1st stage energy will depend on the ion source chosen but it is likely to lie in the range 50-200 keV. The current per source is likely to lie in the 0.5-1 amp region.

6. This concept is also of value in leading to a development program of smaller units which fits in with the requirements of intermediate experiments.

7. The maximum beam angular spread at each stage may be defined approximately. Typically, a maximum perpendicular energy of 300 eV is allowed. These requirements allow a minimum beam 'brightness' to be defined which is exceeded by most present-day high performance sources.

8. The choice of source for 1st stage acceleration is open to some debate. The most likely contenders for D_2^+, D_3^+ production are multihole arrays and high optimised single hole sources. Calutrons need further assessment and Hall accelerators need further experimental development before they can be seen as competitors.

9. Little information is available on suitable D^- sources but the required current density does not appear to be out of the question from consideration of the cross section data available.

10. As an alternative to conventional ion accelerators the Hall accelerator cannot be dismissed and may become competitive if a lower energy than the 1 MeV can be used. However, more experimental information is required at high accelerating potentials and the survival of D_2^+, D_3^+ in the accelerator is open to question.

11. There is a need for a more uniform plasma source with which to illuminate multihole arrays and large plasma boundary ion sources.

12. The neutralisation of high current D_3^+, D_2^+ or D^- beams does not appear to generate serious problems though there is a lack of cross section data and the non-linear consequences of beam plasma instabilities have not been considered in detail.

13. The dumping of un-neutralised beams from D_2^+ or D_3^+ dissociation is a non-trivial problem and may need the development of unconventional techniques. For D^- beams the problems are much less severe.

14. The necessary power supplies represent a reasonable extension of existing technology though the protection of the accelerator in the event of beam collapse may pose some problems.

15. A start has been made on the understanding of the interaction of the injected ion distribution with the reactor plasma. The electric fields generated would appear to be those consistent with momentum balance and the plasma currents may be comparable with the diffusion current. A proper assessment of the instability situation must await better calculation of the energy and angular distribution functions of the injected ions.

16. An estimate of the capital cost of such an injector system is difficult but the allowed cost per kilowatt of injected power leaves a reasonable margin provided the required power is not greatly in excess of that predicted from the elementary scaling laws.

ACKNOWLEDGEMENTS

The authors wish to acknowledge much help from other members of the Laboratory, in particular Drs. J.G. Cordey and A. Gibson, and from Dr S. Blow (Harwell).

REFERENCES

(1) Carruthers, R., Davenport, P.A., Mitchell, J.T.D. The economic generation of power from thermonuclear fusion. Culham Laboratory, CLM-R 85, 1967.

(2) Wort, D. Proc. of the B.N.E.S. Conference on Nuclear Fusion Reactors, Culham Laboratory, September 1969. p.517.

(3) Schlachter, A.S. et al. Phys. Rev., vol. 177, 1969, p.184.

(4) Kelley, G.G. IEEE Trans. Nucl. Sci., vol.14, 1967, p.29.

(5) Cole, H.C., Culham Laboratory, unpublished work, 1970.

(6) Blow, S., Private communication.

(7) Ohkawa, T., Nucl. Fusion, vol. 10, 1970, p.185.

(8) Kolesnichenko, Ya.I., Oraevsky, V.N. Fourth European Conference on Controlled Fusion and Plasma Physics, Rome, 31 August - 4 September 1970. Contributions. (C.N.E.N., Rome, 1970). Paper 180.

(9) Kolesnichenko, Ya.I., Oraevsky, V.N., Atomnaya Energiya, vol.23, 1967, p.289.

(10) Oliphant, T.A., Proc. of the B.N.E.S. Conference on Nuclear Fusion Reactors, Culham Laboratory, September 1969. (British Nuclear Energy Society, 1970). p.306.

(11) Osher, J. and Hamilton, G.W., Annual Meeting of the APS Division of Plasma Physics, Washington D.C., November 1970, paper 4E7. (APS Bull., vol.15, no.11, November 1970, p.1441-abstract).

(12) eg. Rutherford, P.H., Kovrizhnikh, L.M., Rosenbluth, M.N., Hinton, F.L., International Atomic Energy Agency report IC/70/74, 1970.

(13) Rutherford, P.H., Phys. Fluids, vol.13, 1970, p.482.

(14) Spitzer values have been used for the purposes of this discussion.

APPENDIX 1

STELLARATOR HEATING REQUIREMENTS

by

J. Hugill

1. Introduction

The Heating and Injection Study Group concluded that, of the presently available methods for igniting a fusion reactor, neutral injection was the most promising. The present purpose is to consider in more detail the heating of a Stellarator reactor to ignition point, by neutral injection.

As a guide we will take the requirements of the R 85 reactor[A1.3]. Although present designs indicate a stellarator reactor may have to be a factor of 2 to 10 times larger in power output, most of the calculations will follow through on a pro-rata basis.

The maximum heating power and ignition point T_{ig}, have previously been calculated by Wort[A1.1] assuming that the energy confinement time scaled like the Galeev-Sagdeev diffusion time in the intermediate regime. The heating process is envisaged as starting with a neutral gas at the correct density or a 'cold' plasma. During the heating process sufficient power and fuel are supplied to maintain the particle density constant while the temperature increases from $\sim$ 0 to T_{ig}.

The following sections deal with various aspects of this process in relation to a stellarator-like reactor.

2. Power Requirements

Wort's calculation of the power required to ignite a stellarator reactor assumed that the confinement time, τ_c at 20 keV was 0.6 seconds, and scaled as $T^{-3/2}$, as in the Galeev-Sagdeev intermediate regime[A1.2]. This argument neglects

two points.

(a) The confinement time of 0.6 s is an arbitrary one, not related to diffusion theory.

(b) As T increases towards 20 keV the plasma enters the low collision frequency regime where a $T^{-3/2}$, variation of τ_c is pessimistic for tokamaks, but optimistic for stellarators, because of the growing importance of localised particles. This means the use of $\tau_c = 0.6$ s at 20 keV as a normalising point is not valid. When $T < 5$ keV, τ_c bears no simple relation to the value at $T = 20$ keV.

In Table A1.I the confinement times assumed by Wort are compared with values calculated from G-S theory inserting the parameters of the R 85 reactor[A1.3]. Wort's estimate is a factor of 6 below the theoretical value, and so appears pessimistic: however, the same factor is observed experimentally in this regime[A1.4]. We may conclude that Wort's calculation is essentially realistic

Whether $\tau_c = 0.6$ s at 20 keV can be achieved in a stellarator depends very much on plasma behaviour in the low collision frequency regime where localised particle diffusion is important, and which has not been extensively explored experimentally. It has recently been shown that a unidirectional 'Taylor' current is associated with plasma diffusion in this regime, which produces a rotational transform adding to that of the vacuum field[A1.5]. The effect of this on diffusion rate and critical β has not been worked out in a self-consistent manner, but preliminary studies[A1.6] show that the stellarator is subject to the Kruskal limit in the same way as a tokamak.

The net result of Wort's work is that the ignition point of the R 85 reactor is 6.4 keV and the minimum power required is 0.12 W/cm^3 compared with a thermal output of 30 W/cm^3 at the steady working temperature. Thus total power input to the plasma is 1/250 times thermal output. For the R 85 reactor this amounts to 20 MW. This minimum power is of course only just sufficient for ignition. To make the heating time scale comparable with τ_c the power input should be doubled to 40 MW. The heating time will then be ~ 7 seconds.

The R 85 reactor is small compared with those which recent studies[A1.7] indicate may be necessary when fusion reactors might become operational. For reactors of 3 - 6 GW(e) and 40% thermal efficiency the ignition power on a pro-rata basis comes to 30 to 60 MW.

Present optimisation of stellarator reactors shows that if localised particle diffusion is ignored there is a mis-match between the values of B required for equilibrium and for diffusion-controlled confinement, with the former values being higher. Thus it may be necessary to use higher values of B and increase the diffusion rate artificially at the working temperature. However, during the ignition phase, this may not be necessary. It would imply longer confinement times and lower ignition power than indicated above.

In the calculations above we have assumed n constant. However, there is an advantage in using lower densities during the ignition phase. Wort shows the minimum ignitable density in R 85 is $\sim 1.9 \times 10^{14} cm^{-3}$ and the power required is reduced by about 30%.

We conclude that a stellarator or tokamak reactor of the size presently envisaged will require between 14 and 60 MW of power for ignition.

3. Heating Mechanism, Characteristic Times

In heating a plasma by neutral injection it is assumed that the neutral beam is ionized in traversing the plasma and that the high energy ions share their energy with the plasma by classical collisions.

Some characteristic times associated with the heating process are calculated below.

3.1 Values of the slowing down time, τ_s, defined by Spitzer's equation (5-27)[A1.8] are given in Table A1.II. For D^+ ions in the range 100 keV to 1 MeV and plasma temperatures from 100 to 4000 eV this time is < 50 ms, which is two orders less than the corresponding diffusion times in Table A1.I.

3.2 For the parameter ranges given, the fast ions are slowed mainly by plasma electrons, so the electrons are initially heated, and the ions must be heated by electron-ion thermalisation. The classical equi-partition time, τ_{eq}, given by Spitzer(5-31) for hot electrons to heat cold ions is shown in Table A1.III and is of the same order as τ_s, so that the ions will be heated along with the electrons, although the temperature of the latter will be somewhat lower.

3.3 If the injected particle is in the loss region in velocity space, for example because it is localised, it will escape from the confinement region in a time approximately equal to the plasma radius/drift speed in B_φ field gradient.

$$\tau_D = \frac{r}{V_D}$$

$$= \frac{rRB}{EA} \times 10^{-8} \qquad \ldots (A1.1)$$

units: seconds, gauss, eV and A.M.U.

Typically for a reactor $r = 10^2$, $R = 10^3$, $B = 10^5$, $E = 10^6$, $A = 2$,

$$\tau_D = 5 \times 10^{-5} s \ .$$

It is clear that, if the injected particle is in a loss region of velocity space, it will drift out of the system before it loses its energy. This generally means that the parallel velocity of the particle must not be so small that it is mirrored in the helical field gradient and becomes 'localised' (A1.9).

3.4 Another important quantity is the time taken to complete a drift orbit closed in the minor cross-section. If it happens that the particle loses all its energy before returning to the injection point there would be no problem in having an injection 'snout' at this position: thus it may be feasible to inject <u>charged</u> particles rather than neutrals. If so this may greatly simplify the problem of producing the heating beam.

The transit-time of the particle around the major axis

$$\tau_R = \frac{2\pi R}{\gamma v_i} \qquad \ldots \text{(A1.2)}$$

where $\gamma = v_{11}/v$. γ must not be so small that the particle is in the loss-region (see paragraph 3.3). The allowed value will depend on the particle energy, the field strength and configuration and details of the injection point, but might be ~ 0.1.

For a typical stellarator the maximum rotational transform is $\sim 2\pi$ and the effective rotational transform of a particle orbit, ι_{orb}, will be about half this. Thus the time to complete a drift orbit in the minor cross section will be

$$\tau_o = \tau_R \frac{2\pi}{\iota_{orb}} \qquad \ldots \text{(A1.3)}$$

however, unless $\iota_{orb}/2\pi$ is rational the particle will not return to its starting point. Its chance of returning within a distance s of the starting point per transit will be $\frac{s}{\pi r\sqrt{1 + (\frac{\iota_{orb} r}{2\pi R})^2}}$ (Later, s will be put equal to the 'snout' radius). So the mean time to return within a distance s of the starting point will be (for $r \ll R$)

$$\tau_p = \tau_R \frac{\pi r}{s} = 1.4 \times 10^{-5} \frac{RrA^{\frac{1}{2}}}{\gamma s E^{\frac{1}{2}}} \, . \qquad \ldots \text{(A1.4)}$$

Example: for $R = 10^3$, $r = 10^2$, $\gamma = 10^{-1}$, $s = 10$, $E = 10^6$, $A = 2$,

$$\tau_p = 2 \text{ ms} \, .$$

This is an order of magnitude smaller than the slowing down time of ~ 50 ms at ignition point from Table A1.II, which indicates the particle can not lose a large fraction of its energy before returning to near its starting point. However, even if it should have lost only a small part of its energy, the orbit may be so changed by collisions with background gas that it misses the 'snout' anyway. This point will be further discussed in the next section.

The situation becomes slightly more favourable for lower energy injection since $\tau_p \sim E^{-\frac{1}{2}}$ whereas τ_s is $\sim E^0$, so $\tau_p/\tau_s \sim E^{-\frac{1}{2}}$.

3.5 In addition to loss of energy and scattering on the background plasma an injected ion also partakes of the general drifts of the other plasma particles. The magnetic drifts have already been discussed in sections (3.3) and (3.4). There is in addition a convective motion due to electric fields in the plasma. This is only well understood in the collisional range of plasma diffusion which does not apply here, except for $T_e < 500$ eV. However, the time scale of the analogous motion in the intermediate diffusion regime will probably not be an order of magnitude faster. For the M.H.D. regime the time scale is τ_o/ι i.e. ~ seconds. It is therefore unlikely that injected particles will be much affected by $\underline{E} \times \underline{B}$ drifts before losing their energy to the background plasma, and such effects will be ignored in what follows.

4. Geometrical Considerations

In this section we wish to examine the questions of where the neutral atom is ionised, what its subsequent trajectory is, and where the energy is deposited in the plasma.

4.1 The problem of the penetration depth of a neutral beam will be discussed in (A1.10) where it is concluded that a 1 MeV beam is required to penetrate to the centre of a 150 cm radius plasma with $n = 3 \times 10^{14}$ and $T = 10$ keV. However, for the neutral beam energies which we are considering, and for an $\underline{\ell=3}$ stellarator penetration of the neutral beam to the centre may not be necessary. A 1 MeV D^+ ion at $B = 100$ kG has $r_L \sim 2$ cm, $r_p/r_L \sim 75$. For particles of this energy the displacement of the drift surfaces from the magnetic surface can amount to a quarter of the plasma radius in an $\ell=3$ stellarator. The reason for this behaviour is the very low transform in the centre, which means the dominant drift in this region is the toroidal drift. This can carry particles vertically through

a large fraction of the plasma radius before the field transform predominates.

By reversing the orbit one can see that a particle starting near the outside of the plasma can have a drift orbit passing through the centre.

These results will be strongly modified in a reactor at operating temperature where, because of finite β effects and the transform produced by the Taylor current, the stellarator field is modified. It is a matter for calculation whether these effects will be important at temperatures of $\sim$ 5 keV, at which maximum heating is required.

The conclusion of this section is that we may be able to allow lower injected energies than indicated by (A1.10). The geometry is indicated in Figure A1.1.

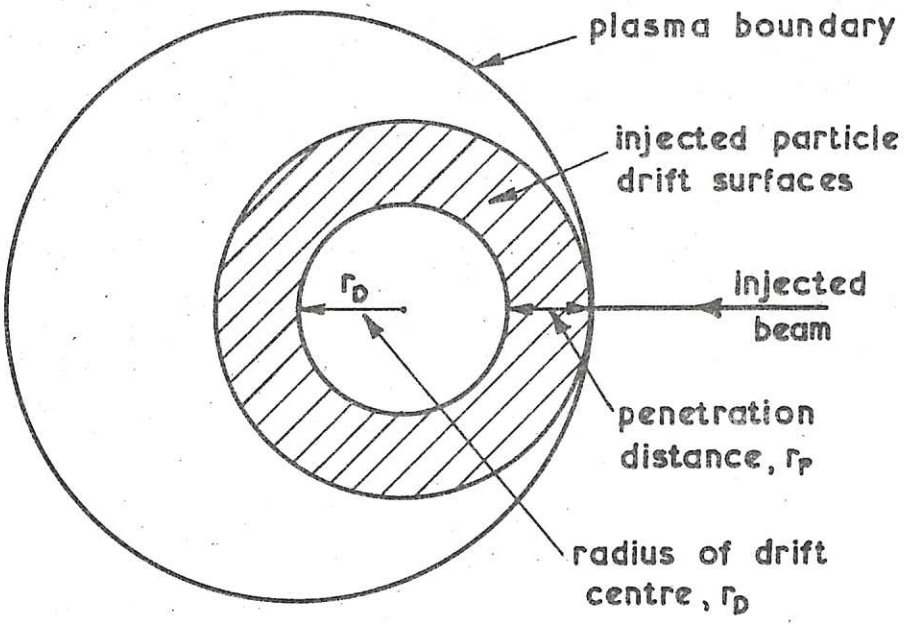

Fig. A1.1

The radius of the centre of the drift surface, r_D is given by the condition that the toroidal drift and transform drift just cancel i.e. with distances expressed as fractions of the plasma

radius.

$$2\pi r_L = r_D \iota \quad , \quad \iota = \text{rotational transform.}$$

For $\ell=3$ stellarators $\iota = r_D^2 \iota_{max}$. The penetration distance is proportional to particle velocity to first order so that

$$r_p = 1 - 2r_D \sim \varepsilon^{\frac{1}{2}},$$

where ε is the energy. $\iota_{max} = 2\pi$, $r_p = 1$ for 1 MeV gives $\varepsilon = 300$ keV.

4.2 The calculations of the last section assumed implicitly that $v_{||}$ was so directed that the toroidal drift and transform were opposite. For particles injected with the opposite velocity the drift orbits are displaced in the opposite direction as shown in Figure A1.2.

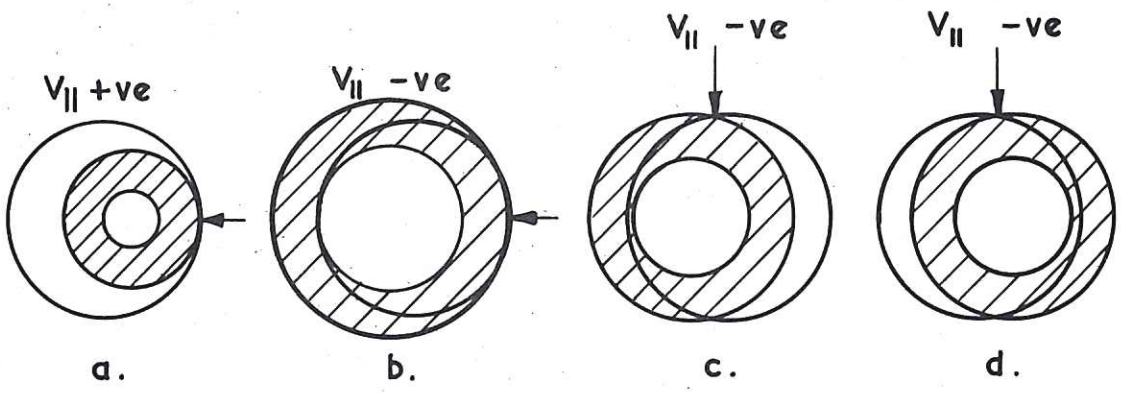

Fig. A1.2

Evidently many different regions of the plasma are accessible with the same injection energy, depending on the angle and position of the injected beam. Using several injectors it will be possible to arrange a very wide dispersion of particle orbits in the plasma being heated.

4.3 For a single particle the drift orbit in a stellarator is closed and drift surfaces are formed corresponding to the magnetic surfaces. However, we have already seen in section 3.4 that the time to 'complete' a drift orbit, in some sense, is comparable with the slowing down time. Since the energy and magnetic moment of the particle are continuously

changing it is not reasonable to expect the particle trajectory to form a drift surface. Two effects may be important. Since the transform is lower the closer the particle to the centre, the particle will spend more time in the centre of the plasma and lose more energy there. In the limit in which all the energy was lost at the centre of the plasma the particle would be stopped at the magnetic axis. The effect is similar to the reduction in apogee of a satellite due to friction with the earths atmosphere at perigee.

Secondly, as the particle loses energy, the displacement of the 'instantaneous' drift axis from the magnetic axis is reduced. This also results in a centering of the particle orbit on the magnetic axis.

4.4 A computer program to test some of the results of sections 4.1 and 4.3 has been written (A1.11). It calculates the trajectory of a particle with given charge, mass, initial position and velocity in a simulated $\ell=3$ stellarator field filled with plasma with specified parameters.

The effect of slowing down and scattering of the injected particle is included via Spitzer's diffusion equations (5-15) to (5-17).

It is hoped to use the program to gain better understanding of some aspects of the orbit theory just discussed. Some preliminary results are shown in Figure A1.3. In these examples the magnetic field is reduced to 20 kG and the plasma density increased to 3×10^{16} cm^{-3}, as compared with 100 kG and 3×10^{14} cm^{-3} for a reactor. The reason for this is to save computing time by increasing the gyroradius and decreasing the slowing down time, however the essential features of the particle orbits should not be very different from those in a reactor. In both cases the inward drift of the particle orbit is apparent.

4.5 From the above remarks it is fairly obviously difficult to ensure that the heating produced by neutral injection in a stellarator field is uniform. However, for $\ell=3$ stellarators at least, this may not be a severe problem. The diffusion and thermal conduction coefficients in the intermediate regime are proportional to ι^{-1} so that in the centre of the plasma, at least, thermal gradients may be removed by conduction on a much shorter time scale than the confinement time. Thermal gradients will also be influenced by the method of injection of cold fuel which is necessary to maintain n constant. At present this appears to be a bigger problem than that of supplying heating power.

5. Interface Between Injector and Stellarator Reactor

5.1 As presently envisaged a stellarator reactor would have the Torsatron configuration in which the confining field is produced by a single set of helical field windings. The space between the winding contains field lines which connect the outside of the confinement region with the 'helical divertor' as proposed by Gourdon (A1.12). The access in this system is very good and the dimensions of the 'holes' available for neutral injection would be typically 50 cm x 50 cm.

5.2 The handling capability of the divertor can be simply calculated from the thermal output of the reactor. The following calculations are for the R 85 reactor.

Thermal output, P	5000 MW
Fractional burn-up, f_b	0.035
Energy release per reaction, Q_T	22.4 MeV

$\therefore$ Equivalent throughput,

$$I = \frac{2P}{Q_T f_b}$$

(1.28×10^4 Amperes.
(
(8×10^{22} particles/second.

Assuming cold fuel is injected and all charged particle energy is deposited in the divertor (3.52 MeV per reaction):

Divertor power	785 MW
Area of divertor surface (≈ area vacuum wall)	4×10^6 cm^2
Approximate divertor loadings	(200 W/cm^2
	(
	(3.2 mA/cm^2 ion current.

Thus the superficial handling capability of the divertor is rather small: not sufficient to act as the beam dump for the neutral injector without careful consideration.

References

(A1.1) Wort, D, Culham Laboratory, unpublished work, 1970.

(A1.2) Galeev, A.A. and Sagdeev, R.A., Zh.E.T.F., vol.53, 1967, p.348.

(A1.3) Carruthers, R. et al., The economic generation of power from thermonuclear fusion, Culham Laboratory, CLM-R 85, 1967.

(A1.4) Bolton, R.A.E. et al., Plasma containment in the Proto-cleo stellarator, Fourth IAEA Conference on Plasma Physics and Controlled Nuclear Fusion Research, Madison, Wisconsin, 17-23 June 1971. Paper CN-28/H-6.

(A1.5) Taylor, J.B.: in a letter to Dr R.S. Pease, 3 March 1969.

(A1.6) Bickerton, R.J., Culham Laboratory. Unpublished information. 1970.

(A1.7) Merz and McLellan, Report on integration of fusion reactors into power networks, August 1970.

(A1.8) Spitzer, L., Physics of fully ionised gases (Interscience Publishers Inc., N.Y., 1956).

(A1.9) Gibson, A., and Taylor, J.B., Single particle motion in toroidal stellarator fields. Phys. Fluids, vol.10, no.12, December 1967, pp. 2653-2659.

(A1.10) Riviere, A.C., See Appendix 2 of this report.

(A1.11) Dixon, V.A., Culham Laboratory, Unpublished information. January 1971.

(A1.12) Gourdon, C. et al., The torsatron, without toroidal field coils as a possible solution to the divertor problem. Fourth European Conference on Controlled Fusion and Plasma Physics, Rome, 31 August - 4 September, 1970. Contributions. (C.N.E.N., Rome, 1970). p.35.

TABLE A1.I

Comparison of theoretical diffusion time (Galeev and Sagdeev) with figures used by Wort [A1.1], for the R 85 [A1.3] reactor

T (keV)	τ_{G-s} (seconds)	Wort's estimate $0.6\ (T/20)^{-3/2}$
0.5	844	152
1.0	312	54
1.5	170	29
2.0	111	19
2.5	79	13.5
3.0	60	10.3
3.5	48	8.2
4.0	39	6.7
4.5	33	5.6
5.0	28	4.8
20	-	0.6

TABLE A1.II

Slowing down time of fast deuterons in a D-T plasma (mean ion mass = 2.5 A.M.U.) at various temperatures $n = 3 \times 10^{14}$, $\ell n\ \Lambda = 20$, $T_e = T_i$, τ_s in ms

Plasma temp.(eV)	100	500	1000	2000	3000	4000	5000	10000
Ion energy								
50 keV	0.22	2.1	5.0	9.8	13	15	16	19
100 keV	0.24	2.3	5.9	14	22	28	33	46
500 keV	0.44	2.7	7.0	18	33	49	67	158
1 MeV	0.83	3.2	7.7	20	36	51	71	188
5 MeV	7.5	9.2	14	28	44	63	84	220

TABLE A1.III

Equipartition times between hot electrons and cold ions in a D-T plasma (mean ion mass = 2.5 A.M.U.) at various temperatures $n = 3 \times 10^{14}\ cm^{-3}$, $\ell n\ \Lambda = 20$, τ_{eq} in ms

T_e (eV)	τ_{eq} (ms)	τ_{eq}/τ_s
100	0.13	0.16
500	1.5	0.46
1000	4.1	0.54
5000	46	0.65
10000	131	0.70

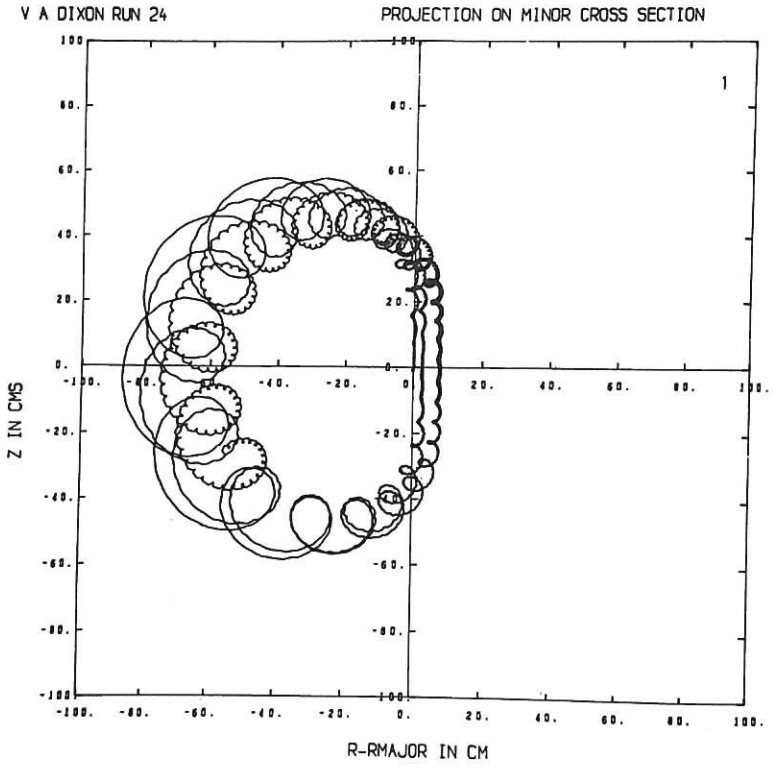

Fig. A1.3(a)

Motion of 1 MeV D^+ ion in $\ell=3$ stellarator field containing plasma.

Field parameters : Major radius 10^3 cm, minor radius 10^2 cm, rotational transform 240^o at 80 cm from toroidal axis, B = 20 kG.

Plasma parameters : $n_e = 3 \times 10^{16}$ cm^{-3}, $T_e = T_i = 1.0$ keV, A = 2.5 A.M.U.

Injected particle : A = 2 A.M.U., E = 1 MeV, initial velocity in the azimuthal direction, starting point on minor axis.

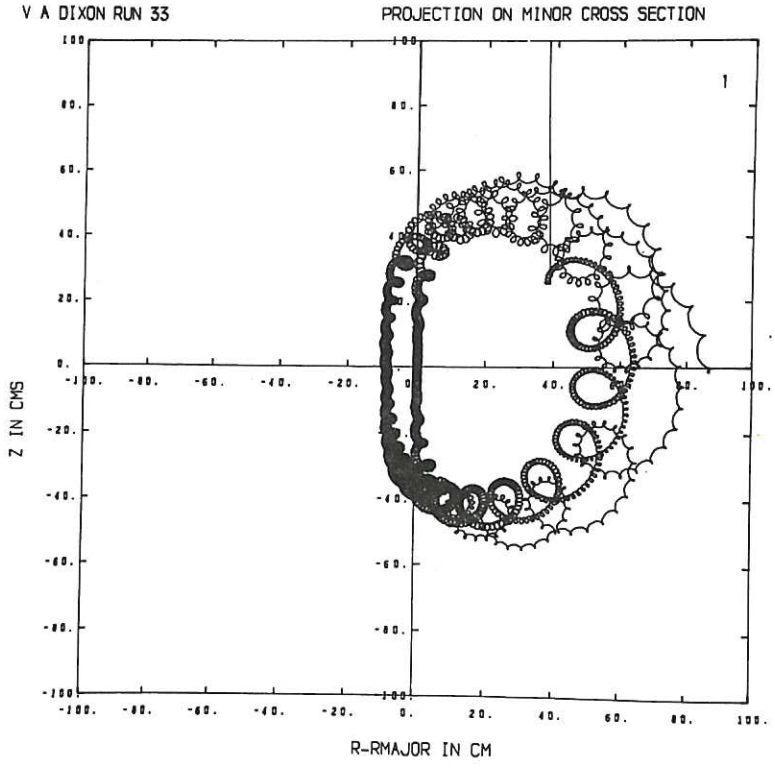

Fig. A1.3(b)

Field and plasma parameters as for Fig. A1.3(a).

Injected particle : A = 2 A.M.U., E = 1 MeV, initial velocity in the azimuthal direction, starting point on median plane, 87 cm from minor axis; chosen so as to make the unperturbed orbit pass near the minor axis.

APPENDIX 2

NEUTRAL ATOM PENETRATION INTO A FUSION REACTOR PLASMA

A.C. Riviere

1. Introduction

The successful injection of a neutral atom beam into a fusion reactor for heating and refuelling the plasma depends on the extent to which the beam can penetrate the plasma. It is important to establish that the rate of ionization is not so high that it prevents the penetration of the beam to the centre of the plasma nor so low that a substantial part of the beam passes right through the plasma. Some preliminary estimates were made by Rose[A2.1] for the attenuation lengths to be expected. Here, the relevant cross section data has been summarised and rate coefficients have been calculated for the appropriate ion and electron energy distributions. The plasma thickness, T, for a 1/e reduction in intensity of the neutral beam has been calculated as a function of energy from these rate coefficients. Finally, the required ratio of T to the product of plasma density and radius is calculated in a simple case and found to be of the order of 0.5.

2. Collision Cross Section Data

The collision processes of interest are:-

(1) Ionization by the electrons, with cross section σ_1 ,

(2) Ionization by the ions (σ_2),

(3) Charge exchange with the ions (σ_3), and

(4) Collisions with the alpha particles in the plasma.

As discussed in Appendix 3, collision cross section data is generally obtained with hydrogen beams, but the values for deuterium beams are the same for equal velocity. Thus to obtain σ for deuterons at energy E the value for protons at 0.5 E can be used.

2.1 Ionization by electrons, σ_1

A review of experimental data on electron ionization was published by Keiffer and Dunn[A2.2] and mean values for atomic hydrogen have been taken from their report. These are plotted in Figure A2.1 up to an electron energy of 800 eV. At high energies the cross section is expected to tend towards one half of that for molecular hydrogen. High energy ionization of H_2 was measured by Schram et al.[A2.3] and their results have been plotted at half their value in Figure A2.1 from 600 eV to 20 keV.

In order to join smoothly from the atomic hydrogen data to the molecular data one can make use of the high energy behaviour of the cross section as predicted by theory using the Born approximation, namely

$$\sigma_1 \sim \frac{A}{E} (\ell n\, E + B). \qquad \ldots (A2.1)$$

A good fit to the data is obtained with $A = 1{\cdot}364 \times 10^{-15}$ cm^2 eV and $B = 1{\cdot}82$. Values obtained from equation A2.1 with these constants have been plotted as crosses in Figure A2.1.

Gryzinski [A2.4] obtained a formula for σ_1 using a classical theory:

$$\sigma_1 = \frac{6{\cdot}513 \times 10^{14}}{E^2}\ g\,(x)\ \text{cm}^2$$

where

$$g(x) = \frac{1}{x}\left(\frac{x-1}{x+1}\right)^{3/2}\left[1 + \frac{2}{3}\left(1 - \frac{1}{2x}\right)\ell n\,(2{\cdot}7 + \sqrt{x-1})\right],$$

E is the electron energy in eV and x is the ratio of the electron energy to the ionization potential which in this case is 13·605 eV. Values obtained with this formula are shown in Figure A2.1 as the solid curve. The 10 per cent discrepancy around 50 eV is of the order of the present experimental uncertainty so that there is little point in adjusting the Gryzinski formula to fit the data more closely and we shall adopt it for the present calculations as a good analytic expression for σ_1.

2.2 Ionization by protons, σ_2

The cross section for ionization of atomic hydrogen by protons was measured by Fite et al.[A2.5] for energies between 7 and 40 keV and by Gilbody and Ireland [A2.6] for energies from 60 to 370 keV. Their data is plotted as solid and open circles respectively in Figure A2.2. The ionization of molecular hydrogen was measured by Hooper et al. [A2.7] at higher energies and their results are plotted at half their measured values between 150 keV and 1 MeV as open squares. At high velocities ionization by protons is expected to be equivalent to ionization by electrons and data on σ_1 is plotted (as crosses) at 500 keV and 1 MeV for electrons of the same velocity as 500 keV and 1 MeV protons respectively.

Theoretical calculations using the Born approximation also predict a dependence of the form of equation 1 at high energies. This is used here in the form

$$\sigma = 3{\cdot}6 \times 10^{12} E^{-1} \log_{10} (0{\cdot}1666\, E) \qquad \ldots (A2.2)$$

which is plotted as the short-dashed curve in Figure A2.2. The Gryzinski formula for ionization by protons is not such a good fit as it was for the electron case so a parabola was fitted to the log-log plot of the experimental data in the low energy region. The result is the expression

$$\log_{10} \sigma = -0{\cdot}8712 (\log_{10} E)^2 + 8{\cdot}156 (\log_{10} E) - 34{\cdot}833 \qquad \ldots (A2.3)$$

which is plotted as the solid curve in Figure A2.2. We have adapted equation A2.2 above 150 keV (proton energy) and equation A2.3 below 150 keV as good analytic expressions for σ_2.

2.3 Charge exchange with protons, σ_3

The cross section for charge exchange by protons in atomic hydrogen was measured by Fite et al. [A2.5] and their data is plotted in Figure A2.3 as solid circles over the energy range from 400 eV to 40 keV. This cross section was also measured at very low energies by Balyaev et al. [A2.8] and a single point is shown as an open circle at 100 eV. At high energies the cross section was measured by

Gilbody and Ryding [A2.9] and their values are plotted as open triangles between 38 keV and 98 keV. The charge exchange cross section for protons in molecular hydrogen was measured at high energies by Barnett et al. [A2.10] and their results are plotted as crosses at half their measured values.

At high energies, i.e., above 50 keV the data seem to fit an energy dependence of the form $E^{-3\cdot3}$. Although a much faster fall off is expected theoretically, more like E^{-6}, this probably occurs at much higher energies than 100 keV and since the cross section is then very small the error introduced will not affect the present results. Any calculation of the charge exchange of the injected beam at high energies to determine for example the wall bombardment must of course use the correct values for those energies and not the approximation used here.

At low energies the cross section is given by the expression

$$\sigma_3^{\frac{1}{2}} = A + B \ln E .$$

This form was combined with the $E^{-3\cdot3}$ dependence at high energies to obtain an empirical expression which fitted reasonably well over the whole energy range. The final expression was

$$\sigma_3 = \frac{0\cdot6937 \times 10^{-14} (1 - 0\cdot155 \log_{10} E)^2}{1 + 0\cdot1112 \times 10^{-14} E^{3\cdot3}} \text{ cm}^2 \qquad \ldots (A2.4)$$

where E is in electron volts. Values of σ_3 derived from equation A2.4 are shown as the solid curve in Figure A2.3 and the equation was adapted as a good analytic expression for σ_3.

2.4 Ionization by alpha particles

The ionization of atomic hydrogen by alpha particles does not seem to have been measured experimentally. Ionization of molecular hydrogen has been measured by Langley et al. [A2.11] from 500 keV to 1 MeV and their results are plotted at half their value in Figure A2.4(a). Since we are dealing with a bare nucleus it is expected from collision theory that at high energies the ionization cross section scales as Z^2 for equal velocity of impact. We assume here that this applies over

the whole energy range of interest and we use the formula for ionization of hydrogen atoms by protons derived above but scaled in this way. The result is plotted as the solid curve in Figure A2.4(a).

2.5 Charge exchange with alpha particles

The capture of electrons from atomic hydrogen by He^{++} was measured by Fite et al.[A2.12] between 0.1 and 38 keV using a He^3 beam and their results are shown in Figure A2.4(b) at the appropriate energy for mass 4. Also plotted in Figure A2.4(b) are the cross section values given by Allison[A2.13] for charge exchange in molecular hydrogen but again plotted at half value. The experimental points were fitted by simple analytic expressions. Above 12 keV

$$\log \sigma = - 14{\cdot}78 - 1{\cdot}33 \, (4{\cdot}5 - \log E)^2 \qquad \ldots \text{(A2.5)}$$

and below 12 keV

$$\log \sigma = - 16{\cdot}54 + 0{\cdot}09 \, (\log E)^2 \qquad \ldots \text{(A2.6)}$$

where E is in electron volts. Values derived from these expressions are shown as the solid curves in Figure A2.4(b).

3. Energy Distribution

In a mirror reactor plasma the electrons will have a Maxwellian energy distribution with a temperature T_e related to the ion injection energy E_o in a way which is dependent on the mirror ratio R (Kuo-Petravic et al.[A2.14]). The value of R will most likely lie between 3 and 10 and in this range we may take $E_o/T_e \approx 7$, although as will be seen later, the electrons have only a small effect on the beam attenuation so the exact value of this ratio is unimportant.

The calculations by Kuo-Petravic et al.[A2.14] show however, that the ion energy distributions are far from Maxwellian. The distributions for $R = 3$ and for $R = 10$ are shown in Figure A2.5(a). Also shown in Figure A2.5(a) for comparison is a Maxwellian distribution with $kT = E_o$ and it can be seen that the mirror distributions lack high energy particles in comparison with the Maxwellian. Analytic expressions have been obtained for both of the distributions. For $R = 3$ the result was

$$f(E/E_o) = - 1{\cdot}316 \, (E/E_o)^2 + 2{\cdot}831 \, (E/E_o) - 0{\cdot}4674 \text{ for } E/E_o < 1 \qquad \ldots \text{(A2.7)}$$

and

$$f\,(E/E_o) = 1{\cdot}684 - 1{\cdot}0526\,(-3{\cdot}69 + 5(E/E_o) - (E/E_o)^2)^{\frac{1}{2}} \qquad \ldots (A2.8)$$

for $1 < (E/E_o) < 2{\cdot}5$. For R = 10 the result was

$$f\,(E/E_o) = 0{\cdot}9123 - 1{\cdot}4251\,(0{\cdot}85 - (E/E_o))^2 \quad \text{for } E/E_o < 1 \qquad \ldots (A2.9)$$

and

$$f\,(E/E_o) = 1{\cdot}417 - 0{\cdot}8857\,(-3{\cdot}69 + 5\,(E/E_o) - (E/E_o)^2)^{\frac{1}{2}} \text{ for } 1 < (E/E_o) < 2{\cdot}5. \qquad \ldots (A2.10)$$

In both cases $\int_o^1 f(E/E_o)\, d(E/E_o) + \int_1^{2{\cdot}5} f(E/E_o)\, d(E/E_o) = 1$

and the distributions were assumed to stop at $(E/E_o) = 2{\cdot}5$.

The alpha particle energy distribution has also been calculated by Kuo-Petravic et al.[A2.14] and is reproduced in Figure A2.5(b) for R = 10. It is assumed here that this distribution is insensitive to mirror ratio and to the injection energy. The solid curve in Figure A2.5(b) shows the values derived from the analytic expression

$$f(E) = 1{\cdot}11 \times 10^{-4} \left\{ 10^{(-1{\cdot}94 - 1{\cdot}55(5 - \log E)^2)} + 10^{(-2{\cdot}61 - 1{\cdot}4(6 - \log E)^2)} \right\} \qquad \ldots (A2.11)$$

where E is in electron volts and this seems to be a reasonable description of the alpha energy distribution.

In toroidal reactors the ion and electron energy distributions are expected to be Maxwellian with $T_e \simeq T_i$.

4. Rate Coefficients

The rate coefficient for a collision process is the effective volume swept out per second by the bombarding particle and is basically the product of collision cross section and velocity of impact. With a wide energy distribution of particles in the plasma the definition of the rate coefficient becomes

$$\langle \sigma v \rangle = \int_o^{E_{max}} f(E_p)\, \frac{1}{4\pi} \int \sigma\,(E_c)\, |\bar{v}_p - \bar{v}_o|\, d|\bar{v}_p - \bar{v}_o|\, d\,E_p$$

where E_p and E_c are the energy of the plasma particle and the effective bombarding energy for the collision respectively and $\bar{v}_p$ and $\bar{v}_o$ are the

velocity of the plasma particle and velocity of the beam atom respectively. The plasma distribution is assumed to be isotropic in ϕ, the azimuth about the beam. This means, that for a mirror reactor the distribution in ϕ is taken to be that for $R = \infty$. The distribution is also isotropic in θ, the angle with respect to the beam. The relative collision velocity depends only on θ so that

$$\langle \sigma \cdot v \rangle = \int_{E_{min}}^{E_{max}} f(E_p) \, \tfrac{1}{2} \int_{o}^{\pi} \sigma(E_c) \, (v_p^2 + v_o^2 - 2 v_p r_o \cos\theta)^{\frac{1}{2}} \sin\theta \, d\theta \, dE_p \qquad \ldots(A2.12)$$

In a mirror reactor the electron velocity is always much greater than the atom beam velocity so that the integration over θ can be replaced by $\sigma(E_p) \cdot v_p$. Using a Maxwellian distribution and the analytic form for σ_1 the integration was performed for the electrons by using Simpson's rule with $E_{max} = 200 \times T_e$, E_{min} = ionization potential and taking 100 steps. The result is plotted in Figure A2.6 from T_e = 100 eV to 1 MeV. The effect of relativistic changes in velocity were included.

For proton ionization in a mirror reactor the integration over θ was carried out as a simple summation in 50 steps from 0 to π. The integration over E_p was also carried out as a simple summation in 50 steps with the energy distribution both for R = 3 and R = 10 and the results are plotted in Figure A2.7(a). The change from R = 3 to R = 10 is within the experimental errors on σ_2 so we will use R = 3 only in calculating the total rate coefficient. It should be noted here that the beam energy is coupled to the plasma "temperature" E_o and was taken equal to E_o in Figure A2.7(a).

The same number of steps and integration method were used to calculate the charge exchange rates and the results are shown in Figure A2.7(b) for R = 3 and R = 10. However, if the fast neutral formed by the collision is heading within an angle θ_{min} of the beam and its energy is greater than E_o the injected atom beam could not be said to have been attenuated. The effect of excluding such events with $\theta_{min} = 0.2$ is shown in Figure A2.7(b) where it can be seen that the effect only becomes appreciable at high energies. The reason for this is that σ_3 is large

at low energies and falls rapidly with energy so that at high plasma and beam energies only those collisions with low relative velocity contribute to the rate and these are just the ones which lie within θ_{min}. Here again the effect of changing from R = 3 to R = 10 is not very great except at high energies where in fact the rate is small. The R = 3, θ_{min} = 0.2 result will be used in calculating the total rate coefficient.

We have, from the previous section, analytic expressions for the cross sections for alpha particle collisions and the alpha energy distribution. These were used in the same way as for the proton collisions above to obtain the rate coefficients except that the alpha energy distribution was divided into 100 parts rather than 50. The results are shown in Figure A2.8 for the two processes.

All rates are summarised for a mirror reactor with R = 3 in Figure A2.9 but now as a function of deuteron energy. It can be seen that the electrons play a minor role and that the choice of $T_e = \frac{1}{7} E_o$ is not critical.

The rate coefficients for a toroidal reactor plasma were obtained by using a Maxwellian energy distribution but allowing for the relative velocity between beam and plasma particles. The expressions for the cross sections derived above were used and the results are shown in Figure A2.10 for various hydrogen atom beam energies. The emphasis with the toroidal reactor is on the use of neutral injection as a means of heating the plasma up to ignition temperatures so that we choose cases where the beam energy is much greater than the plasma temperature. It can be seen that charge exchange has a very small rate and that electrons only have an appreciable rate at low plasma temperatures. The attenuation of the atom beam is mostly due to collisions with ions leading to ionization and this process is almost independent of plasma temperature since the beam atoms are moving at a much higher velocity than the plasma ions. Total rate coefficients are plotted in Figure A2.11(a) as a function of deuteron plasma temperature for deuteron beam energies of 256 keV, 1·024 MeV and 2·048 MeV.

5. Attenuation Thickness, T

The thickness of plasma which will attenuate the atom beam by 1/e is given by

$$T = \frac{\text{velocity of beam}}{\text{rate coefficient for collision processes}} = \frac{v_o}{\langle \sigma \cdot v_r \rangle} \quad \text{cm}^{-2}.$$

Values of T calculated for the toroidal reactor case are plotted in Figure A2.11(b) for deuteron beam energies of 256 keV, 1·024 MeV and 2·048 MeV respectively.

For the mirror reactor case values of T are plotted in Figure A2.12 as a function of E_o the characteristic energy of the plasma. In this case we also consider injection energies different from E_o as it may be desirable to inject at several energies simultaneously. Values of T are plotted for E_{inj}/E_o equal to 2, 1 and 0·5 but neglecting the effect of the alpha particles. The effect of an alpha population of 10 per cent is shown for $E_{inj}/E_o = 1$ and also for this beam energy the values of the parameter T are shown for injecting tritium atoms into a pure tritium plasma. These results show the range of values of T to be expected and the exact value will depend on the deuteron-tritium-helium concentration ratios.

6. Radial Distribution of Injected Particles in a Cylindrical Plasma

We assume the reactor plasma has cylindrical symmetry simply to be able to say that particles ionized beyond the axis will precess around the axis at constant R. We assume also for the present discussion that the density distribution of the plasma is independent of radius, that is, a "top-hat" distribution. The consequence of this assumption is that the number of particles between r and r + dr increases linearly with r and this distribution is the one to be matched by the injected distribution. The intensity of the atom beam at radius r on the incoming side of the axis of a plasma of radius R_o and density N_o is simply

$$I_1(r) = e^{-\frac{N_o R_o}{T}(1 - r/R_o)}$$

where the initial beam intensity is unity. We replace $\frac{N_o R_o}{T}$ by γ and

r/R_o by R, the injected distribution is then

$$\left| \frac{d\, I_1\,(R)}{d\, R} \right| = \gamma\, e^{-\gamma(1-R)} \quad . \qquad \ldots (A2.13)$$

Beyond the axis the beam intensity is

$$I_2\,(R) = e^{-\gamma}\, e^{-\gamma R}$$

and the injected distribution resulting from this attenuation is

$$\left| \frac{d\, I_2\,(R)}{d\, R} \right| = \gamma\, e^{-\gamma}\, e^{-\gamma\, R} \quad . \qquad \ldots (A2.14)$$

The total trapped distribution is simply the sum of A2.13 and A2.14;

$$\frac{dI}{dR} = \gamma\, e^{-\gamma} \left(e^{\gamma R} + e^{-\gamma\, R} \right) = 2\gamma e^{-\gamma} \cosh\,(\gamma R) \quad .$$

This distribution for $\gamma = 2$ and $2{\cdot}5$ is shown in Figure A2.13 in comparison with the desired distribution $\frac{dI}{dR}$ = constant x R. The fraction of the beam which penetrates to the far side of the plasma is $e^{-2\gamma}$ and for $\gamma = 2$ and $2{\cdot}5$ is $1{\cdot}8$ and $0{\cdot}7$ per cent respectively. It can be seen that a value of γ near 2 would be acceptable but that relatively more injection occurs at the edges and on the axis than at intermediate radii. The density of the plasma would increase rapidly on the axis in fact but it seems plausible that the exact density distribution required can be obtained by varying injection energy and the direction of injection, that is, by some off axis injection.

For toroidal plasmas with densities of 3×10^{14}, T_e = 10 keV and R_o = $1{\cdot}5$ metres a deuteron energy of about 1 MeV is required. For mirror reactors with injection E_o = 300 keV and R_o = $1{\cdot}4$ metres the plasma density should not exceed about $1{\cdot}0 \times 10^{14}$ cm^{-3}. These results indicate the possibility of neutral injection but the actual requirements will depend on more exact information about the reactor plasmas.

References

(A2.1) Rose, D.J., Private communication, 1968.

(A2.2) Keiffer, L.J. and Dunn, G.H., Rev. Mod. Phys., vol. 38, pp. 1-35, 1966.

(A2.3) Schram, B.K., De Heer, F.J., Wiel, M.J.V.D. and Kistemaker, J., Physica, vol. 31, pp. 94-112, 1965.

(A2.4) Gryzinski, M., In: Atomic Collision Processes, Ed. M.R.C. McDowell, (North-Holland Publishing Company, Amsterdam, 1964) pp.226-236.

(A2.5) Fite, W.L., Stebbings, R.F., Hummer, D.G. and Brackman, R.T., Phys. Rev., vol. 119, 1960, pp.663-668.

(A2.6) Gilbody, H.B. and Ireland, J.V., Proc. Roy. Soc., vol.277A, 1964, pp.137-141.

(A2.7) Hooper, J.W., McDaniel, E.W., Martin, D.W. and Harmer, D.S., Phys. Rev., vol.121, 1961, pp.1123-1127.

(A2.8) Balyaev, V.A., Brezhniev, B.G. and Erastov, E.M., Proc. of the Vth Int. Conf. on the Physics of Electronis and Atomic Collisions, Leningrad, July, 1967 (Publishing House NAUKA, Leningrad, 1967). pp.156-158.

(A2.9) Gilbody, H.B. and Ryding, G., Proc. Roy. Soc., vol. 291A, 1966, pp.438-443.

(A2.10) Barnett, C.F. and Reynolds, H.K., Phys. Rev., vol.109, 1958, pp.355-359.

(A2.11) Langley, R.A., Martin, D.W., Harmer, D.S., Hooper, J.W. and McDaniel, E.W. Phys. Rev., vol.136A, 1964, pp.379-385.

(A2.12) Fite, W.L., Smith, A.C.H. and Stebbings, R.F., Proc. Soc., 268A, 527-536 (1962).

(A2.13) Allison, S.K., Rev. Mod. Phys., vol.30, 1958, pp.1137-1168.

(A2.14) Kuo-Petravic, L.G., Petravic, M. and Watson, C.J.H., Proc. of the B.N.E.S. Conference on Nuclear Fusion Reactors, Culham Laboratory, September 1969. (British Nuclear Energy Society, 1970). Paper 2.4.

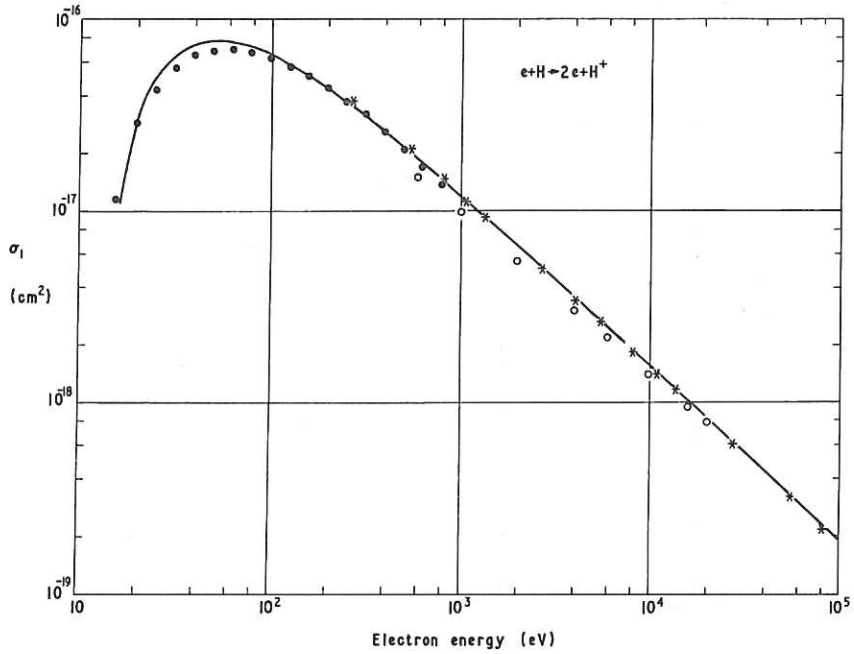

Fig. A2.1 The cross section for ionization of atomic hydrogen by electrons.
● - average of experimental data for H [Ref. A2.2],
O - 0.5 x value of experimental data for H_2 [Ref. A2.3],
* - extrapolation of experimental data using equation (A2.1),
—— Gryzinski [A2.4] formula for σ_1.

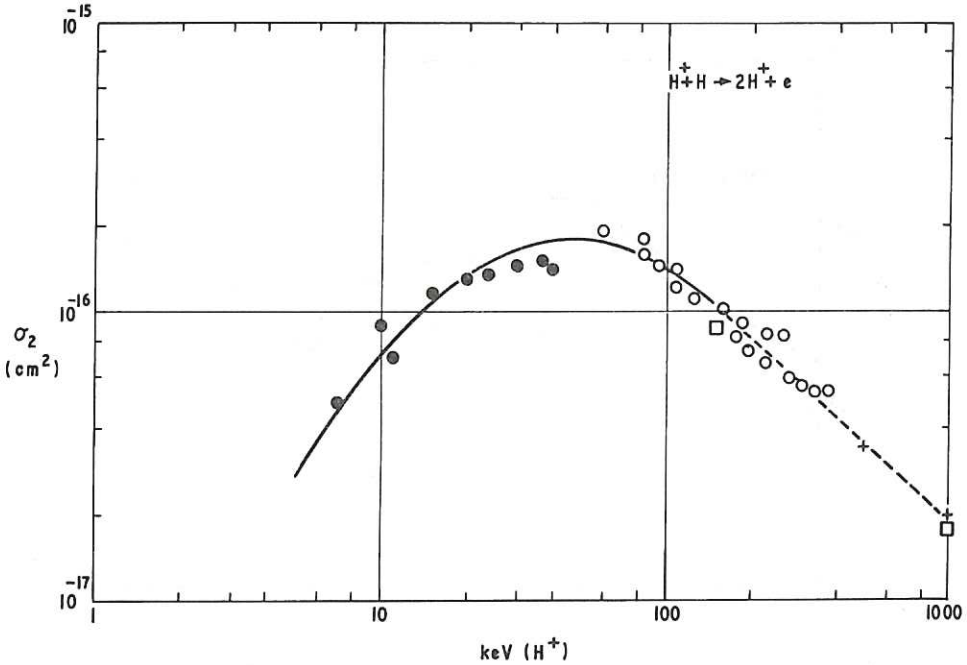

Fig. A2.2 The cross section for ionization by protons in atomic hydrogen.
● - experimental points for H [Ref. A2.5],
O - experimental points for H [Ref. A2.6],
□ - 0.5 x value of experimental points for H_2 [Ref. A2.7],
+ - electrons in H at same velocity [Ref. 2.4],
--- equation (A2.2),
—— equation (A2.3).

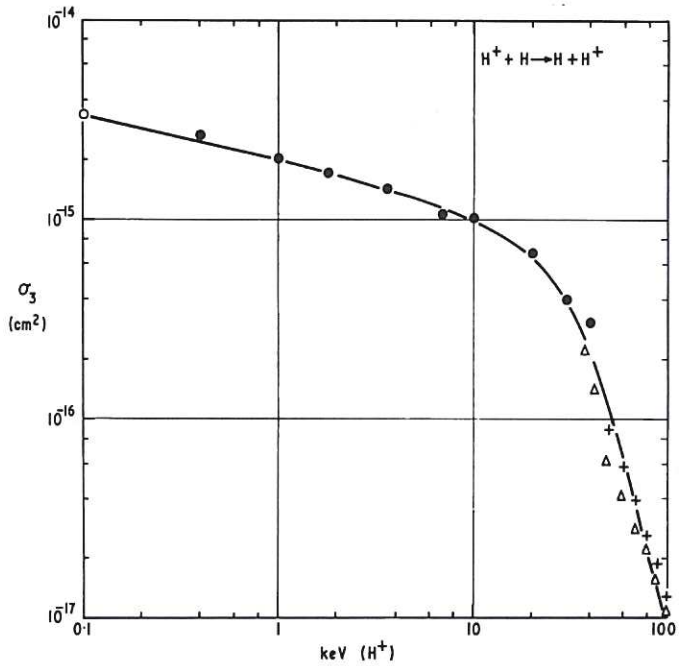

Fig. A2.3 The cross section for charge exchange by protons in atomic hydrogen.
O - experimental points for H [Ref. A2.8],
● - experimental points for H [Ref. A2.5],
Δ - experimental points for H [Ref. A2.9],
\+ - 0.5 x value of experimental points for H_2 [Ref. A2.10],
—— equation (A2.4).

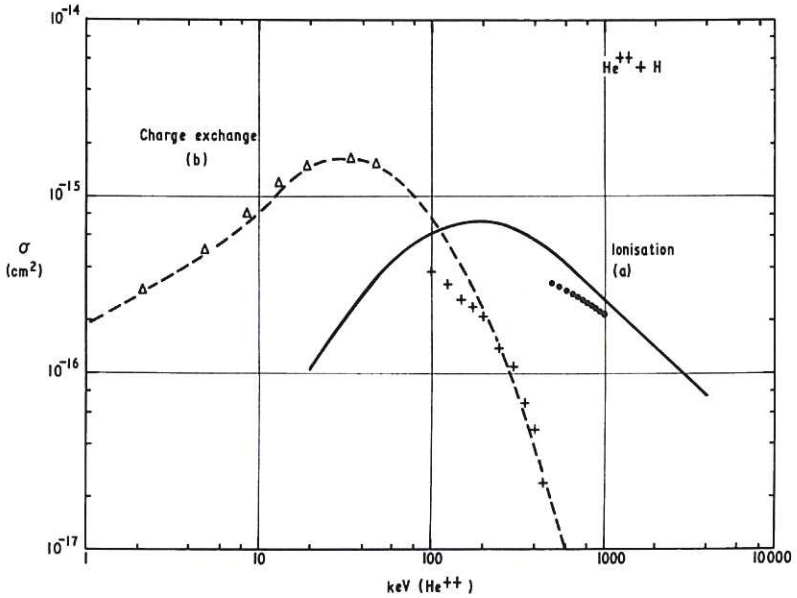

Fig. A2.4 (a) the cross section for ionization of atomic hydrogen by H_e^{++}.
● - 0.5 x value of experimental points for H_2 [Ref. A2.11],
—— equations (A2.2) and (A2.3) scaled as Z^2 and plotted at equal velocity,
(b) the cross section for charge exchange by H_e^{++} in atomic hydrogen.
Δ - experimental points for He^3 ions scaled to the correct energy for the He^4 ions [Ref. A2.12],
\+ - 0.5 x value of experimental points for H_2 [Ref. A2.13],
—— —— equation (A2.5), above 12 keV, equation (A2.6) below 12 keV.

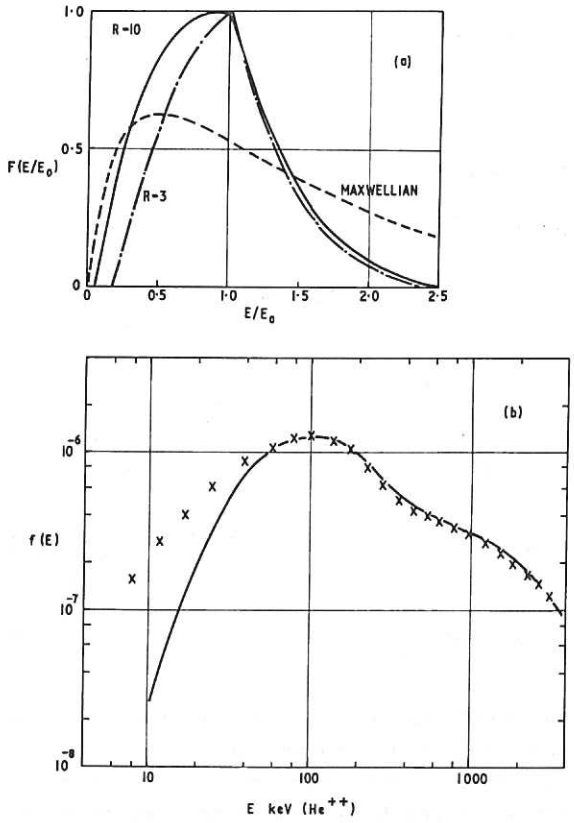

Fig. A2.5 (a) ion energy distributions for a mirror reactor with R = 3 (equations (A2.7) and (A.2.8) and R = 10 (equations (A2.9) and (A2.10)) and a Maxwellian distribution with $T_i = E_o$.
(b) H_e^{++} energy distribution for a mirror reactor with R = 10.
X - computed results from [Ref. A2.14],
—— equation (A2.11).

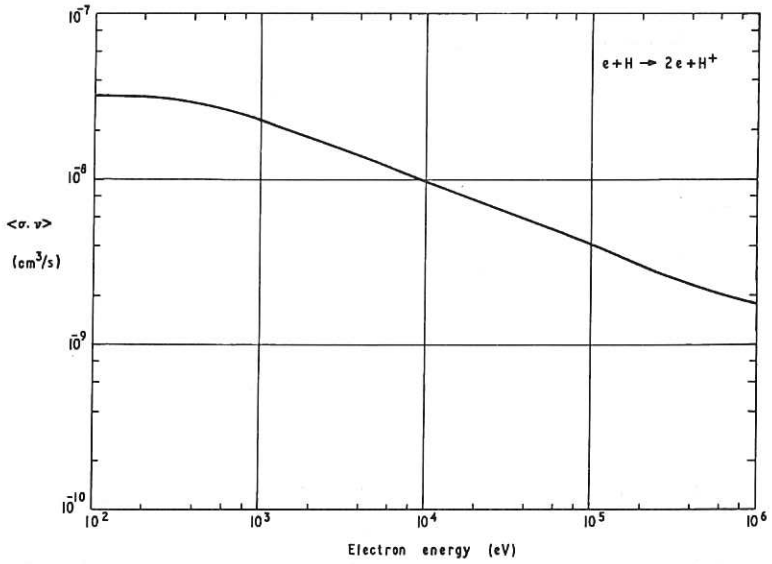

Fig. A2.6 Rate coefficient for the ionization of atomic hydrogen by electrons with Maxwellian energy distribution.

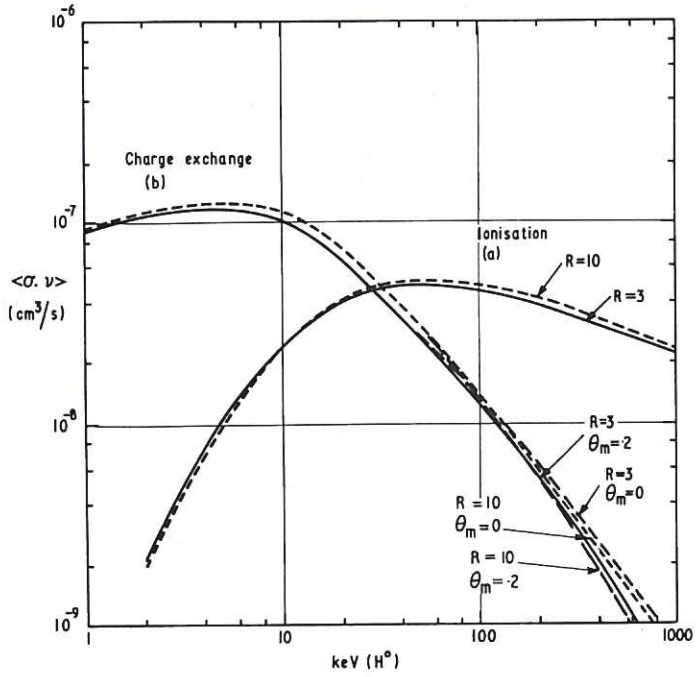

Fig. A2.7 Rate coefficients for a mirror reactor plasma obtained from analytic expressions for the cross sections and ion energy distributions. (a) Ionization of atomic hydrogen by protons for R = 3 and R = 10; (b) Charge exchange by protons in atomic hydrogen for R = 3 and R = 10 and with and without rejection of forward events within a cone of semi-angle θ_{min} and of energy greater than E_o.

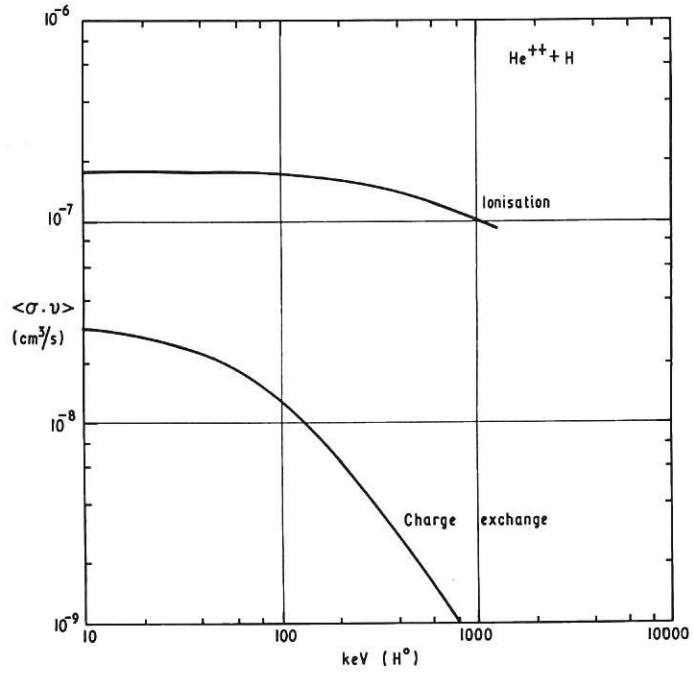

Fig. A2.8 Rate coefficients for collisions with H_e^{++} in a mirror reactor plasma as a function of characteristic plasma 'temperature' E_o.

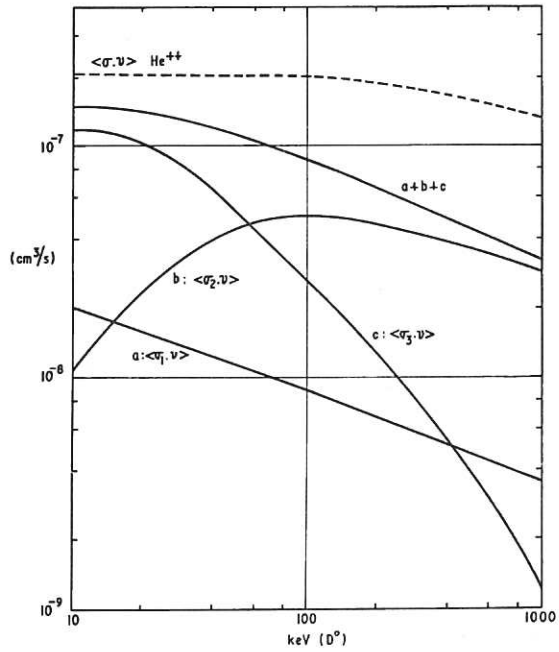

Fig. A2.9 Summary of rate coefficients for a deuterium atom beam with energy E_o entering a mirror reactor plasma.
a: electron ionization with $T_e = E_o/7$.
b: proton ionization for R = 3
and c: proton charge exchange for R = 3, $\theta_{min} = 0.2$
— — — sum of H_e^{++} rates given in Figure A2.8.

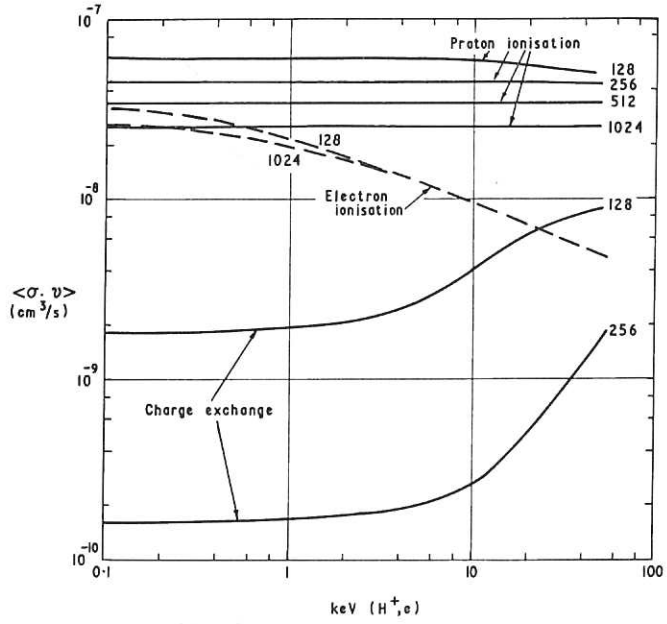

Fig. A2.10 Rate coefficients for a reactor plasma with Maxwellian ion and electron energy distributions and with $T_e = T_i$. Results are plotted as a function of plasma temperature for indicated H^o beam energies in keV.

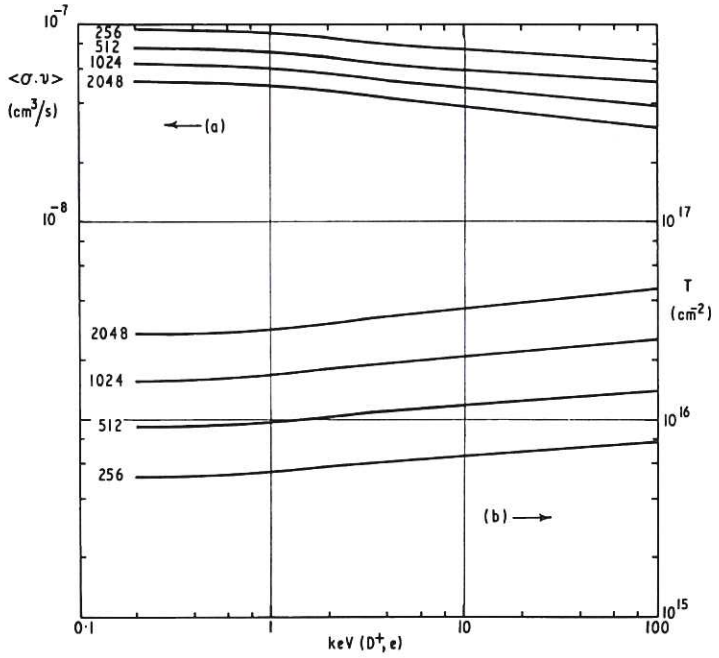

Fig. A2.11 (a) Total rate coefficients for attenuation of deuterium atom beam entering a pure deuterium plasma.
(b) Attenuation thickness R for an e^{-1} reduction in beam intensity.
Results are plotted as a function of plasma temperature for indicated D^0 beam energies in keV, and are for a plasma with Maxwellian energy distribution.

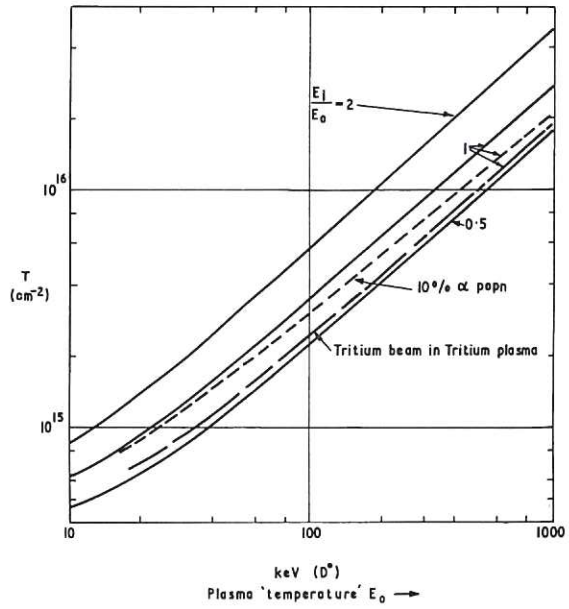

Fig. A2.12 Attenuation thickness T for an e^{-1} reduction in beam intensity as a function of charactersitic plasma 'temperature' E_0 of a mirror reactor. Curves labelled 2,1, 0.5 refer to beam energies 2, 1 and 0.5 times E_0. — — — as for 1 but with an alpha particle population of 10 per cent.
— - — as for 1 but for a tritium atom beam entering a pure tritium plasma.

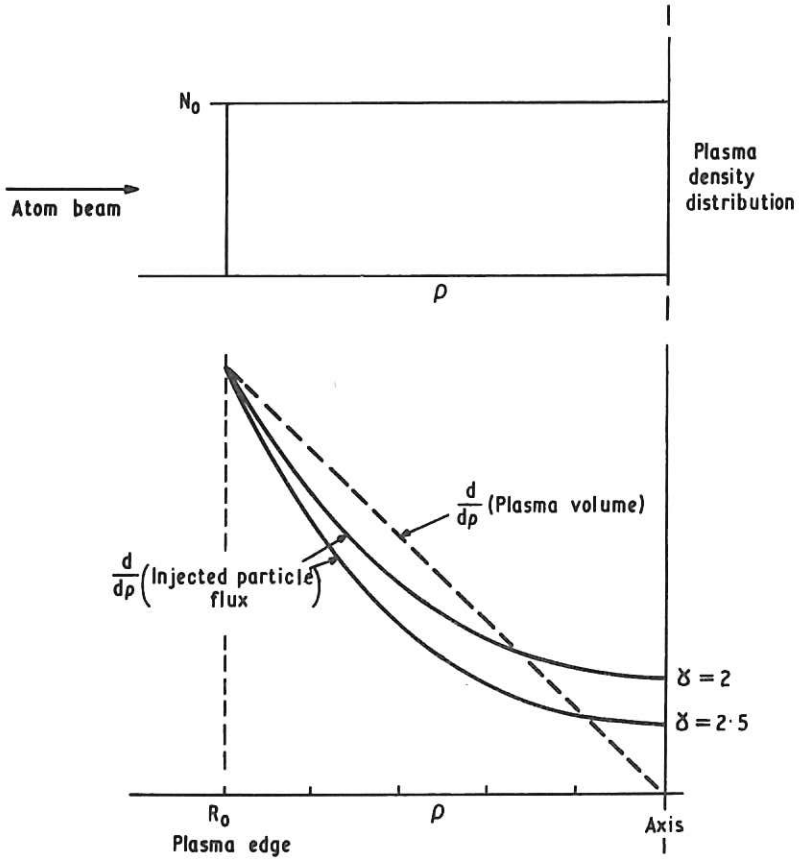

Fig. A2.13 Lower diagram shows trapped ion distributions produced in a simple cylindrical plasma in which ions precess around at constant radius. The broken line shows the distribution required if the number of particles per unit volume is to be the same throughout the plasma. Top diagram shows assumed plasma density distribution.

APPENDIX 3

NEUTRALISATION EFFICIENCY

A.C. Riviere

1. Introduction

An essential part of the injector is the conversion of the ion beam into a beam of fast atoms and the expected power efficiency for this process is calculated here for a range of beam energies and for several ion species.

To obtain the beam of atoms the ion beam, after acceleration to the required energy, is passed through a gas target. A fast atom is formed when either an electron is captured by a positive ion, a molecular ion is dissociated or an electron is lost by a negative ion. The effectiveness of these processes is generally known or can be calculated since most of the cross sections required have been measured.

For a reactor a beam of deuterium or tritium atoms is required whereas the cross section data has generally been measured using hydrogen ions. The collisions causing the processes mentioned above mainly involve electronic interactions and the differences in the electronic wave functions between the isotopes are extremely small. There are differences in the vibrational energy levels between the isotopic forms of the molecular ions but the effect of these on the cross sections are small and will be neglected. In what follows it will be assumed that the cross sections depend only on the velocity of the particles but not on their mass and at equal velocities the data obtained using hydrogen ions can be used for deuterium and tritium.

In a full scale injector the gas in the neutraliser will become ionized to some extent. The effect of this on the performance of the neutraliser

will be simply related to the sum of the effect of the collisions with the neutral molecules and the effect of the collisions with the ions and electrons. The electrons in the plasma can be assumed to be cold and because of the relatively high velocity of the ions in the beam the effect of the ions can be taken to be equal to the effect of the electrons. Where possible the effect of a pure electron gas has been calculated and the net efficiency can be expected to lie somewhere between that of the un-ionized gas and that of an electron gas.

2. Available Data on the Yield of Atoms per Beam Ion

D^+ primary beam

The only possible process in this case is electron capture. In the present energy range the formation of negative ions can be neglected so that the equations describing the formation and destruction of D^0 and D^+ ions become

$$\dot{D}^0 = \sigma_{10} \cdot D^+ - \sigma_{01} \cdot D^0 \qquad \ldots (A3.1)$$

$$\dot{D}^+ = \sigma_{01} \cdot D^0 - \sigma_{10} \cdot D^+ \qquad \ldots (A3.2)$$

where differentiation is with respect to target thickness, D^0, D^+ are the fractions of the beam in each charge state, σ_{01} is the electron loss cross section and σ_{10} is the electron capture cross section. After a sequence of collisions an equilibrium is reached and equations A3.1 and A3.2 then show that the fraction of the beam in the neutral state is simply

$$F_{0\,\infty} = \frac{\sigma_{10}}{\sigma_{10} + \sigma_{01}} \quad . \qquad \ldots (A3.3)$$

With increasing energy σ_{10} falls approximately as E^{-6} whereas σ_{01} falls approximately E^{-1}. Thus the value of $F_{0\,\infty}$ falls off as about E^{-5}, that is, very rapidly. Values of $F_{0\,\infty}$ are given in Figure A3.1 for a D^+ beam passing through a hydrogen and a helium neutraliser. These were taken from the summary of data published by Allison and Garcia-Munoz (A3.1), but

where $F_{o\,\infty}$ was not measured directly it was obtained from cross section values through equation A3.3. Other materials give values of $F_{o\,\infty}$ which are equal to or less than those shown. Ionization of the gas will result in smaller capture cross sections and a reduction in $F_{o\,\infty}$.

D_2^+ primary beam

In this case electron capture and/or dissociation of the molecule can produce fast neutrals. Although the electron capture cross section falls rapidly with energy the dissociation cross section falls only as about E^{-1}. When the molecular ions are dissociated there is no feasible return path for reforming them and the yield of atoms for thick targets becomes that obtained for atomic ions in the previous section. At intermediate target densities the yield of atoms goes through a maximum and at high energies this can give a high efficiency compared with electron capture alone.

There are four possible constituents to the beam as it penetrates the target gas, D_2^+, D_2^o, D^+ and D^o. The four equations determining the rate of change of each component are rather unwieldy to handle as is also their analytic solution. A simplification can be made if the reaction $D_2^+ \rightarrow D_2^o$ is assumed to be the reaction $D_2^+ \rightarrow 2D^o$. There is then no channel feeding the D_2^+ component and its intensity can be written as

$$D_2^+ = \exp\,(-\,t\,.\,\Sigma\sigma) \qquad \ldots(A3.4)$$

where $\Sigma\sigma$ is the sum of the cross sections for all the processes leading to the loss of D_2^+, t is the target thickness and the primary beam intensity is assumed to be equal to 1.0. The equations defining D^o and D^+ are then

$$\dot{D}^o = (\sigma_{d1} + 2.\sigma_{d2})\,.\,\exp(-\,t.\Sigma\sigma) - \sigma_{01}\,.\,D^o \qquad \ldots(A3.5)$$

$$\dot{D}^+ = (\sigma_{d1} + 2.\sigma_{d3})\,.\,\exp(-\,t.\Sigma\sigma) + \sigma_{01}\,.\,D^o \qquad \ldots(A3.6)$$

where σ_{d1} is the cross section for dissociation into $D^o + D^+$, σ_{d2} that for forming $2D^o$, and σ_{d3} that for forming $2D^+$. The contribution to D^o

from electron capture by D^+ is neglected. Substituting for D_2^+ from A3.4 equation A3.5 becomes of the form

$$\frac{dy}{dx} = A \exp(-Bt) - Cy \qquad \ldots (A3.7)$$

which has the solution

$$y = \frac{A}{C - B} \left\{ \exp(-Bt) - \exp(-Ct) \right\} . \qquad \ldots (A3.8)$$

This goes to zero incorrectly at $t = \infty$ because the electron capture by D^+ was neglected but this is only important for thick targets whereas y goes through a maximum at intermediate values of t. The maximum value of y is given by

$$y_m = \frac{A}{B} \left(\frac{B}{C} \right)^{\frac{C}{C-B}} \qquad \ldots (A3.9)$$

at

$$t = \frac{1}{C - B} \ell n \left(\frac{C}{B} \right) . \qquad \ldots (A3.10)$$

For the maximum value of the yield of atoms $A = \sigma_{d1} + 2.\sigma_{d2}$, $B = \Sigma\sigma$ and $C = \sigma_{01}$. The maximum atom yield in H_2 gas calculated from equation A3.9 is plotted as a function of energy in Figure A3.2 as the curve marked H_2(calc). Values of σ_{d1}, σ_{d2} and σ_{d3} for H_2 gas have been taken from Sweetman[A3.2] and McClure[A3.3]. Experimental values of the maximum atom yield are available for Li, Mg, Zn, and Hg from D'yachkov[A3.4] and for H_2O from Sweetman[A3.5]. These are also shown as individual points on Figure A3.2.

The dissociation of H_2^+ ions by electrons has been measured by Dunn and Van Zyl[A3.6] and by Dance et al.[A3.7]. It was shown by Dunn that the same results were obtained with D_2^+ ions. Their experiments did not differentiate between reactions leading to $H^o + H^+$ and those leading to $H^+ + H^+$. Some indication was obtained by Dance et al.[A3.7] that the second reaction was of the order of 10 percent of all reactions and this assumption was used to obtain the electron curve in Figure A3.2. The transition energies for the two processes (obeying the Frank Condon principle) are about 11 eV and 29 eV respectively and if the Grysinski[A3.8] formula for ionization is

used to calculate the cross section for dissociation it is found that the second reaction will occur in 25 percent of the reactions at the highest energy and in 10 percent at the low energies. The electron-gas curve is probably in doubt to the same extent. The cross section σ_{01} for electron impact has been measured by Fite and Brackman (A3.9) and their values are used here. The electron curve indicates the maximum atom yield to be expected for a fully ionized target.

D_3^+ primary beam

This case is similar to D_2^+ but with additional reaction paths available. Cross sections for all the reaction paths from H_3^+ were measured by Sweetman (A3.10) in hydrogen for energies from 1 to 3 MeV and cross sections for H^+ and H_2^+ production were measured by Barnett (A3.11) from 40 to 200 keV.

The cross section for $H_2 \rightarrow H_2^+ + e$ was extrapolated as E^{-1} from the last value given by McClure at 100 keV, i.e. 2×10^{-16} cm^2. The cross sections for the processes leading to 2H, H_2^+, $H + H^+$ and $2H^+$ from H_2 were assumed to be inversely proportional to the excitation energy required for each reaction. These energies were taken to be 7, 15.6, 30, and 45 eV respectively.

The rise and fall of the various beam components in traversing the gas target can be described by a set of simultaneous differential equations whose coefficients are all known. The solution of these equations for H_2 gas has been carried out and the result for 1.5 MeV H_3^+ is shown in Figure A3.3. The maximum yield of atoms per incident H_3^+ ion is 0.6 and variation of the H_2 break-up cross sections by $\pm$ 30% causes this to change from .57 to .63 only. Variation of the relationship between the various channels into which H_2 break-up can go will have an effect but what variation is most likely is not known. The results in Figure A3.3 also show what proportion of the beam appears as H_3^+, H_2^+ and H^+ at maximum yield.

The results for the atom yield calculated as above for a range of deuterium atom energies are shown in Figure A3.4 with the results of some recent measurements made at Culham (Middleton, Payne and Riviere).

A measurement of the yield of atoms and molecules was made by D'yachkov[A3.4] in Li vapour and his results are also shown in Figure A3.4.

No data has been found on the collision of electrons or ions with H_3^+.

D⁻ primary beam

Because the outer electron of the negative ion is bound by only 0.75 eV to the atom the cross section for electron loss by D^- is much greater than that for D^0. It is possible therefore to convert a large part of a D^- beam to a D^0 beam without producing an appreciable population of D^+ ions. The yield of atoms passes through a maximum as a function of target thickness as for the H_2^+ molecular ions above and equation A3.9 can be used to determine the maximum yield.

The cross section for electron loss by H^- in hydrogen gas is known. The data used here was taken from Allison and Garcia Munoz[A3.1] and the result of evaluating equation A3.9 neglecting electron capture by D^+ is shown in Figure A3.5 as a function of energy. A direct measurement was also made by D'yachkov[A3.4] for H^- in Li and his results are also plotted in Figure A3.5.

The cross section for electron detachment from H^- by electrons has been measured by Dance et al.[A3.12]. Their results were used with equation A3.9 to obtain the maximum atom yield for electron impact as a function of energy and the result is plotted in Figure A3.5.

It is evident that very high yields of atoms can be obtained through the use of negative ion beams. However, the production of these ion beams must also be considered. Although it is possible to extract negative ions directly from an ion source, present source performances are rather low. The production of negative ions by electron capture occurs when an ion beam is passed through a gas target, and the maximum yield is obtained under equilibrium (or thick target) conditions. A summary of the available information on the maximum yield of negative ions produced in this way is shown in Figure A3.6 as a function of energy. More data is available on other materials but the H^- yield is not greater than that shown. The data of Figure A3.6 suggests that at any ion energy high enough to produce a high ion

current the negative ion yield is too small for reactor purposes if produced in this way.

He^{3+} primary beam

The production of a beam of neutral helium atoms may be required if a reactor operating on the D He^3 reaction is required. Data is included here on the yield of He^3 atoms as a function of energy when He^3 ions are neutralised by electron capture. Thick target yields are shown in Figure A3.7 for the H_2 and He gas. These were taken from the cross sections and ratios published by Allison and Garcia-Munoz(A3.1). The same problem exists as for the production of D^o by electron capture, namely that the capture cross section and therefore the yield falls rapidly with energy. Molecular ions, such as He_2^+ and HeH^+, have been observed but very little information is available on the yield of these ions from a high current source. Some measurements have been made by Wilson(A3.16) on the collisional break-up of 560 keV He^4 H^+ ions in hydrogen and helium gases. He^3 H^+ ions of the same velocity would have an energy of 450 keV and the energy of the He^3 atoms arising from the dissociation of this ion would be 340 keV. Sufficient information was given by Wilson to use equation A3.9 above for calculating the expected maximum yield of fast He^3 atoms. This was found to be 0.12 for both gases and is substantially higher than could be obtained by electron capture at 340 keV although still a very low yield.

3. Neutraliser Power Efficiency

The power efficiency of the neutraliser is defined as

$$\eta_o = \frac{\text{Power in beam of atoms leaving neutraliser}}{\text{Power in ion beam entering neutraliser}} .$$

In the previous section the yield of atoms per incident ion was calculated for various cases and in the case of electron capture this number is equal to η_o. In the case of D_2^+ and D_3^+ the atom yield figures have to be divided by 2 and 3 respectively and in the D^- case η_o is again simply equal to the atom yield. A summary of the values of η_o for primary beams of D^+, D_2^+, D_3^+ and D^- is shown in Figure A3.8. In the absence of a high

current D^- source the most efficient ion beam is D_3^+ although the effect of ionization of the neutraliser gas is not known.

Values of η_o for He^3 beams can be read directly from Figure A3.7 and there is a single value $\eta_o = 0.09$ for 340 keV He^3 obtained from an He^3H^+ ion beam.

4. Data Still Required

The most important collision cross sections for D^o production which are not yet known are those for the dissociation of H_3^+ ions under electron impact. These are required in the electron energy range of 20 to 300 eV.

For any proposed use of He beams with energies above about 200 keV it would be necessary to investigate sources of high current beams of molecular helium ions and to measure the collision processes involving these ions.

References

(A3.1) Allison, S.K. and Garcia-Munoz, M., In: Atomic and Molecular Processes, (Academic Press, New York, 1962). Chapter 19, pp.722-782.

(A3.2) Sweetman, D.R., Proc. Roy. Soc., vol. 256A, 1960, pp. 416-426.

(A3.3) McClure, G.W., Phys. Rev., vol. 130, no. 5, 1 June 1963, pp. 1852-1859.

(A3.4) D'yachkov, B.A., Soviet,Physics-Tech. Phys., vol. 13, 1969, pp. 1036-1045.

(A3.5) Sweetman, D.R., Unpublished data, 1960.

(A3.6) Dunn, G.H. and Van Zyl, B., Phys. Rev. vol. 154, 1967, pp. 40-51.

(A3.7) Dance, D.F., Harrison, M.F.A. and Rundel, R.D., Proc. Phys. Soc., vol. 92, 1967, pp. 577-588.

(A3.8) Cryzinski, M., In: Atomic Collision Processes, Ed. M.R.C. McDowell, (North-Holland Publishing Company, Amsterdam, 1964). pp. 226-236.

(A3.9) Fite, W.L. and Brackman, R.T., Phys. Rev. vol. 112, 1958, pp. 1141-1151.

(A3.10) Sweetman, D.R., Unpublished data, 1961.

(A3.11) Barnett, C.F., Unpublished data from Oak Ridge National Laboratory report ORNL-3113, 1964.

(A3.12) Dance, D.F., Harrison, M.F.A. and Rundel, R.D., Proc. Roy. Soc., vol. 299A, 1967, pp. 525-537.

(A3.13) Schlachter, A.S., Bjorkholm, P.J., Loyd, D.H., Anderson, L.W. and Haeberli, W., Phys. Rev., vol. 177, 1969, pp. 184-190.

(A3.14) Schmelzbach, P.A., Gruebler, W., Konig, V. and Marmier, P., Helv. Phys. Acta, vol. 41, 1968, pp. 310-312.

(A3.15) Futch, A.H. and Moses, K., UCRL, Unpublished data, 1966.

(A3.16) Wilson, W.D., University of California, Lawrence Radiation Laboratory, Berkeley, report UCRL-16308, 1965.

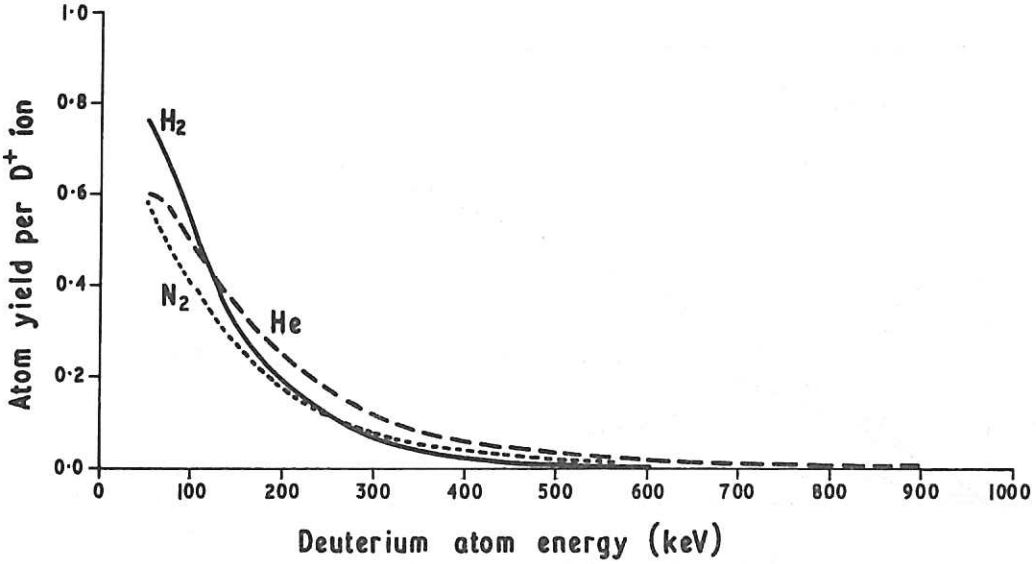

Fig. A3.1 Atom yield per incident D^+ ion for thick gas targets.

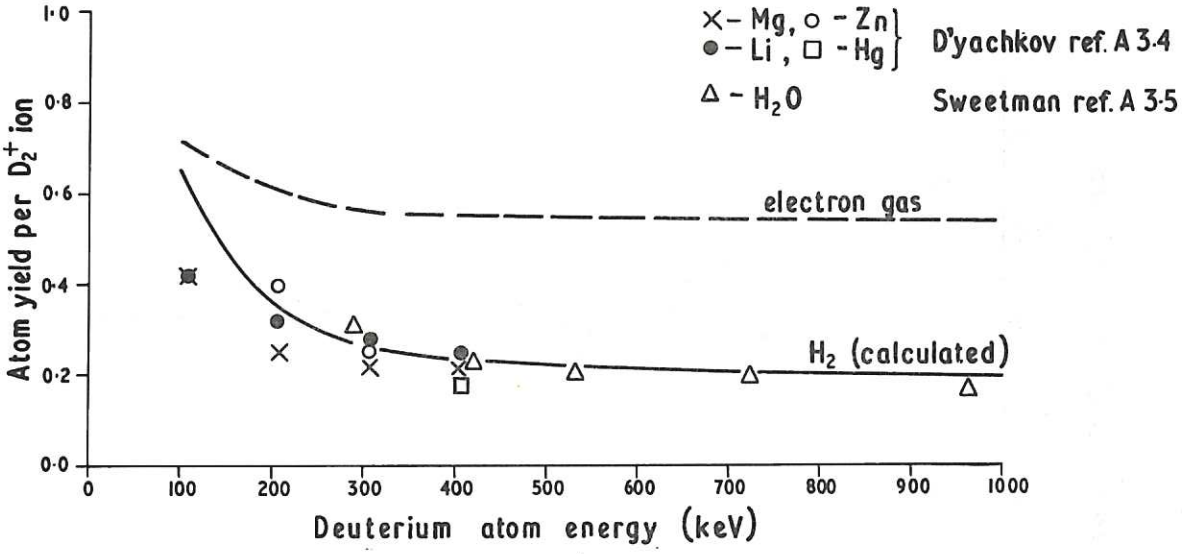

Fig. A3.2 Atom yield per incident D_2^+ ion for optimum target thickness.

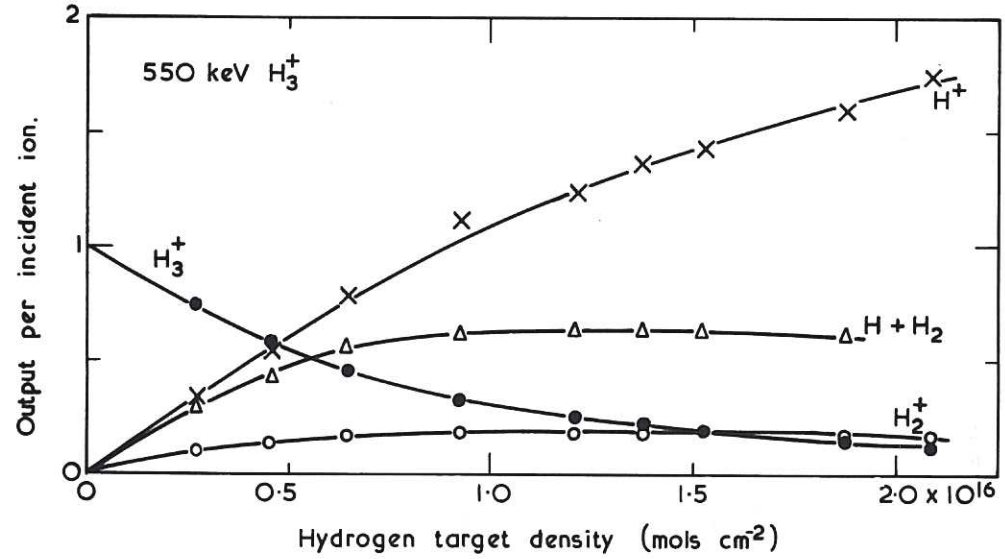

Fig. A3.3 Variation of atom yield per incident H_3^+ ion as a function of H_2 gas target thickness.

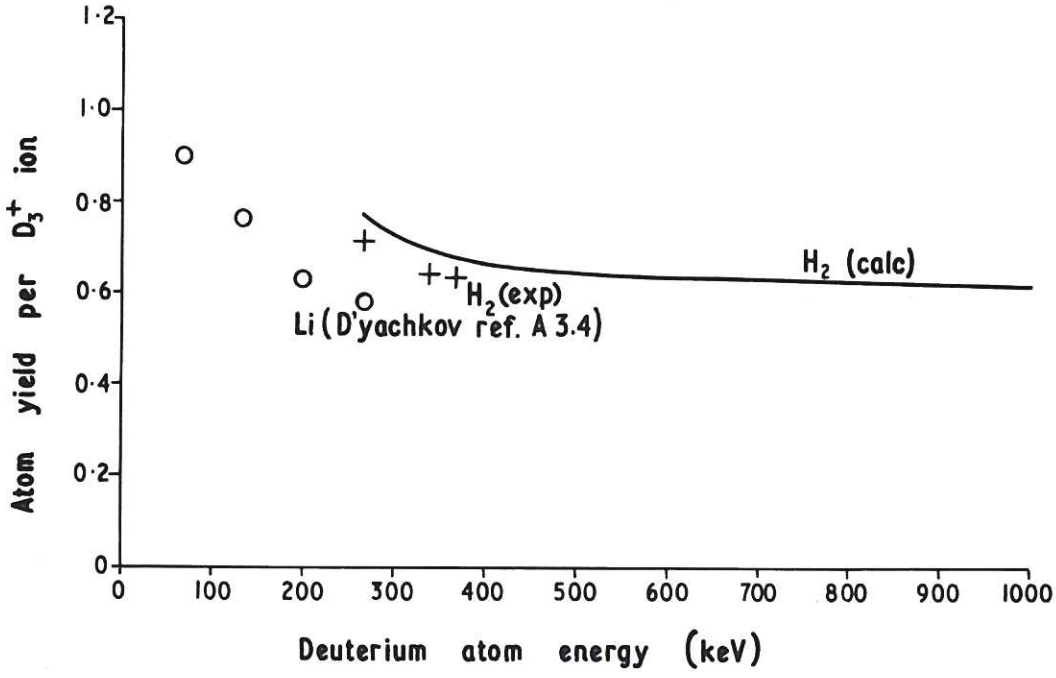

Fig. A3.4 Atom yield per incident D_3^+ ion for optimum target thickness.

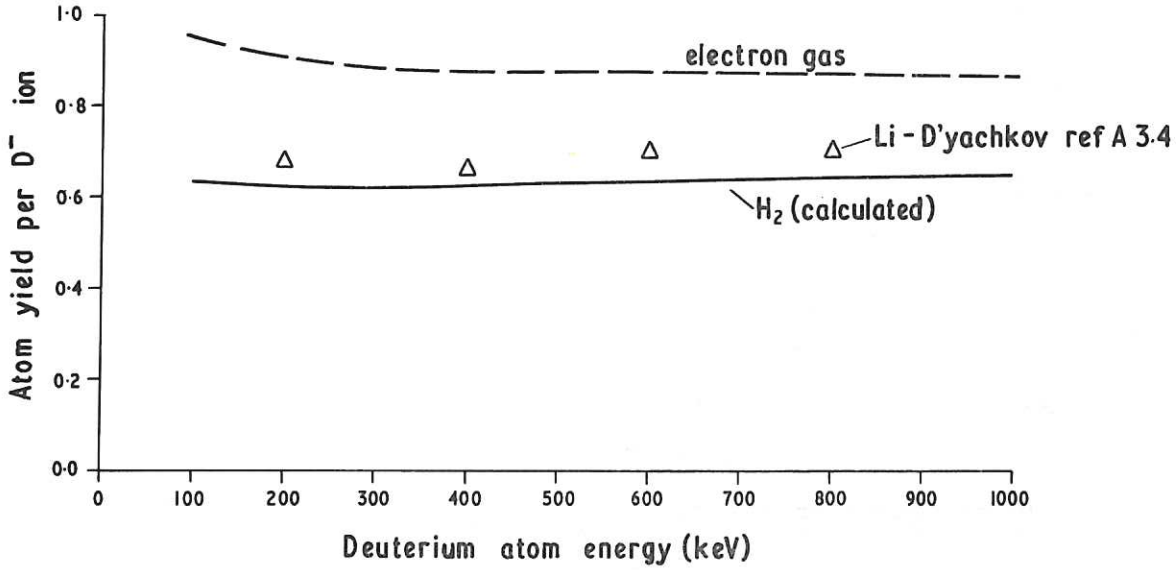

Fig. A3.5 Atom yield per incident D^- ion for optimum target thickness.

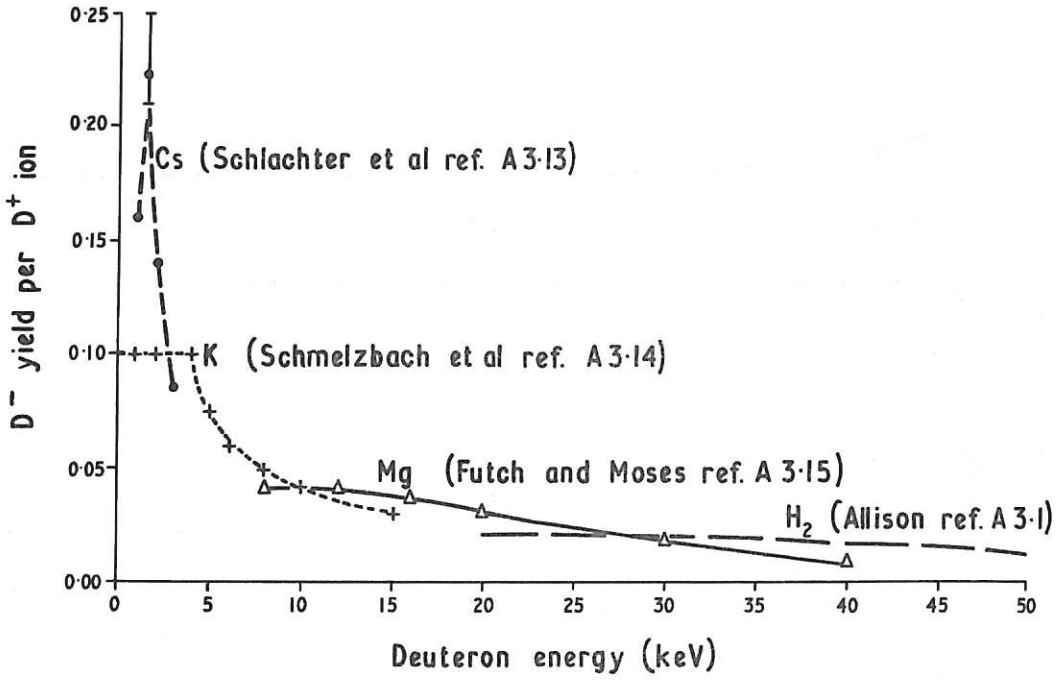

Fig. A3.6 D^- ion yield per incident D^+ ion for optimum target thickness.

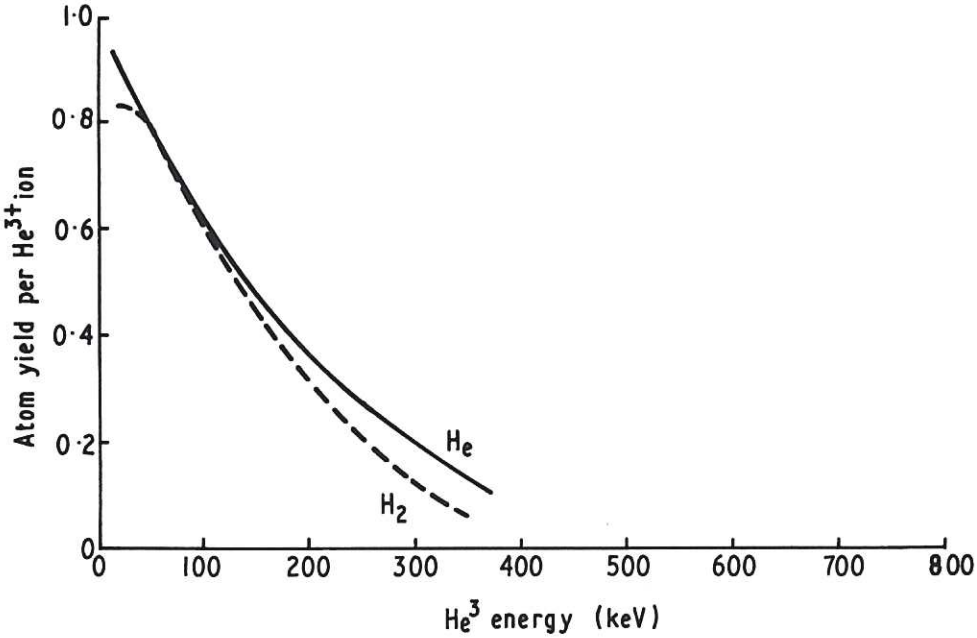

Fig. A3.7 Helium atom yield per incident He^{3+} ion for thick gas targets.

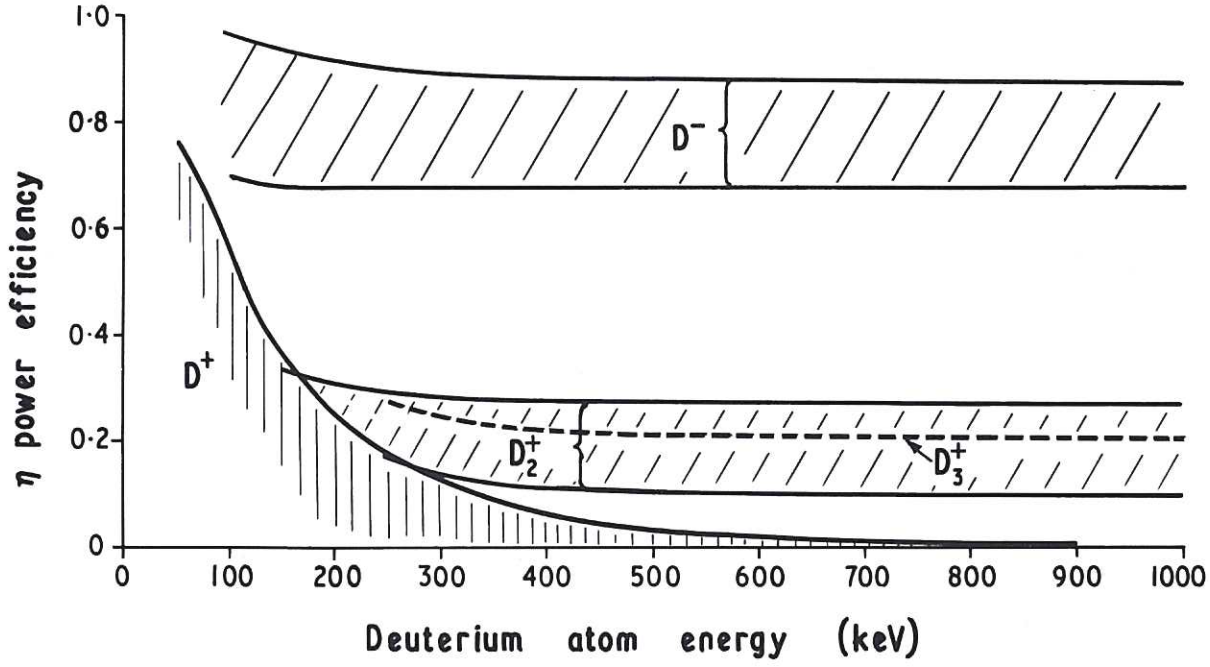

Fig. A3.8 Power efficiency for atom production from D_1^+, D_2^+, D_3^+ and D^- beams. Hatched area indicates variation with degree of ionisation of target. Ionisation reduces η for D^+ and increases η for D_2^+ and D^- ions.

ION SOURCE AND ACCELERATOR CONSIDERATIONS

D.P. Hammond and E. Thompson

The requirement considered is for a 10 A beam of D_3^+ with beam energy in the region 1 - 3 MeV. We discuss the problems of producing the required beam current and also the separate, but very closely related, problem of accelerating such a beam to the final required energy. Possible solutions are also put forward.

1. High Intensity Ion Sources and Their Possible Development for Reactor Injection

Introduction

There are two separate properties of ion sources which we should consider. Firstly, the equivalent electron perveance defined as

$$\mu_e = \left(\frac{M}{m} \right)^{\frac{1}{2}} \cdot \frac{I}{V^{3/2}}$$

where M is the ion mass, m the electron mass, I the total extracted current in amperes, and V the extraction potential in volts. The perveance is a geometrical figure of merit and, as defined above, comparison can be made between electron guns and ion sources, the values of μ_e obtained being similar for both devices, ($\simeq 10^{-6}$). The perveance determines the amount of beam obtainable at a given energy. The "optical quality" of this beam is measured by the second fundamental parameter, viz: the normalised emittance, defined as

$$\varepsilon_n = \frac{\beta\gamma}{\pi} \left[\begin{array}{c} \text{Area in phase space with coordinates of} \\ \text{beam radius and the ratio of radial to} \\ \text{axial momentum} \end{array} \right]$$

where $\beta = \frac{v}{c}$ and $\gamma = (1 - \beta^2)^{-\frac{1}{2}}$ where v is the ion velocity. This quantity is then an invariant of the beam, (excluding scattering) and is conserved throughout its motion(A4.1). A high quality beam has a low value of normalised emittance and this leads to a concept of normalised "brightness" defined as

$$b = \frac{2I}{\pi^2 \varepsilon_n^2} \qquad \text{(ref A4.2)} .$$

Examination of these parameters is the only real quantitative method of obtaining a comparison between different source systems. Unfortunately, these parameters are not always measured by experimenters (especially in the case of ribbon beams) and this leads to some confusion and ambiguity.

The definition of brightness given by Kelley(A4.3) may be used as a simple approximation to b in which case ε_n is replaced by the normalised acceptance of the stop system through which the beam must be transmitted. As such, this definition gives a lower limit to the real normalised brightness.

Types of Plasma Sources and Extraction Systems

The commonly used sources for high current beam production are

1. Duoplasmatron (in various versions)
2. R.F.
3. Calutron

using one of these extraction geometries

1. Modified Pierce
2. Grids
3. Calutron
4. Single or multiple disc apertures.

The most common grouping is a duoplasmatron coupled to a "modifed

Pierce" extraction geometry[A4.4,A4.5,A4.6]. Although not amenable to theoretical treatment, very high currents (0.5-1 A) of protons or molecular ions can be extracted from these systems, at extraction voltages up to 100 kV.

The R.F. sources used at CERN and RHEL have plane gridded extraction systems. This leads to very high perveance and also low emittance, as shown in Table II of the main report.

The calutron has been widely used and gives total extracted currents of the order of 1.0 A, and Golovin has reported a calutron giving 0.5 A of neutrals. The "ALICE" injector[A4.7] for example, has the following characteristics:

ENERGY	10 - 18 kV
EXTRACTED CURRENT	500 mA at 18 kV
μ	9×10^{-6} at 20 kV
	14.7×10^{-6} at 9 kV
EMITTING AREA	2.21 cm^2 (3" x 0.1" slit)
EXTRACTION GAP	1.5 cm
ION SPECIES	H^+

Although it gives large currents, we are of the opinion that the source is not well understood and is somewhat inflexible. It relies on anomalous diffusion across field lines in order to supply the plasma boundary and also has a low gas efficiency ($\sim$ 2 - 5%). Also one of the supposed advantages of side extraction across the magnetic field - that of "stiffening" the plasma boundary does appear to be obtained, since the perveance is observed to decrease at high energy. No measurements of emittance have been found, but the beam quality is not very high since the current transmitted through the ALICE injector (admittedly very restrictive) is $\sim$ 20% of the extracted current and it is not clear how the usable output can be increased.

The aperture disc system however is fairly well understood[A4.8,A4.9]. The theoretical perveance can be 6×10^{-6} or more and values of 4 or 5×10^{-6}

have been obtained by Hamilton et al.[A4.10]. At Culham we obtained $\mu = 1.9 \times 10^{-6}$ for focussed H_3^+ which represents about 60% of the total beam and similar values of μ appear to be obtained in space thrustor devices. The extraction gap for such a system determines the rest of the geometry for a given perveance, and for purposes of comparison with the calutron with an extraction gap of 1.5 mm as in the above example, we find by using three disc-aperture systems (to give the same emitting area as the calutron), we can expect the same output for a value of $\mu_e \sim 2.5$ per hole which in fact, refers to usable currents. We see then that in terms of total output, the calutron appears to have no advantage over the disc aperture system even using conservative values for μ_e. It is found experimentally that the emittance of a disc aperture is quite low (.07 rad.cm) but more work is needed to obtain a full relationship between perveance and emittance for various geometries.

The major problem to be resolved with multiaperture-disc systems is that of uniform illumination of a large array of extraction systems by a quiescent plasma of the required density and ion species. This problem is at least well defined and does not appear to be insurmountable. It is because the problems of plasma production are largely decoupled from those of ion extraction that we favour multiaperture (or multi slit) systems over the calutron as being the most promising method of obtaining high current ion beams suitable for reactor start-up.

Parameters for a 10 A Ion Source Using Multiple Apertures

Since the current per hole is solely determined by the perveance the number of apertures required for 10 A can be determined as a function of energy. The result of this trivial calculation for D_3^+ ions is shown in Fig. A4.1 where we have assumed $\mu_e = 3 \times 10^{-6}$.

Since the hole size is determined for a given extraction gap we can also calculate the current density at the emission surface as a function of

energy for any assumed variation of extraction gap with energy. Fig. A4.2 shows the current density if we assume that the extraction gap is limited by vacuum breakdown according to the relationship $V = k\, d^{\frac{1}{2}}$ where d is the gap and k a constant[A4.11]. This curve represents the smallest gap and hence highest current density attainable for the assumed value of μ_e; also shown is a curve which assumes that the gap is a factor of 5 greater than that for vacuum breakdown (comparable to our presently used values) and this of course results in a lower current density at the emitting surface. We also indicate on Fig. A4.2 the maximum value of emitted current density we have obtained experimentally for H_3^+ from a single aperture. Our preliminary measurements indicate that higher current, and hence ion densities, results in break-up of the molecular ion prior to extraction and this may set an upper limit to the maximum allowable current density at the plasma boundary. (If we assume that the molecular ion has thermal velocity, this limit corresponds to a density of H_3^+ of $\sim 10^{13}$ cm^{-3}).

Taking this limit we see that the extraction energy must be $\gtrsim$ 30-50 keV in which case we need to illuminate an area of some tens of cm^2 containing $\sim$ 50 apertures in order to obtain 10 amperes of ion current. It is important to note that the analysis <u>assumes</u> that the extraction gap scales as the square of the voltage as in vacuum breakdown - another scaling law would yield a different result but as long as the gap varies as V^n where $n > 0.4$ then the highest current densities are obtained at the lower extraction energies.

<u>Conclusion</u>

Experimental investigation into the scaling of the fundamental parameters of a single aperture extraction system to voltages higher than our presently used 15-25 keV, would appear to be the first step in assessing the validity of this approach to the production of a source capable of extrapolation to reactor injection conditions. Also, development of the existing single

aperture system to a multiple aperture system will form a complementary program which could also be of great benefit to present and planned injection experiments.

2. Accelerating Systems for High Current Injection

Introduction

Some of the highest current injectors of the present time are found in high energy nuclear physics and a review of some parameters of typical existing devices are given in Table II of the main body of this report. Generally the beam brightness falls as the total current is increased presumably due to space charge[A4.12,A4.13,A4.14].

Some of these pre-injector accelerating stacks are worthy of study in our present context. The existing CERN machine[A4.15] accelerates 100 mA to 540 kV across 12.6 cm, and a tube to accelerate, eventually, the full 500 mA output of the ion source to 1.4 MeV has been constructed and tested in the absence of beam[A4.16]. A total voltage of over 1 MV has been sustained across 6 cm. This extremely high performance is attributed to the use of polished titanium electrodes and very clean vacuum conditions. The source is pulsed for 50 μsec bursts approximately. Fig. A4.3 shows the arrangement of the existing CERN device, and Fig. A4.4 shows the equipotentials and beam trajectories in the central region. The advantages of this type of accelerator tube for high current acceleration are very marked. Because the beam sees only one gap, loading due to electron multiplication is significantly decreased. Because of the short column length, both the gas ionization and space charge expansion are reduced - and, demonstrably, the optics are extremely favourable. The normalised emittance for this device of 6×10^{-1} cm mrad has to be compared with say, the admittance of the largest port which can be allowed through the field coils of a plasma trap or, ultimately, the blanket of a reactor. For example, the normalised acceptance of a tube 10 cm in diameter and 2 metres long is 7.3 cm mrad at 1 MeV. The Los Alamos MPF injector[A4.17].

uses a Pierce type accelerating tube of interesting design, with a planned final gradient of 40 kV/cm. The DCX 2 machine at Oak Ridge has for some years been used with an injector of H_2^+ ions operating at 600 keV. In this case, the accleration is accomplished over 45 cm and the operation is D.C. Of an extracted 300 mA, 50 mA is actually injected(A4.18), but no figure for normalised emittance is available.

In the nuclear physics field, demands for higher injected currents for experiments like the CERN storage rings, the study of low yield nuclear reactions and isotope production, have met a barrier due to space charge effects in the circular machines. At some critical density, the space charge field of the beam has been found to modify the focussing properties of the guide field and certain instabilities are excited,(A4.19). One machine, the CERN Booster Injector, overcomes this problem by maintaining four beams in separate orbits until the energy has been increased above the level at which space charge effects are significant in the main ring. In general, the peak current of circular machines is of the order of a few tens of milliamperes, but the normalized brightness and peak power levels can be very high (Fig. A4.9).

Thus, the provision of an accelerator to handle currents like 10 amperes at energies of 1-3 MeV represents a significant technological advance, but interest is strong in fields other than fusion. A dominant factor influencing the design will be the effect of space charge. The design may attempt to use space charge as a major focussing force or the space charge interactions may be minimised by the use of a short high gradient column(A4.15), with possibly sub-division of the beam at low energy. The space charge may by modified by externally applied fields, either electrostatic, as in Pierce geometry, or magnetic as in Brillouin flow.

Beam Profiles

A. Space charge dominated profile

The problem of an ideal beam expanding under the action of space charge forces during acceleration has been treated, with some approximations, by

C. Moak[A4.20]. Fig. A4.5 shows the profile obtained by this calculation for a 10 amp D_3^+ beam, being accelerated up to 1 MeV. Some typical values have been assigned to the final beam radius, and the tube length. Intensity contours at 50% and 25% are shown, (calculation assumes uniform current density throughout and zero divergence at the beam waist). The injection angle at the beam edge for the case shown is as much as 55°, but this figure is sensitive to the field gradient and the assumed final radius. Tangents drawn to the three curves at the injection energy converge at a point inside the accelerator, emphasizing that this treatment is valid only for a zero emittance source system. In practice a finite input velocity - space spread will cause some divergence at the tube exit, and may make it necessary to use a high energy lens, e.g. a magnetic quadrupole.

In addition to the space charge forces, the beam will be influenced by the lens action at the tube input and exit and by the focussing action of the tube itself. This effect is well known, and is treated by Elkind[A4.21]. Analysis of the optics of the system of Fig. A4.5 by this method shows that, with the virtual object presented by the injection scheme, the tube focussing forces have very little effect in this case.

For the case shown, the beam current density increased some ten times over the flight path, from 13 mA/cm^2 at 50 kV to 127 mA/cm^2 at the tube exit. From present sources, beams of the order of 100 mA can be extracted from a single aperture of 0.5 cm diameter[A4.8,A4.9,A4.10], so the necessary input current density could be achieved by clustering sources of this type on a mesh size of 2.7 cm spacing.

The beam profile, being space-charge dominated, will be sensitive to neutralisation due to electrons in the beam. It can be shown that, due to the high field gradients, electrons produced by ionization of background gas or by secondary emission are so rapidly removed that their contribution to the total space charge is negligible.

In general, the electrons will have a more serious effect by loading the power supply, with consequently poor efficiency and high radiation levels. In Fig. A4.6 is shown a simplified scheme of some processes leading to electron loading in an accelerator tube. From the viewpoint of total load, electrons produced directly from a process involving one or more ionization cross-sections will be insignificant. ($n_o v \ell = 10^{11} \times 10^{-16} \times 10^{2} = 10^{-3}$ for some typical numbers.) Loading caused by secondary emission can be a more serious problem, being determined by $\delta e \times M$, where δe is the secondary emission coefficient for electrons and will be in the range 1 - 10, and M is the multiplication due to the electrode geometry.

In modern Van der Graaf ion accelerators the number of electrons (and their average energy) is greatly reduced by inclining the tube electrodes, so that secondary electrons are accelerated with a significant radial component of velocity and strike subsequent electrodes at some radial distance from the aperture(A4.22). The chance of further secondaries then being accelerated is small. Similarly the CERN accelerator has tilted electrodes, and in this case the electrodes are also remote from the beam envelope, although no quantitative information on tube loading is available in this case.

B. <u>The separated trajectory accelerator</u>

The principal disadvantages of the scheme outlined under 'A' are:

(1) The analysis(A4.21) is approximate and at most valid only for the case of a zero emittance source and a long beam path. In this case, Liouville's theorem does not apply and the trajectory transformation of Fig. A4.5 is unreliable. The case of a beam expanding under the combined influence of space charge and finite emittance has been studied by Walsh (A4.23,A4.24) and Starling (A4.25), and for practical values of emittance found in existing sources, the modification to Moak's treatment can be significant.

(2) Due to the reliance on space charge, the design, e.g. the distribution of the sources, is inflexible and applies to one current and voltage only.

These objections are somewhat reduced if the system is sub-divided not only as far as the plasma boundary in the ion source, but so that the identity

of separate pencils of rays is maintained until the energy has increased to the point at which space charge forces are becoming negligible. Each pencil, or group of pencils, of rays can be electrostaticlly shielded from its neighbours over the sensitive low energy region. By this means the optics of each group of rays can be arranged to take advantage of the focussing action of an accelerator when given a real object distance, the actual magnitude of which can be controlled by a focus electrode in the usual way. Each pencil will be subjected to symmetrical distortion of its envelope by space charge, but as the trajectories are considered to be diverging on injection, the overall effect will be to shorten the object distance. Adjustment of the focussing field to compensate should be possible. The subdivision could be accomplished in a number of ways, e.g. 100 apertures at 100 mA/aperture, as one extreme, or preferably, something like 10 groups of a total of 1 A each.

To demonstrate the benefit of this system, curves are given (Figs. A4.7 and A4.8) of a 100 mA beam expanding in free space and a 1 A beam being accelerated to 200 keV at which point it is visualised that it would begin to mix with the other beams.

Conclusions

The approach to the problem of the 10 A multi-MeV beam should concentrate initially on the effect of space charge on the beam while it is at low energy prior to and during the initial stages of acceleration. No complete theory for the effect of space charge on finite emittance sources is known, but a great deal could be done by studying the optics of a small cluster of sources, extracting at low energy and accelerating to ~ 100 keV. The mechanics of "blending" low current units to make the final beam require some investigation at this stage. Studies of the very important features of loading and beam profile at this energy would be essential before proceeding to a further stage. At the same time, the problem of miniaturization of the

ion source could be tackled in order to 'cluster' the sources at the required input density.

Should a negative ion source become a practical proposition, it is expected that beam loading effects could be troublesome, due to the fact that electrons produced by ionization while the beam is at low energy will now tend to be accelerated the full length of the tube. This effect is observed in Van der Graaf tandem accelerators where, in the case of unsuppressed tubes, a few microamperes of negative ions produce as much radiation as hundreds of microamperes in positive ion machines.

In general, the feasibility of a 10 A MeV injector is summarised by Fig. A4.9. Here, parameters of known devices are plotted in terms of brightness against peak power. The values of existing injectors lie to the left of the figure. The target point is also shown.

References

(A4.1) Judd, D., Annual Review of Nuclear Science, vol. 8, p.181 at seq.

(A4.2) Septier, A, Focussing of Charged Particles, p.123 et seq. Academic Press, New York, 1957.

(A4.3) Kelley, G., IEEE Trans. Nucl. Sci., vol. 14, 1967, p.29.

(A4.4) Kelley, G., et al., Nucl. Inst. Methods, vol. 10, 1961, p.263.

(A4.5) Poroshin U.F. and Kutan, Z.H., Formation and investigation of intense hydrogen ion beams. Culham Laboratory, Translation, CTO/115, 1964.

(A4.6) Rose, P., Nucl. Inst. Methods, vol. 28, 1964, p.146.

(A4.7) Gordon, F. and Damm, C., Rev. Sci. Instrum., vol.34, no.9, September 1963, pp. 963-970.

(A4.8) Harrison, E., J. App. Phys., vol. 29, no.6, June 1958, pp. 909-913.

(A4.9) Coupland, J. and Thompson, E., The production of high current, high quality beams of ions and neutral particles. Culham Laboratory Preprint. CLM-P 251, 1970.

(A4.10) Hamilton, G., Hilton, J.L. and Luce, J.S., Plasma Phys., vol.10, no. 7, July 1968, pp. 687-697.

(A4.11) Hawley, R., Vacuum, Vol. 10, 1960, p.310.

(A4.12) Sluyters, IEEE Trans. Nucl. Science, vol. NS-16, no.3, 1969, p.29.

(A4.13) Wroe, H., Nucl. Inst. and Methods, vol. 58, 1968, p.213.

(A4.14) Coupland, J. Private communication.

(A4.15) Huguenin, J., et al. Proceedings of the 1966 Linear Accelerator Conference, Los Alamos, October 1966. Los Alamos Scientific Laboratory report LA-3609. pp. 355-364.

(A4.16) CERN Courier, vol.10, no.3, March 1970, pp. 82-83.

(A4.17) Emigh et al. IEEE Trans. Nucl. Science, vol. NS-16, no.3, 1969, p.46.

(A4.18) Kelley, G.G., Lazar, N.H. and Morgan, O.B., Nucl. Inst. and Methods, vol. 10, no.4, April 1961, pp. 263-271.

(A4.19) Martin et al. IEEE Trans. Nucl. Science, vol.NS-16, no.3, 1969, p.479.

(A4.20) Moak, C., AERE Harwell, report R-3255, 1960.

(A4.21) Elkind, Rev. Sci. Instrum., vol.24, no.2, 1953, p.129.

(A4.22) Pyrsen, K., et al., Rev.Sci.Instrum., vol.36, no.4, 1965, p.453.

(A4.23) Walsh, T.R., Plasma Phys. (J. Nucl. Energy, Part C), vol.4, 1962, pp. 53-54.

(A4.24) Walsh, T.R., Plasma Phys., (J. Nucl. Energy, Part C), vol. 5, 1963, pp. 17-22.

(A4.25) Starling, P.P., Plasma Phys., (J. Nucl. Energy, Part C), vol. 6, 1964, pp. 405-407.

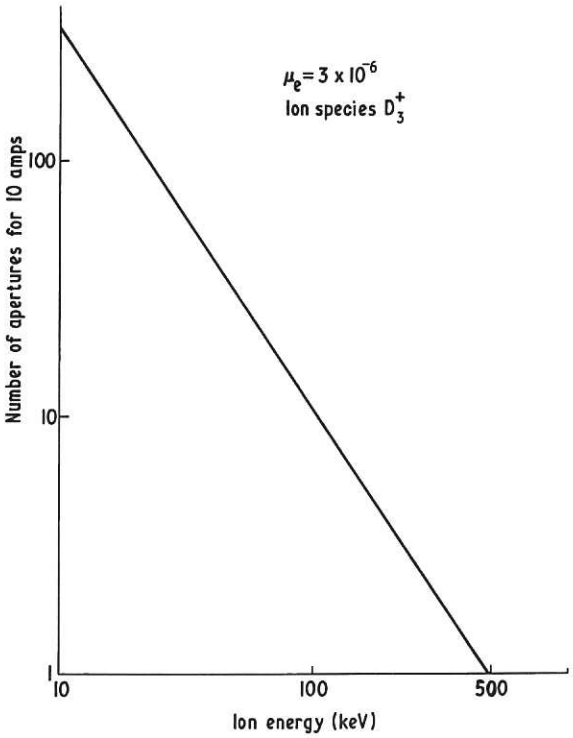

Fig. A4.1 Performance of multi-aperture source. No. of apertures vs. ion energy.

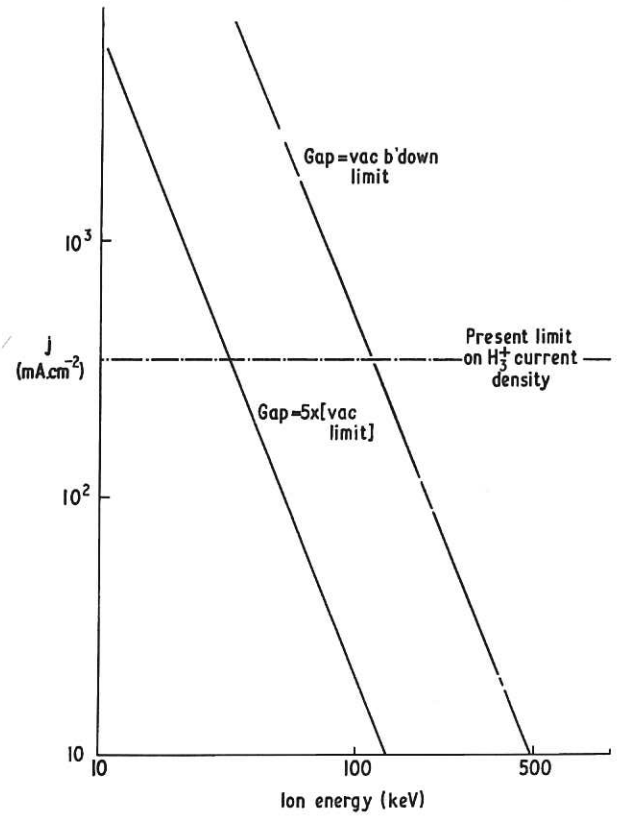

Fig. A4.2 Performance of multi-aperture source. Current density vs. ion energy.

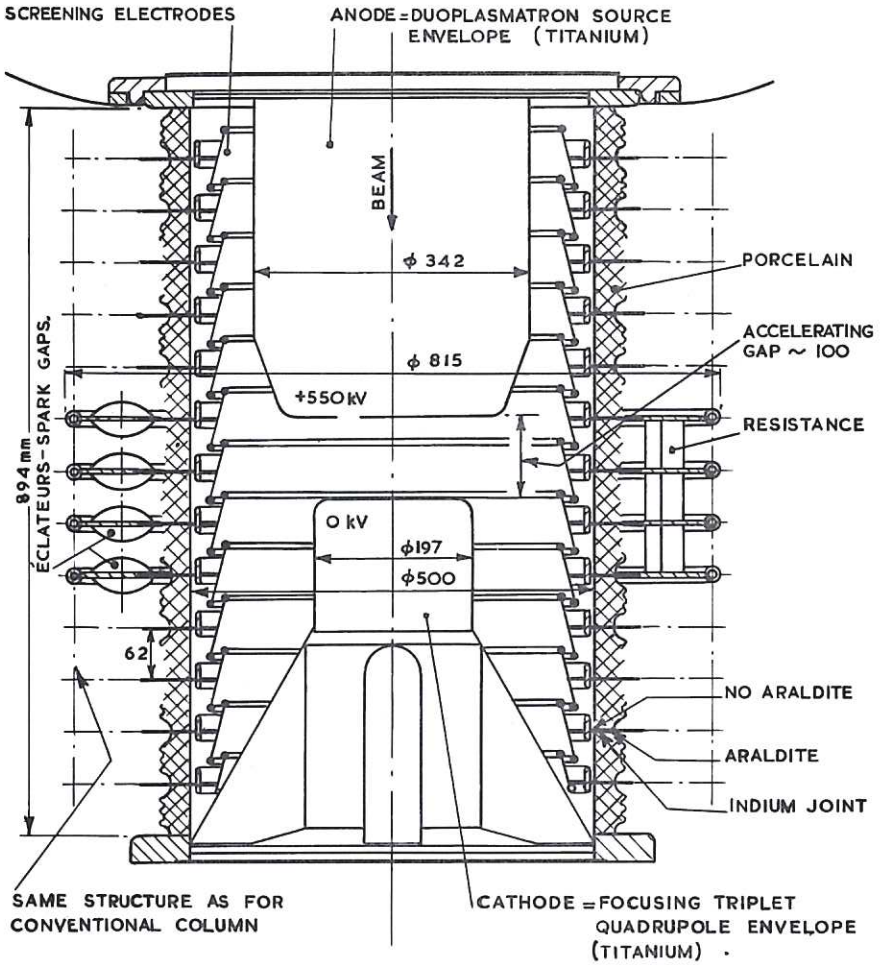

Fig. A4.3 Air at Atmospheric Pressure - Schematic drawing.
(Reproduced by permission of CERN).

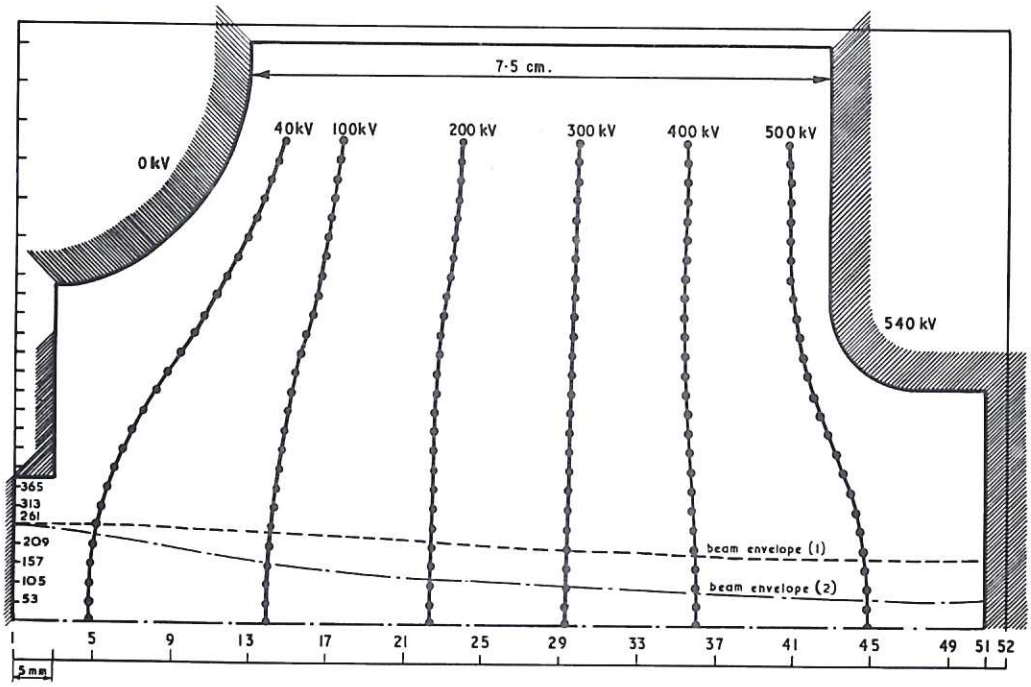

Fig. A4.4 Potential field of the Duoplasmatron and Short Column.
(Reproduced by permission of CERN).

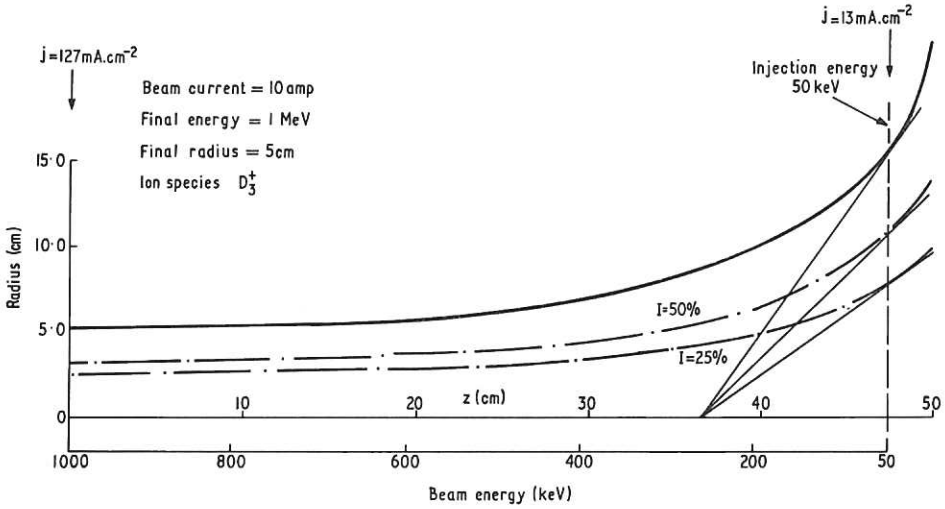

Fig. A4.5 Beam profile under uniform acceleration.

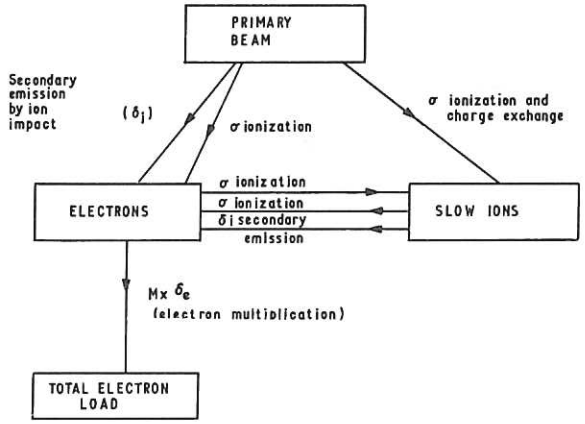

Fig. A4.6 Processes leading to electron loading.

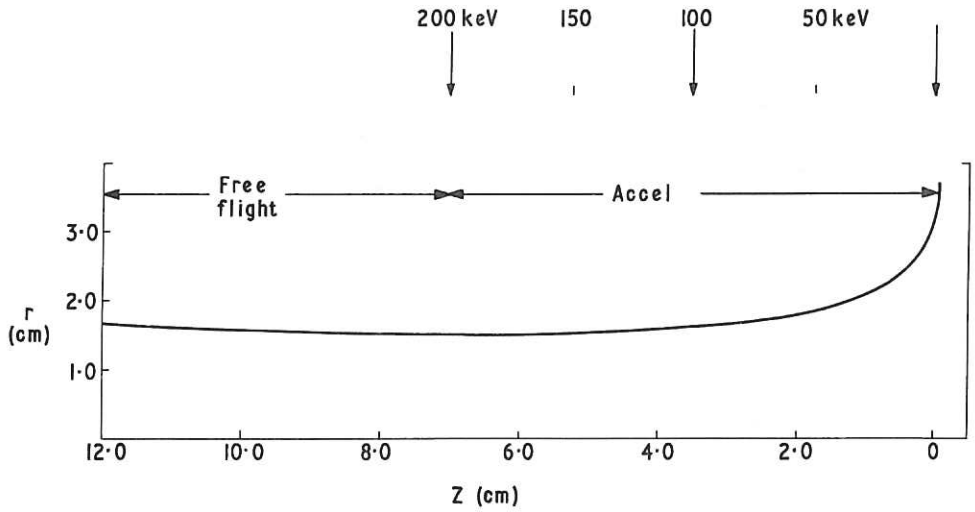

Fig. A4.7 Separated orbit 1 amp 200 keV.

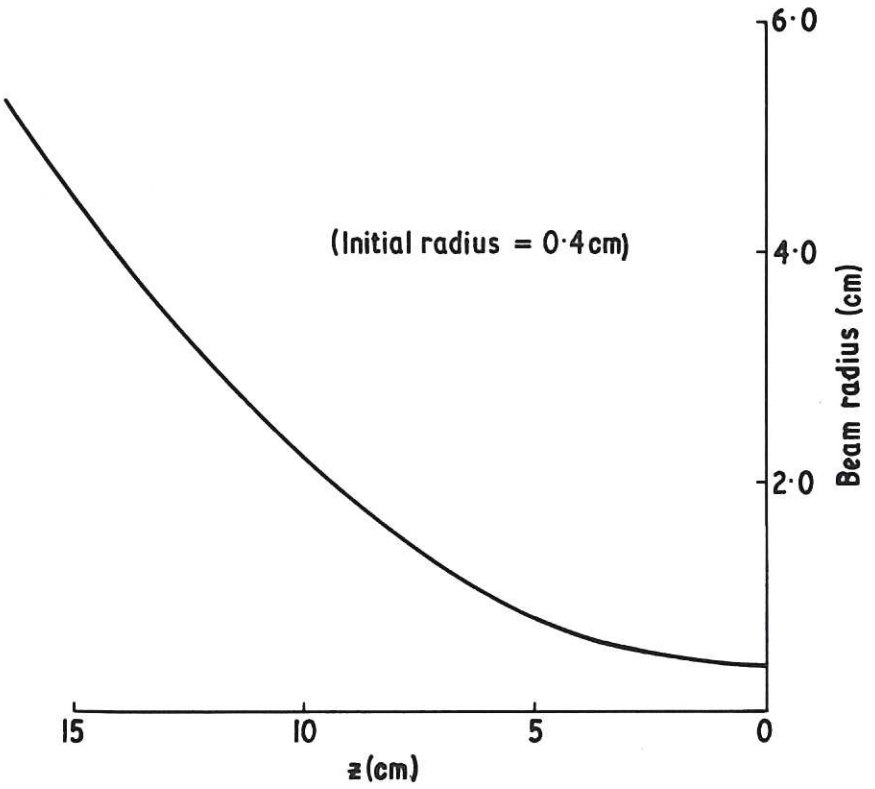

Fig. A4.8 Beam profile of 100 mA 50 keV beam due to space charge.

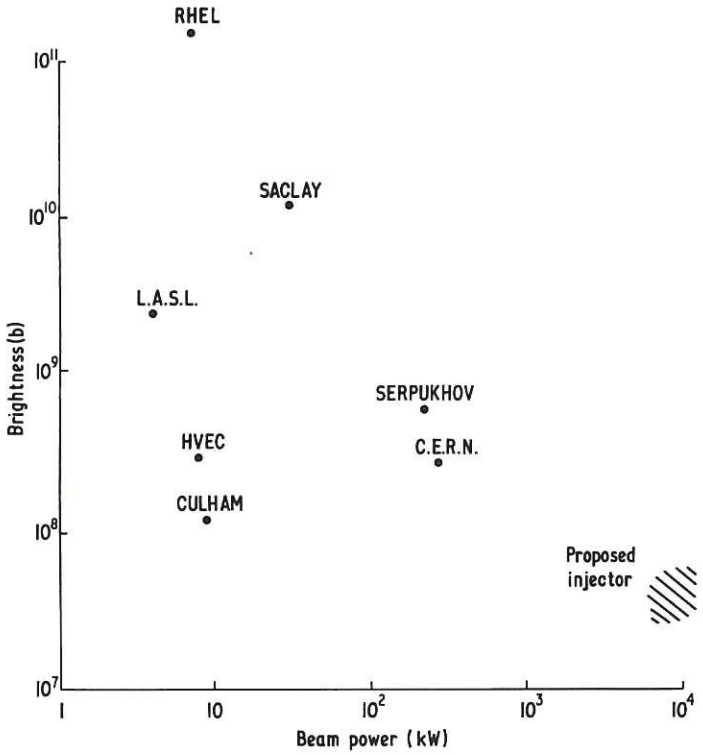

Fig. A4.9 Performance of existing injector systems.

APPENDIX 5

PLASMA HEATING BY NEUTRAL INJECTION IN A STELLARATOR REACTOR USING A HALL ACCELERATOR

by

H.C. Cole

1. Introduction

A fusion reactor can be started, in principle, by injecting plasma at the required operating density and temperature. However, it has been shown[A5.1] that this is unlikely to be a viable proposition because of the power loading at the point of injection, and fundamental difficulties associated with the injection process itself.

Neutral injection, however, offers considerably more promise, particularly if it is considered as a means of heating an existing cool plasma.

This paper discusses the use of a Hall type accelerator to produce the primary beam of ions from which the neutral atoms are produced by charge exchange before injection into the reactor.

As discussed elsewhere, the total beam requirements before neutralization are ~ 75 A of D_2^+ at 2 MeV in order to provide 30 MW for our standard reactor.

2. Hall Accelerator Characteristics

An experimental Hall accelerator is shown in Fig. A5.1. This is similar to that described in[A5.1] and [A5.2] and operates in the same manner. These experiments showed that output plasma beams of $\sim$ 500 A equivalent could be obtained at energies of a few keV. More recent experiments have shown that the efficiency of the accelerator can be increased from the earlier figure of $\sim 16\%$ [A5.1] and [A5.2] to values $> 60\%$. This means that plasma flows in excess of $\sim$ 1500 A equivalent can now be obtained. The Hall accelerator is therefore clearly capable of producing the required beam current. However, the problem of scaling up to potential

differences of ~ 2 MV remains.

There are two results which indicate that such a scaling may be possible. Firstly, the electric field in the accelerator is, to a first approximation, directly proportional to the magnitude of the radial magnetic field, particularly at low current densities, and secondly, the electric field increases as the current density is reduced. The latter result is illustrated in Fig. A5.2 which shows the electric field in volts/cm/kG as a function of the current density. It should be noted that when the current density is ~ 1 A/cm^2 the electric field is ~ 1 kV/cm/kG.

3. The 2 MV Accelerator

If we assume that the above results are still valid at magnetic fields of 10 kG it should be possible to achieve electric fields of ~ 10 kV/cm. The total effective stage length then required for a 2 MV accelerator would be ~ 200 cm. However, if the field is set up using an iron cored system the overall length would need to be increased to ~ 400 cm in order to accommodate the magnetizing winding. A possible arrangement of the iron cores for a 1 MV accelerator is shown in Fig. A5.3. A 2 MV accelerator would require the addition of a further five 20 cm stages. The initial stages are made shorter in order to avoid ion trapping at the lower energies. Output collimation is improved by using equal stages over most of the accelerator as the ratio of Larmor radius to stage length then decreases as the ions are accelerated.

The efficiency of an accelerator with sixteen stages is not known at present. However, for a given cross-section the wall area is proportional to the length, so for similar operating conditions it is reasonable to suppose that efficiency will decrease with increasing length. It is proposed , therefore, that a further increase in magnitude of radial magnetic field coupled with a corresponding reduction in length is desirable.

This cannot easily be done using an iron cored system, but by discarding cores altogether and constructing a system using superconducting coils, it should

be possible to reduce the overall length to less than 2 metres.

Problems that have not yet been considered include the breakup of D_2^+ ions during the acceleration and the vacuum criteria imposed by wall loading in the accelerator.

It should be pointed out that the Hall accelerator might be particularly valuable if consideration of particle drifts in the reactor allowed injection at an energy well below the 1 MeV assumed above.

References

(A5.1) Cole, H.C. Hall accelerators in fusion research. Proc. of the B.N.E.S. Conference on Nuclear Fusion Reactors, Culham Laboratory, September 1969, (British Nuclear Energy Society, 1970). Paper 5.6.

(A5.2) Cole, H.C. A high current hall accelerator. Nuclear Fusion, vol.10, no.3, September 1970, pp. 271-275.

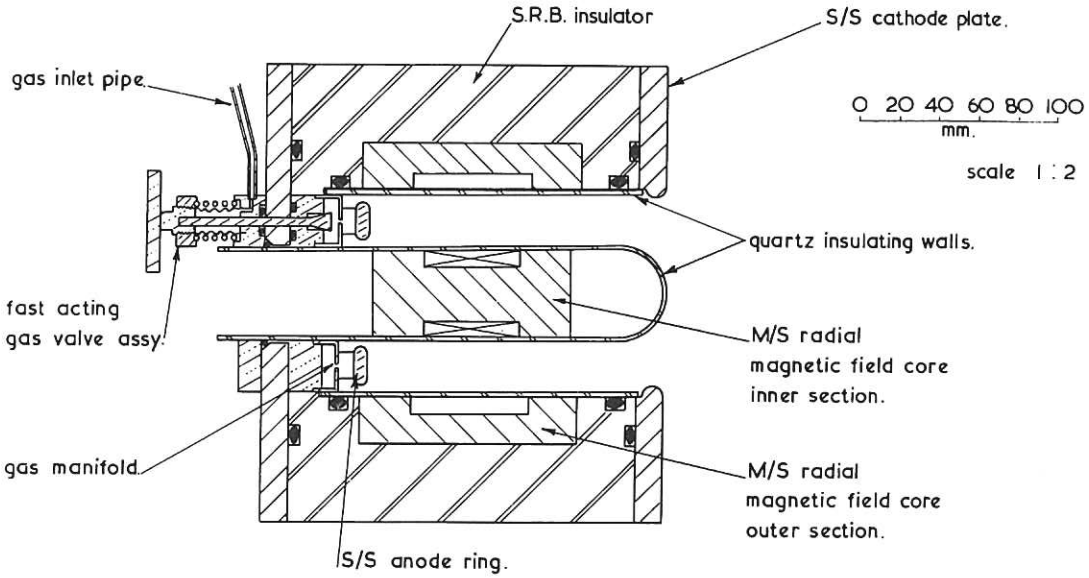

Fig. A5.1 Experimental high current Hall acceleration.

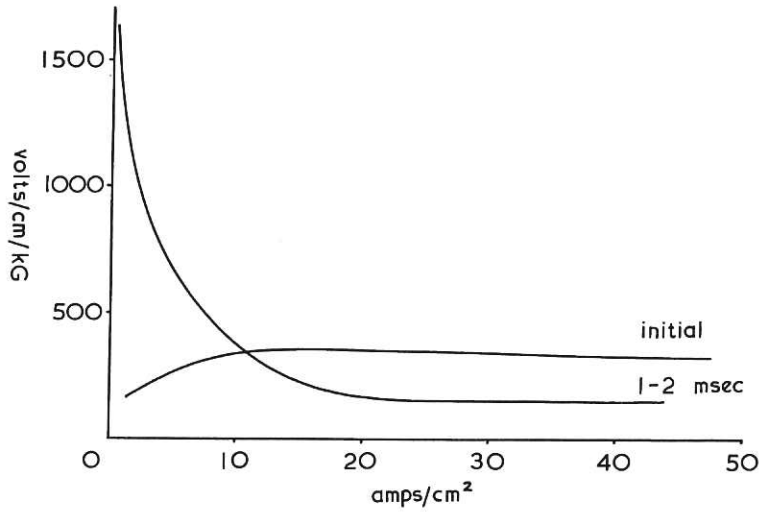

Fig. A5.2 Electric field variation with current density in experimental Hall accelerator.

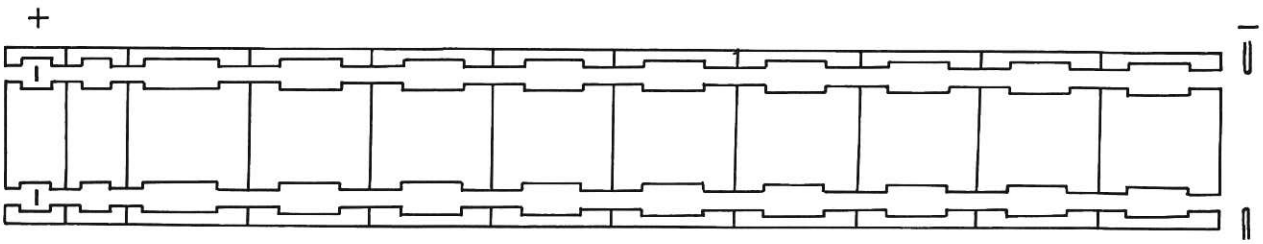

Fig. A5.3 Core assembly for a 1 MV accelerator (5 more stages required for a 2 MV accelerator)

PUMPING REQUIREMENTS OF NEUTRAL INJECTORS

G.M. McCracken

1. General Considerations

There are two main gas sources in the neutral particle injectors, firstly the neutral gas flow from the ion source and, secondly, the gas resulting from those ions which are not neutralized in the charge exchange cell. In addition there is the possibility of ions being dissociated or charge exchanged on the residual gas in the system, and the probability of this happening will obviously be greatest near the ion source where the pressure is high. Although at first glance it might seem that these neutrals resulting from dissociation on the background gas could be used, it seems impractical to accelerate them sufficiently before they are neutralised.

The relation between the gas flow and the ion currents in the various parts of the system are shown schematically below.

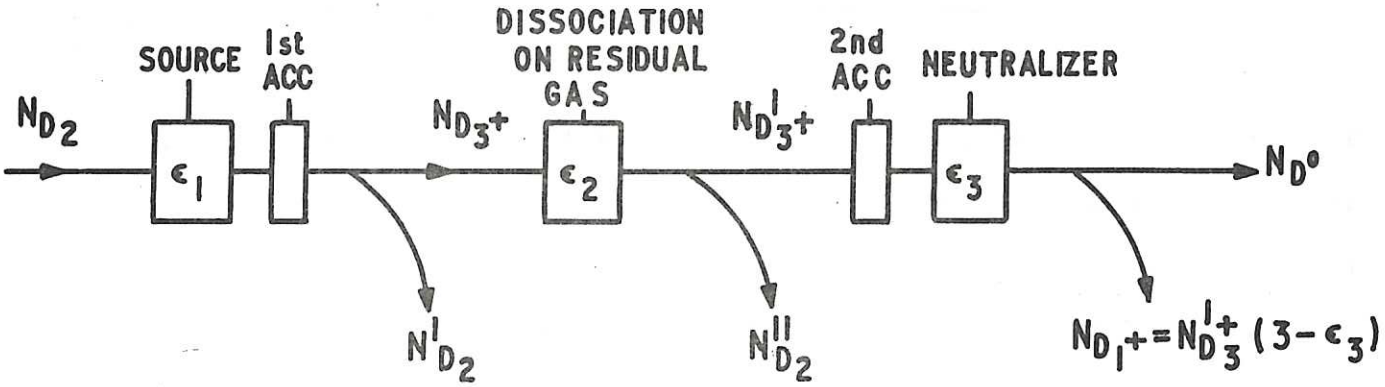

The N's define the flow in number of particles/second and the efficiencies, ε_1, ε_2, ε_3 are defined as follows:-

The gas efficiency of the source $\varepsilon_1 = \frac{3}{2} \frac{N_{D_3^+}}{N_{D_2}}$.

The factor $\frac{3}{2}$ has been introduced so that ε_1 will be 1.0 when all gas molecules are converted to D_3^+ ions.

The efficiency of transmission through residual gas $\varepsilon_2 = \frac{N'_{D_3^+}}{N_{D_3^+}}$.

The efficiency of the neutralizer $\varepsilon_3 = \frac{N_{D^o}}{N'_{D_3^+}}$.

It is to be noted that the total charged particle flux from the neutralizer, i.e. D_1^+, D_2^+, D_3^+ has been put in terms of its D_1^+ equivalent flux. It is convenient to write all gas flows in terms of the defined neutral output of the injector, thus -

$$N'_{D_2} = \frac{1}{2}\left(2N_{D_2} - 3N_{D_3^+}\right) \qquad N_{D_1^+} = N'_{D_3^+}\,(3 - \varepsilon_3)$$

$$= \frac{3}{2} N_{D_3^+}\left(\frac{1}{\varepsilon_1} - 1\right) \qquad = \frac{N_{D^o}\,(3 - \varepsilon_3)}{\varepsilon_3}$$

$$= \frac{\frac{3}{2} N_{D^o}\left(\frac{1}{\varepsilon_1} - 1\right)}{\varepsilon_2\,\varepsilon_3} \quad \cdots (A6.1) \qquad = N_{D^o}\left(\frac{3}{\varepsilon_3} - 1\right) \quad \cdots (A6.2)$$

The value of ε_2 depends on ε_1 since the probability of ions dissociating on the background gas depends on how much gas comes out of the source. Even in the case where one has a pump with unity sticking coefficient on the walls, dissociation can take place on gas streaming from the source.

The density of the gas immediately outside the source will be given by:-

$$n_o = \frac{N'_{D_2}}{Av} = \frac{\frac{3}{2} N_{D^o}\left(\frac{1}{\varepsilon_1} - 1\right)}{Av\,\varepsilon_2\,\varepsilon_3} \qquad \cdots (A6.3)$$

where v is the gas velocity and A the total area of the source. The density will decrease as the beam moves away from the source (although the decrease will be small within a distance comparable with the dimensions of the source). Let us assume that the beam travels an equivalent distance d in a density n_o

(i.e. $d = \int n(r)dr/n_o$). But we know that ε_2 is determined by n_o and d from

$$\sigma_T \, n_o d = 1 - \varepsilon_2 \qquad \ldots (A6.4)$$

where σ_T is the sum of the cross sections for all reactions leading to dissociation. Thus from (A6.3) we have:-

$$\frac{A}{d} = \frac{\frac{3}{2} \sigma_T \left(\frac{1}{\varepsilon_1} - 1\right) N_D o}{v \, (1 - \varepsilon_2) \, \varepsilon_2 \, \varepsilon_3} \, . \qquad \ldots (A6.5)$$

But the current density of D_3^+ at the source is given by

$$J_{D_3^+} = \frac{eN_D o}{A \varepsilon_2 \varepsilon_3} \, . \qquad \ldots (A6.6)$$

If we assume a circular source and that the equivalent path length in the gas is proportional to the diameter of the source D, (i.e. $d = fD$), then using (A6.5) and (A6.6) we obtain

$$J_{D_3^+} = \frac{\pi \varepsilon_2 \varepsilon_3 \, ev^2 \, (1 - \varepsilon_2)^2}{9 \sigma_T^2 \left(\frac{1}{\varepsilon_1} - 1\right)^2 N_D o \, f^2} \, . \qquad \ldots (A6.7)$$

The gas velocity v is calculated assuming deuterium gas at 300^oK, σ_T is estimated from McClure's data[A6.1] to be 6.8×10^{-16} cm^2 at 50 keV, and a value of $\varepsilon_3 = 0.6$ for 3 MeV D_3^+ is taken from Appendix 3, hence

$$J_{D_3^+} = \frac{213}{f^2 I_o} \, \varepsilon_2 \, (1 - \varepsilon_2)^2 \left(\frac{\varepsilon_1}{1 - \varepsilon_2} \right)^2 \qquad \ldots (A6.8)$$

where I_o is the equivalent current of neutrals.

If we now specify $\varepsilon_2 \geq 0.95$ in order to minimize beam loss, take $\varepsilon_1 = 0.5$, $f = 1.0$ and $I_o = 10$ A we have $J_{D_3^+} \leq 50$ mA/cm^2. As we allow ε_2 to decrease $J_{D_3^+}$ increases and $N_D o$ increases but the ratio $N_D o / J_{D_3^+}$ decreases, as

is obvious from equation (A6.6), thus making less efficient use of the ions produced.

Using equation (A6.5) the source diameter has been calculated as a function of gas efficiency ε_1 for some values of ε_2 (Fig.A6.1) It is clear that if ε_2 is relaxed to 0.9 the current density limitation is not a serious one for a 10 A neutral beam. If the limitation was serious, as for a larger current source, then by using a slit source rather than a circular one it should be possible to reduce the effective path length in the streaming gas. The value of d will obviously depend markedly on how directional the gas flow from the source is and therefore on the details of the extraction system design.

2.1 Pumping of source gas

Now consider the gas coming out of the source. After it has streamed out initially, it must be rapidly pumped so that the residual gas pressure in the chamber outside the source makes a very small contribution to reducing ε_2. Let us consider the criterion.

$$\sigma_T \, n_o' \, d' = (1 - \varepsilon_2) = 0.02 \qquad \cdots (A6.9)$$

where n_o' is the contribution to n_o from the background gas. If we assume the chamber length d' is 100 cm

$$n_o' = 3 \times 10^{11} \text{ moles/cm}^3 \simeq 10^{-5} \text{ torr pressure}.$$

If conventional pumps are used, or even using cryopumping panels with radiation shields, the effective capture coefficient over the pump surface is $\simeq 0.2$. Thus an equivalent pumping speed of $31 \times 0.2 \; \ell \; s^{-1} \; cm^{-2}$ is obtained for deuterium. Now the gas flux obtained from equation (A6.1) taking $\varepsilon_1 = 0.5$, $\varepsilon_2 = 0.95$, $\varepsilon_3 = 0.6$ is $5t\ell/s$ for a 10 A neutral beam. Thus the surface area required is $\sim 1 \times 10^5 \text{ cm}^2$ implying, say, a cylindrical pumping surface ~ 2 m long by

1.5 m diameter. This would obviously be done most conveniently by cryopumping. If the radiation load from the ion source can be minimized so that direct condensation without radiation shields can be used one could possibly reduce the pump area by a factor of 5. These calculations are only order of magnitude and should be more carefully done, for example using a Monte Carlo analysis, when the angular distribution of the gas emitted from the source is known.

2.2 Thermal loading on cryopumps

The thermal load will be composed primarily of radiation from surrounding surfaces and the heat in the condensed gas. The enthalpy of deuterium at $300^{o}K = 2.06 \times 10^{3}$ cals/mole(A6.2). Hence if we assume the gas flow calculated above we have the heat load $W_1 = 2.5$ watts. The latent heat of vapourization is 108 cals/gm, thus the heat load due to latent heat is $W_2 = 0.12$ watts.

Radiation can be simply calculated in two extreme cases. Firstly if we assume that the pumping surface is covered with a liquid nitrogen cooled baffle with a molecular transmission of 0.2. Then, as before, a surface area of 1.0×10^{5} cm^2 is required and the radiation load will be:-

$$Q_{77} = m \sigma A T^{4} = 6 \text{ watts for an emissivity } m = 0.3.$$

Using an unbaffled surface the area can be decreased by a factor of about 5 but the radiating temperature will be $300^{o}K$, thus

$$Q_{300} = 280 \text{ watts.}$$

This last figure might be reduced substantially if the geometry can be arranged so that the surface looks in on itself.

3. Pumping of Unneutralized Beam

From equation (A6.2) we have that the flux of charged ions from the neutralizer is given by

$$N_{D_1}^{+} = N_{D}^{o} (3/\varepsilon_3 - 1).$$

For $\varepsilon_3 = 0.6$ and a neutral beam of 10 A we thus have a gas load $F = 4t\ell/s$. This calculation makes the assumption that particles leaving the source come out

either as D_3^+ or as neutral gas. In fact there is bound to be an appreciable fraction of D^+ and D_2^+ coming from the source as well. Unless these are separated out at low energy they will increase the gas load at the neutralizer end and decrease the load at the source end. They will however be neglected in the following.

Three methods have been considered for pumping the unneutralized beam, firstly dumping the energetic beam directly in a metal surface, secondly allowing it to pass through a thin metal foil, and thirdly letting the beam pass through a hole, thermalising it, and pumping by conventional means.

3.1 Trapping in solids or liquids

It has been shown experimentally that energetic hydrogen ions can be trapped with efficiencies $\eta \sim 0.97$ in a number of hydride forming metals (e.g. Li, Ti, Zr, Er) over the temperature range 300-600^{o}K and the energy range 3-60 keV(A6.3,A6.4). At the higher energies being considered, trapping should be better. In non hydride forming metals the re-emission of incident ions is primarily by a diffusion mechanism and the net trapping efficiency will be close to zero for the ion current density, time and temperature with which we are concerned. In the hydride forming metals there appear to be two main release mechanisms:(a) a component due to the finite dissociation pressure of the partial solution of hydrogen in the metal, which is temperature and concentration dependent and (b) the re-emission of the incident ions by backscattering with an appreciable fraction of their incident energy. Backscattering depends on the atomic number of the target and on the incident ion energy (approximately as $E^{-3/2}$)(A6.5).

By working at temperatures below 600^{o}K and concentrations of hydrogen in the metal less than 1 at. % the dissociation pressure should be small compared with 10^{-6} torr and so the effective trapping efficiency determined by re-emission should be $\geq$ 99%. If the beam were decelerated to low energy, backscattering could contribute to re-emission, Fig. A6.2, but at 1 MeV the backscattering is expected to be $\sim 10^{-4}$ of the incident beam. The gas load will therefore be less than

1% of that calculated above or .04 tℓ/s, and thus a pumping speed of ~ 10^4 ℓ/s would probably suffice; this could then be pumped by a conventional diffusion pump.

The current density which can be tolerated will depend in the steady state on the rate at which the deuterium can be removed from the trapping surface. The removal would probably have to be by causing the trapping surface to move continuously out of the system to desorb the gas. Trapping in liquid lithium (A6.3) which can be pumped through the system is probably the simplest way of doing this.

For pulsed operation it may be simpler to dump the ions in a metal plate which can be removed between pulses. Assuming that the transport of deuterium in the metal is by thermal diffusion it can be shown that under these circumstances the maximum current density allowable is given by

$$J_M = \left(\frac{\pi D}{4t}\right) C_M^2$$

where D is the diffusion coefficient at the operating temperature, C_M is the maximum allowable concentration at the surface which will keep the dissociation pressure less than 10^{-7} torr, and t is the length of time for which ions are trapped. Values of D and C_M are not very reliable but from the available data (A6.6, A6.7) a value for J_M has been calculated for zirconium to be 6 mA cm^{-2} for a 100 s pulse. The data for titanium is inconsistent, while that for Nb and V gives considerably higher values of J_M, if it were possible to maintain the bombarded surface at low temperature ~ 300°K.

The major difficulty of this technique will not be the ion trapping but dumping the energy. If, for example, the power density has to be limited to ~ 100 W/cm^2 then the total area for 40 MW (the power in the unneutralized beam) will be 4 x 10^5 cm^2. Thus the particle density will be 0.1 mA/cm^2. Operating at this lower flux a larger total dose of ions may be trapped. However there is a serious difficulty in trying to trap ions and remove the energy deposited in the same surface, because the thermal conductivity of the trapping materials is in

general low. Moreover the upper temperature which they can be allowed to reach is determined by the dissociation pressure. For zirconium this is $\sim 550^{o}K$. If the temperature rise is specified as $200^{o}K$ and the heat flux as 100 watts/cm^2 then the maximum thickness of zirconium is determined as 3 mm, and the allowable thickness will of course be inversely proportional to the heat flux.

A slightly different approach to beam dumping is possible if low current densities are used. Low doses of hydrogen may be trapped in non hydride forming metals if the temperature is low, so that the diffusion coefficient is low. For example, molybdenum and stainless steel will trap up to $\sim 10^{17}$ ions/cm^2 of 30 keV D^+ ions at around room temperature. The number trapped would be expected to increase with primary beam energy. Such a target would therefore be capable of trapping a beam of 0.1 $\mu A/cm^2$ for $\sim$ 100 s. The deuterium could be then thermally desorbed by increasing the target temperature a few hundred degrees. The main difficulty will again be maintaining a sufficiently low temperature under ion bombardment.

At energies of $\sim$ 1 MeV the sputtering coefficient for metals by deuterons is low. Even for the worst case, copper, the sputtering coefficient is $\sim 5 \times 10^{-4}$ atoms/ion[A6.8]. Thus the rate of erosion is negligible at the current densities determined by the thermal load.

3.2 Beam dumping through thin foils

One method of pumping the ions which should work in principle is to pass them through a thin foil which could maintain a pressure gradient from the injector and allow the gas to be pumped conventionally at high pressure on the other side of the foil. Three aspects of this technique have been considered; the energy lost in the foil, sputtering and back diffusion of gas through the foil.

Since the energy lost in the foil must be small compared with the beam energy in order that the beam gets through and in order that the temperature

rise is limited, the foil must be thin. Thus it must be radiation cooled. We can thus equate energy lost by the beam to heat radiated i.e.

$$m \sigma T^4 = s\ n\ J \qquad \ldots (A6.10)$$

where m is the emissivity of the surface, σ the Stefan Boltzman constant, T the equilibrium temperature of the target, n the target thickness in atoms/cm^2 and s the stopping cross section for deuterons in eV cm^2/atom.

The foil, however, will be sputtered by the beam and if we say that the lifetime of the foil is determined by the criterion that it must not be reduced to less than half its original thickness then we have

$$0.5\ n \geq 6.3 \times 10^{18}\ J\ S\ t$$

where S is the sputtering coefficient and t is the foil life. Combining this inequality with equation (A6.10) we find

$$J \leq \left(\frac{0.5\ m\ \sigma}{6.3 \times 10^{18}\ \varepsilon\ S\ t} \right)^{\frac{1}{2}} T^2 \ . \qquad \ldots (A6.11)$$

If we consider D^+ ions of 1 MeV then the atomic stopping cross section varies from about 1.5 to 3.0 x 10^{14} eV cm^2/atom depending on the atomic number of the target material[A6.9]. We must choose a refractory material such as carbon, molybdenum, or tungsten. We also require a low sputtering coefficient. It is shown later molybdenum is not satisfactory from the point of view of diffusion. No information is available for carbon on either sputtering or diffusion so we will consider tungsten. The sputtering coefficient at this energy is estimated to be $\sim 10^{-4}$ atom/ion[A6.10]. We will assume the emissivity $m = 0.5$ and that a lifetime of 10^4 s is required. Thus,

$$J \leq 2.9 \times 10^{-9}\ T^2\ A/cm^2$$

or for $T = 1300^{\circ}K$, $J \leq 5 \times 10^{-5}$ A/cm^2.

Taking the maximum value of J we get from equation (A6.10) that the thickness $n \simeq 100\ A^{o}$. This is obviously impractically thin when the total current of unneutralized beam is ~ 40 A (D_1^+ equivalent) implying a foil area of ~ 10^4 cm^2. The current density could be reduced by say an order of magnitude increasing the target thickness and area proportionally, but the technical difficulties of producing such a foil would be formidable. Moreover radiation damage in the foil may set an even more severe limit than sputtering, on the current density.

We must consider now the effectiveness of the foil as a barrier to the gas. Such a thin foil at high temperature will obviously allow the gas to diffuse back into the vacuum system. Reliable measurements of diffusion of hydrogen through tungsten and molybdenum tubes .02 cm thick have been made (A6.11). Provided the foil is structurally sound it should be satisfactory to scale the permeation rate inversely with thickness provided permeation is diffusion limited. We will specify that the gas flow back through the foil is less than 10% of the gas equivalent of the ion beam i.e. < 0.4 tℓ/s. Then for a foil thickness of 1000 A^{o} and the area 10^5 cm^2 the permeation rate must be < 4 x 10^{-6} t.ℓ cm^{-2} s^{-1}. Moreover in order to justify the use of foils we must be able to maintain a higher pressure than in the injector in order to reduce pumping speed - let us say 10^{-4} torr. Extrapolating the results for tungsten a permeation rate 4 x 10^{-6} tℓ cm^{-2} s^{-1} should be obtained below 1200°K whereas with molybdenum it would be necessary to keep below 800°K. The lower temperature would reduce the current density for a 1000 A^{o} thick target down to ~ 10^{-5} A/cm^2.

3.3 Differential pumping

If the beam is extracted through a sufficiently small hole then it may be possible to thermalize it and pump it conventionally at a relatively high pressure relying on differential pumping to keep the pressure in the injector line lower. The difficulty is that the three charged particle beams resulting from break up of D_3^+ in the neutralizing cell will have different radii in a deflecting field. This will be further complicated if D_2^+ and D^+ species are also accelerated in the beam. However, it should be possible to at least arrange a cross-over of

the beams and allow them to escape through a hole of approximately the same diameter as the primary beam. If we assume this to be 20 cm (corresponding to a current density of 50 mA/cm^2 in the primary beam) and that the hole is 20 cm long, then a pumping speed of ~ 5000 ℓ/s will be obtained. In this case using two pumps of 10^5 ℓ/s would maintain a pressure of 2×10^{-6} torr in the injector. Pumping gas in these conditions will be much less difficult than near the ion source since the actual speed is less and space will be less critical. A further improvement may be obtained by combining differential pumping with surface trapping of the beam.

4. Conclusions

The pumping of a netural injector appears to be practical. It will however depend on the use of large cryopumps at least at the ion source. The design of these pumps will need to be closely co-ordinated with the ion source design. The gas efficiency of the source is an important parameter which has a bearing on the maximum current density which can be used.

The design of the unneutralized beam dump is determined primarily by the necessity to remove the large amount of energy associated with the beam. This energy makes it difficult to use a hydride forming metal to trap the beam but this may still be possible. The use of foils which transmit the unneutralized beam but prevent the back flow of the resultant gas is considered impractical because of the technical difficulty of making foils thin enough over the required area.

A partial focussing of the three beams although adding extra complexity and cost would greatly reduce pumping problems by allowing differential pumping. Differential pumping together with the surface trapping of the beam would produce the best vacuum conditions in the injector line.

References

(A6.1) McClure, G.W., Phys. Rev., vol.130, no.5, 1 June 1963, pp 1852-1859.

(A6.2) Woolley, H.W., Scott, R.B. and Brickwedde, G., J. Research, vol.41, 1948, pp. 379-475.

(A6.3) Erents, S.K., McCracken, G.M. and Goldsmith, P., J. Phys. D., Appl. Phys., vol.4, 5, May 1971, pp. 672-676.

(A6.4) McCracken, G.M., Jefferies, D.K. and Goldsmith, P., Proc. 4th Int. Vac. Congress, Manchester, 1968. Part 1, pp. 149-154.

(A6.5) McCracken, G.M. and Freeman, N.J., J. Phys. B., Atom. Molec. Phys., vol.2, no.6, June 1969, pp. 661-668.

(A6.6) Sof'ina V.V. and Pavlovskaya, N.G., Russian J. Phys. Chem., vol.34, 1960, p.525.

(A6.7) Mallett, M.N. and Albrecht, W.M., J. Electrochem. Soc., vol.104, 1957, p. 142.

(A6.8) Carter, G. and Colligan, J.S., Ion Bombardment of Solids, (Heinemann, London, 1968), p.339.

(A6.9) Whaling, W.,Handbuch der Physik, (Springer Verlag, Berlin, 1958), vol.34, p.200.

(A6.10) No measurements are available for sputtering of tungsten by deuterons but it is assumed that it will be a factor of 2 to 5 less than copper because the sublimation energy is higher, cf. ref. A6.8, Ch. 7.

(A6.11) Frauenfelder, R., J. Chem. Phys. vol. 48, 1968, p. 3955.

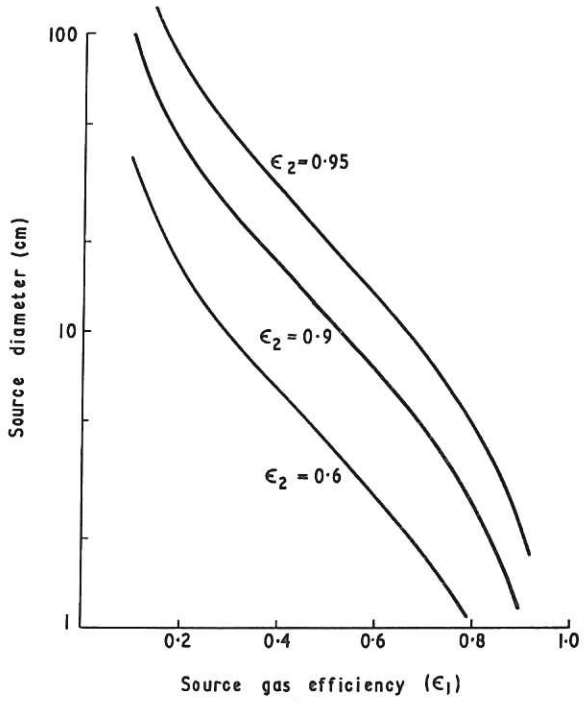

Fig. A6.1 The effect of source efficiency and charge exchange in the accelerator on the size of source required for 10 A of neutrals.

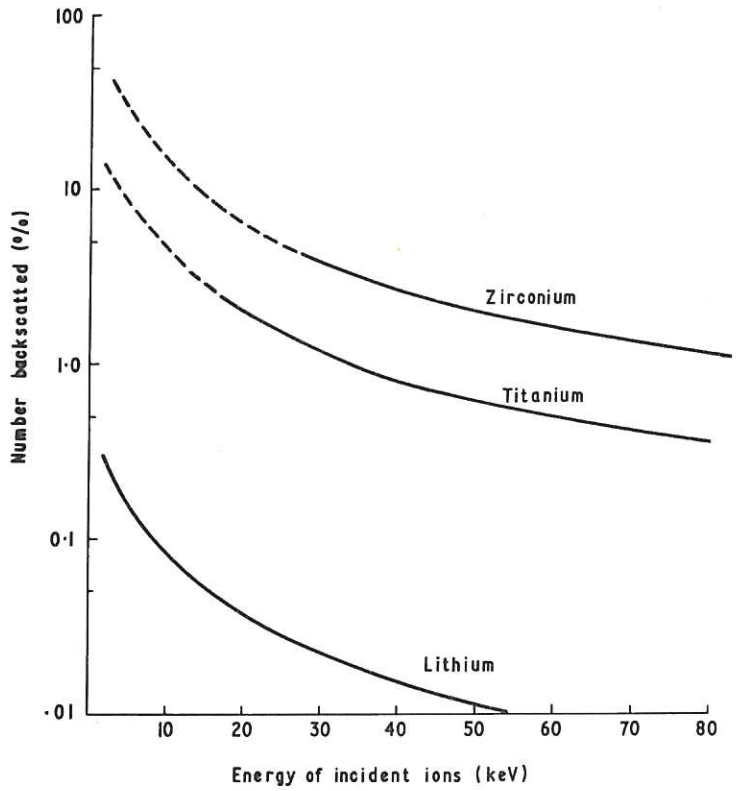

Fig. A6.2 The calculated number of ions backscattered with energy greater than 1 keV for some trapping materials, assuming Rutherford scattering: -------- The effect of screening is greater than 10%.

NOTES ON POWER SUPPLIES

FOR

NEUTRAL INJECTION INTO TOROIDAL SYSTEMS

F.A. Julian

1. Introduction

High voltage accelerators available today seldom give power outputs greater than ten kilowatts, whereas fusion injectors of this type require several tens, or even hundreds, of megawatts. The voltage requirement is well within our experience but the (C.W.) power required represents an extrapolation of three orders of magnitude beyond presently available high voltage accelerators. The principles and methods of generation applying to such large accelerators may differ widely from those in use today. All known methods of power generation should be examined for technical feasibility, operating efficiency, economy and reliability, including capital costs, maintenance and depreciation.

These notes attempt, very tentatively, to assess the technical feasibility of some possible methods of high voltage generation which might be worthy of further investigation. They do not deal with the difficulties of ion beam production acceleration and neutralisation but merely assess the generation problems which are likely to arise when optimistic assumptions of beam handling are made.

Before dealing with the generation requirements we make a brief assessment of the likely demands of the accelerator for a toroidal reactor and optimistically estimate probable losses. The term "accelerator" here is intended to include the accelerating tube and the ion source, together with their corona shields, potential divider, and enclosing vessel.

2. Simple Considerations of the Power Requirements.

Assuming that the neutral particle flux required to ignite the reactor is 100 A of D^0 at 1 MeV then the power to be injected is P_n = 100 MW and the total power to be generated is:

$$P_G = \frac{P_n}{\eta_n \eta_a} = 550 \text{ MW} \qquad \ldots(A7.1)$$

where the neutralization efficiency η_n = 20% (see Section 2.4) and the acceleration efficiency η_a = 90% (see page A7-6, Equation (A7.9)).

With the difficulties of beam handling in mind it is assumed that injection will take place at ten points around the reactor, each injector producing 10 A of D^0 at 1 MeV from an accelerated 3 MeV D_3^+ ion beam of 16.6 A. At this stage the possibility of a 3 MV distribution system from one generator to a number of accelerators seems to be remote, we prefer to assume that each accelerator will be supplied by its own isolated D.C. generator, the output of which must be at least 55 MW at 3.0 MV.

Thus the beam power of the accelerator for each injector is to be $V_B I_B$ = 50 MW where V_B and I_B are beam energy and current respectively. To this power requirement must be added unavoidable power losses within the accelerator:

(a) Ion Source and Extraction System Losses

Let the ion source extraction voltage be V_e

the ion beam current reaching the neutralizer be I_B

the electrical efficiency of the ion source be η_s

the beam extraction efficiency be η_e

and the source power supply system efficiency be η_G.

Then the input power to the ion source is given by:

$$P_m = \frac{V_e I_B (1 - \eta_e)}{\eta_s \eta_G} . \qquad \ldots(A7.2)$$

The extraction potential will depend on the type of ion source used but for the sake of discussion we choose V_e = 70 kV and assume that, η_e = 70%; η_s = 90% as obtained at present in ion thrustors. Assuming also that the ion source power is derived from a motor-generator set, then typically η_G = 80% and the power to be fed directly to the ion source is:

$$P_m \approx 500 \text{ kW}.$$

(b) The Accelerating Tube and Losses

This simple description of a probable tube arises from a preliminary glance at some of the difficulties. Any tube suitable for high power beams of this magnitude will be much larger and heavier than existing (1 mA) tubes. At this stage it is extremely difficult to envisage the physical size and shape of a practical tube and what follows is little more than a guess.

Potential division along the tube will probably occur at 100 kV intervals.

Assuming that beam focussing and tube admittance are good to such an extent that only 1% of I_B is intercepted by tube electrodes, and that the intercepted current I_i is distributed along the tube in such a way that most current impinges on electrodes at the upstream end of the tube, we infer that the power deposited by I_i within the tube is

$$P_b < \tfrac{1}{2} \; I_i \; V_B \simeq 250 \text{ kW} \qquad \ldots (A7.3)$$

It is fairly clear that the accelerating tube will be force cooled, that each of its electrodes will be hollow and contain circulating fluid to keep the electrodes cool in the presence of this standing loss, and also to give further protection during beam adjusting periods. Thus at this stage we envisage the accelerating tube to consist of say 35 electrodes at a pitch of about 3 in., (100 kV per gap) each electrode being about 2 in. thick, with a wall thickness of say 0.1 in., giving an overall accelerating tube length of about 10 feet and an O.D. of say 7 feet.

So far we have taken no account of retrograde electron current i_e which must inevitably occur. Experience with 6 MeV 1 mA tubes shows that i_e can

be up to 5 times greater than I_i, but if magnets are fitted within each electrode this retrograde electron current can be reduced by about 2 orders. In our case therefore we might reduce i_e' to about 10 mA, where i_e' is retrograde electron current directly due to beam impact on electrodes.

But we must also consider retrograde electron currents i_v born of beam interaction with residual gas molecules throughout the length of the accelerating tube. The literature (A7.1, A7.2) indicates that the cross section q for electron production in thesecircumstances lies between about 10^{-16} and 10^{-15} cm^2 per molecule.

If the average pressure in the accelerating tube is 10^{-5} torr and in this case we assume the magnetic suppression coefficient μ to be 0.1, then the retrograde current due to residual gas effects will be

$$i_v = I_B N q l\mu \approx 0.050 \text{ A} \qquad \ldots(A7.4)$$

where N is the number density of gas molecules $\sim 10^{11}$ cm^{-3}

and l is the length of the accelerating tube ~ 300 cm .

Thus total retrograde electron current (i_e) in our case is roughly assessed as

$$i_e = i_e' + i_v \quad 0.010 + 0.050 \simeq 0.060 \text{ A}, \qquad \ldots(A7.5)$$

indicating a probable power loss directly due to retrograde electron current of

$$P_e \approx \tfrac{1}{2} i_e V_B \approx 90 \text{ kW} \qquad \ldots(A7.6)$$

This power (P_e) will be dissipated in the area of the ion source extraction system and clearly the beam defining apperture plate must be force cooled. Also pumps must be carried within the H.T. terminal to ensure good vacuum at the upstream end of the tube.

A further loss which occurs in all accelerators is due to the production of X rays by the impact of i_e on electrodes and beam defining apperture plates. These X rays produce ionization in the insulant gas surrounding the H.T. section of the accelerator and give rise to a current i_g which flows from H.T. terminal

through the insulant gas to the walls of the pressure vessel. Experience with 6 MeV 1 mA accelerators enclosed in 9 ft. diameter pressure vessels containing (200 p.s.i. N_2/CO_2) insulant gas shows that, when target materials such as beryllium backed by lead or uranium are used the magnitude of i_g can be ten times greater than i_e; and the X radiation measured at the surface of the vessel reaches several rad. per hour (A7.3). Clearly, in our present case the X radiation is likely to be enormous unless revolutionary methods of suppression can be adopted. However, if we assume that i_g is ten times greater than i_e and that it flows mainly from the H.T. terminal then the power loss due to i_g is:

$$P_g = i_g V_B \simeq 0.6 \times 3 \times 10^6 \simeq 2 \text{ MW} . \quad \ldots(A7.7)$$

Assuming a pressure vessel diameter of 16 feet (accelerator only) then the power deposited at the vessel top cap surface would have a density of about 4 kW per square foot.

In addition to the foregoing losses directly and indirectly due to the ion beam we must also consider the heat losses of a potential divider, which will probably be shared by the generator and accelerator. For this divider to be effective it must draw current i_d at least one order greater than i_e; assuming it to be a passive element (resistance) then the power loss in the divider will be

$$P_d = i_d V_B \approx 0.6 \times 3 \times 10^6 \approx 2 \text{ MW} . \quad \ldots(7.8)$$

The picture of the accelerator, as far as it has formed at this stage, is that of a 16 foot diameter, 25 foot long, water jacketed, pressure vesssel surrounded by radiation shielding. The vessel contains the complete ion source and accelerating tube within a potentially divided stack which also encloses a force cooled potential divider. Each stage of the force cooled accelerating tube is fitted with electron suppression magnets and radiation shields to minimise i_e and i_g.

The generator is considered to be housed in a separate vessel which will not require radiation shielding, and connections between generator and accelerator are made through pressurised branch pipes connected between the two vessels.

The total, roughly estimated, accelerator losses which we have arrived at by this stage are:

Ion source losses P_m	~500 kW
Intercepted beam current losses P_b	~250 kW
Losses directly due to retrograde electrons P_e	~ 90 kW
Losses indirectly " " " P_g	~2.0 MW
Potential divider losses P_d	~2.0 MW
Total losses P_t	~4.84 MW

Based on the foregoing simple optimistic assessments the efficiency of the accelerator will be:

$$\eta_a \approx \frac{P_o}{P_o + P_t} \approx \frac{50}{50 + 4.84} \approx 90\% \quad . \qquad \ldots (A7.9)$$

Several of the above values are based on such flimsy evidence that they should not be taken too seriously. Up to this point we have merely attempted to get some idea of the achievable accelerator efficiency so that the generator output requirements can be defined reasonably closely. A more thorough accelerator assessment must be the subject of a separate study.

We turn now to the main subject of these notes, namely High Voltage Generation in the 55 MW 3 MV range.

3. High Voltage D.C. Generators

Our requirements are well beyond present experience and all methods of generation should be considered. In particular, commercially successful methods of low power high voltage generation must be examined and compared as to their suitability for high power application. These notes are restricted to a comparison of relatively conventional methods with regard to their technical feasibility, efficiency, reliability, and safety, simply on the basis of a cursory examination of the more obvious factors. Where known, the capital costs of commercially available equipment are given and the recommended method is chosen on economic grounds taking into account likely development costs as well as production capital costs.

There are two distinct commercial classes of DC high voltage equipment in use today:

(a) Convertors used in DC power transmission systems at voltages up to ± 600 kV and powers up to 2000 MW. The present capital cost of such convertors lies in the region £5 - £10 per kW for each convertor. Figure A7.1 is taken from Miller (A7.4).

(b) High voltage generators generally associated with particle accelerators or test equipment at voltages up to 6 MV and powers up to 60 kW. The present capital cost of such generators lies between £1000 and £10,000 per kW.

In our case the environment and geometry of the generator, accelerator and their inter-connecting links can be chosen in such a way that we need not extrapolate beyond present good insulation practice; and it is clear that power supplies of several million volts with outputs up to thousands of MW are entirely practical in a controlled environment. The question is merely whether using low capital cost equipment they can be made compact and cheap to operate.

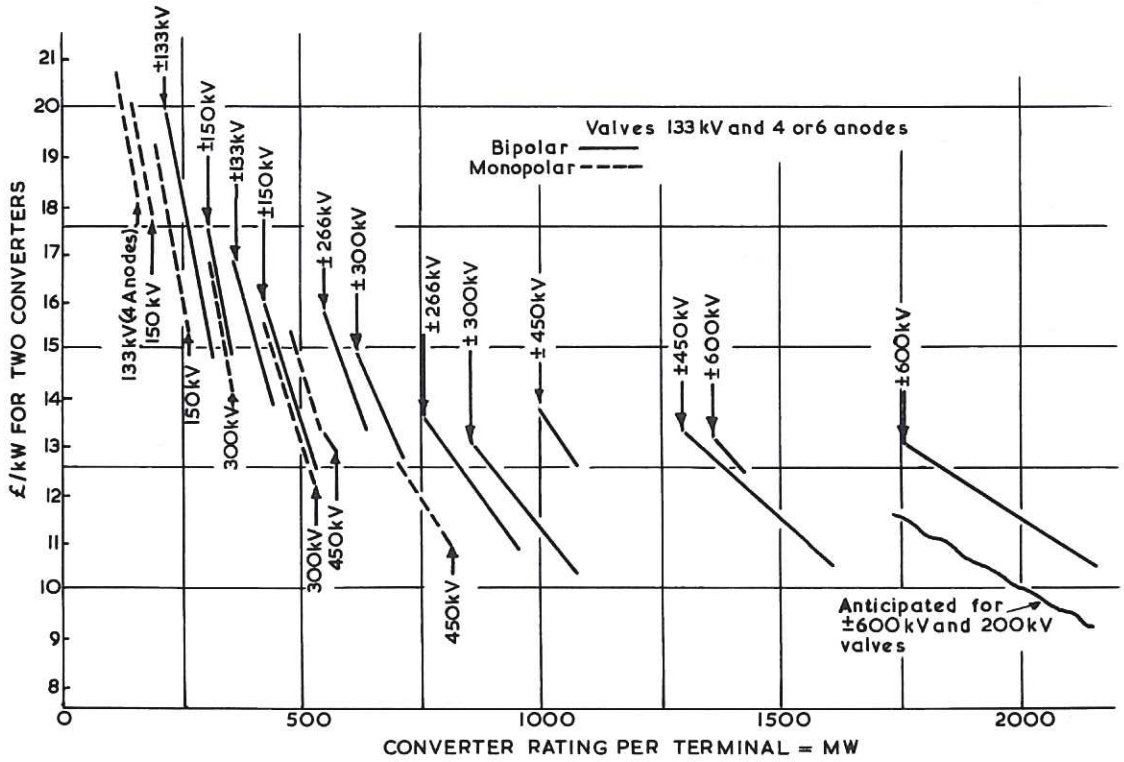

Fig. A7.1 Basic capital costs for converter plant (A.C. switchgear and P.F. correction excluded).

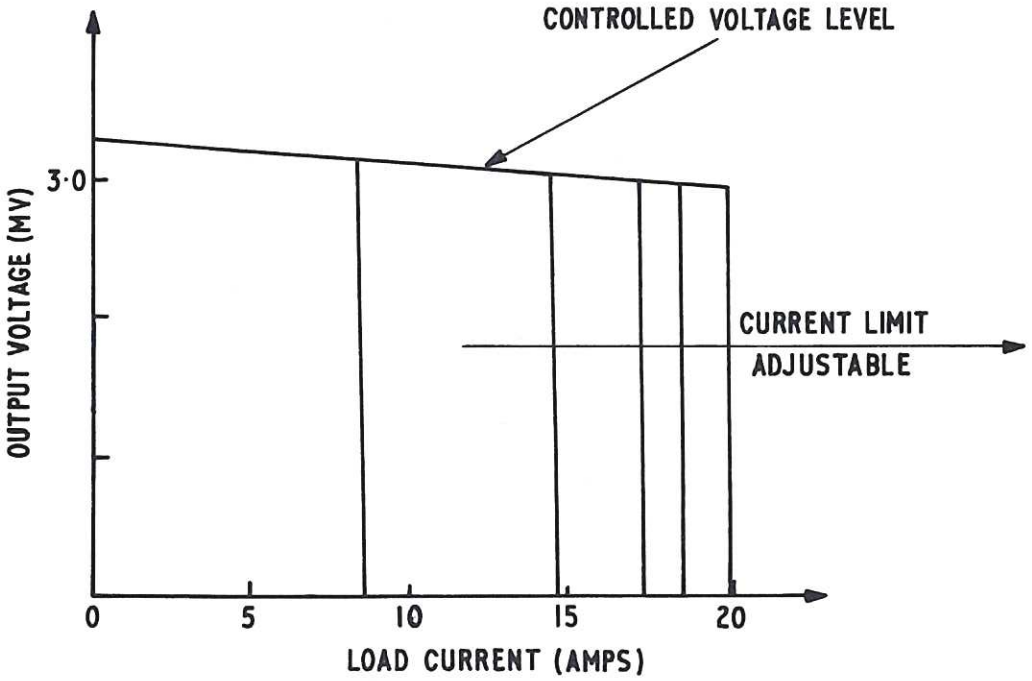

Fig. A7.2 Required generator output characteristic.

CLM-R 112

Obviously, the larger the power output of the generator the more economical it becomes to invest in control and protection equipment. Consequently we should not lose sight of the possibility that it could be more economic to supply several accelerators from one large generator via a 3.5 MV bus bar.

Turning now from these simple commercial considerations to points of general technical interest: both classes of equipment referred to above and, for that matter, all practical high voltage D.C. generators, have one major characteristic in common, namely their output volt-amp characteristics must be of the general form shown in Figure A7.2. In other words, in the interests of control and protection the output of a high voltage D.C. generator must be voltage regulated and adjustably current limited according to the demands of the load.

This is an imperative requirement of all high voltage D.C. systems. Present success with large ($\sim$ 1000 MW) D.C. power links is very dependent on the operating characteristics of mercury arc rectifiers. Used in conjunction with conventional tranformers and chokes these rectifiers shape the output characteristics of the overall conversion equipment to conform with Figure A7.2. The need for this arises from the fact that no effective high voltage D.C. switch or circuit breaker has yet emerged: the protection of these large systems is entirely dependent on the "blocking" and "clamping" ability of grid controlled mercury arc rectifiers (response time $\simeq$ a few milliseconds) and the A.C. circuit breakers (response time $\simeq$ 50 milliseconds). At the present time high voltage applications of the S.C.R. (Thyristor) are developing fast and compact 100 kV thyristor units should be commmercially available within the next few years.

Although it might be possible to develop an explosively detonated fuse for catastrophic emergencies, such an approach does not appear to be practicable for normal overload protection intended to deal with relatively minor load instabilities.

Our present requirement is no exception to these general considerations, short circuit protection must be included as an integral part of the generator.

With the foregoing considerations in mind, the following preliminary functional specification of the generator is intended to meet the minimum requirements. We note that Mirror Systems need much larger continuously rated generators[A7.5] and the chosen method of generation should be capable of being extended to produce a continuous power output of up to 1000 MW.

3.1 Preliminary Functional Specification of the Generator

(a) To provide a continuous power output of at least 55 MW for the reactor ignition period (say 1 minute). This implies that the generator need not be continuously rated but it must be essentially C.W.

(b) Output Voltage: 3.5 MV D.C. (for tube conditioning)

To be stabilised at any chosen value from 2.5 to 3.5 MV.
Voltage regulation to be less than 12% at full load.
Voltage ripple to be less than 5% (RMS) at full load.

(c) Output current: To be smoothly controlled from 0-20 A , and limitable at any intermediate value.

(d) Overload and short circuit protection to be provided for both generator and accelerator.

(e) Input power to be derived from a "prime mover" independent of CEGB mains supply. (In line with normal power station practice.)

(f) Efficiency of the overall generation system must be reasonably high ($> 60\%$) so that the total capital cost can be minimised.

(g) Safety standards to be at least as effective as conventional power systems.

(h) The stored energy of the system to be minimised to facilitate (d) and (g) above.

(i) Each component of the system to be as compact as possible.

(j) The total capital cost of the system to be minimised.

(k) R and D costs to be minimised.

Note: The most suitable method of generation will be the one which satisfies (a) to (g) of the Preliminary Functional Specification in the most economic way.

3.2 Possible Methods of Generation

Seeking the most economic relatively short term solution, only the more conventional methods of generation are examined here. For example, MHD generators are not considered on the basis that they represent a subject as vast as Fusion itself.

At this point it is noted that the overall problem of high voltage insulation is common to all methods and the assumption is that the generator will be housed in a vessel containing insulating fluid or pressurised gas, the breakdown strength of which is greater than 100 kV cm^{-1}.

For purposes of selection conventional methods of generation can be divided into three broad groups:

A - Electromagnetic Methods

B - Electrochemical Methods

C - Electrostatic Methods .

Each of these groups can be further sub-divided into types, the advantages and limitations of which are mentioned below.

The method selected in Section 4 is finally chosen from these types not because it is the only method but because it appears to offer the most direct and economic solution and to require rather less development work than other methods. Probably the most important reason for its selection is that it involves capital cost in production close to those of present commercial D.C. high voltage transmission systems.

Turning now to a simple examination and comparison of possible types of generator:

Group A - Electromagnetic Methods

All the machines in this group rely on electromagnetic induction, they

are fundamentally A.C. machines and are voltage rather than current generators. Although strictly speaking the Homopolar Generator (a D.C. machine) belongs to this group we discard it because in practical geometries it is limited to low voltage generation. Thus for our purpose all the machines in Group A must be used in conjunction with rectifiers and there are three types of rectifier available commercially, viz:

The Mercury Arc - at present available in units suitable for operation at up to about 100 kV and up to about 400 A.

The Thyristor - rapidly developing and at present available in composite units similar to the Mercury Arc.

The Vacuum Valve - at present available in units suitable for operation at up to about 100 kV and up to about 5 A.

Of these types of rectifier the thyristor promises to become the most compact in the near future.

The machines in Group A divide into two classes rotating and non-rotating.

Rotating electromagnetic machines are compact, efficient (95%) and are successfully established commercially (capital cost about £20 per kW at 50 MW output). In practice, the insulation difficulties associated with high voltage rotating electromagnetic machines are greater than those encountered by non-rotating machines. Present day commercially available alternators seldom exceed output voltages of a few tens of kilovolts; they do not lend themselves to economic application in the 3 MV regime, but as an intermediate component used in conjunction with a non-rotating A.C. to D.C. high voltage convertor they are essential in such arrangements as shown in Figure A7.3(a).

Non-rotating machines performing the functions of rectification and voltage transformation are well-established commercially in the 3 MV regime. Examples of successful types are compared below:

The Transformer Rectifier

The most suitable circuit on which high power, high voltage D.C. transmission

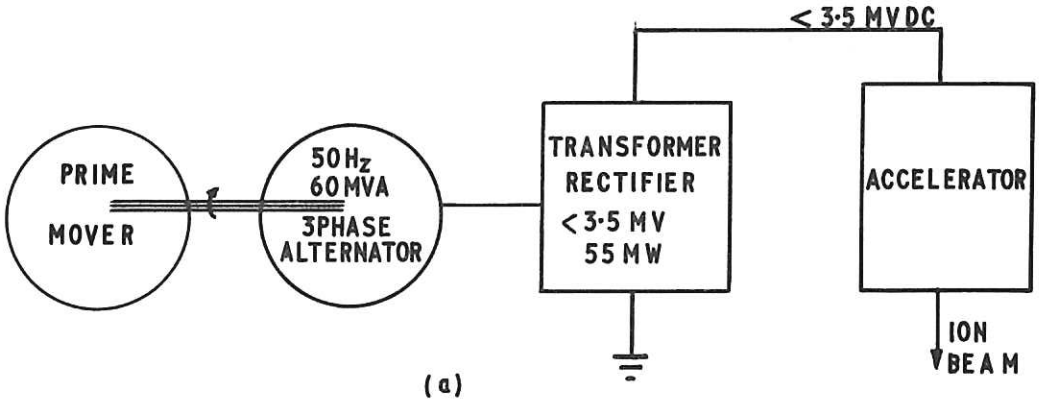

(a)

Alternator-transformer-rectifier arrangement

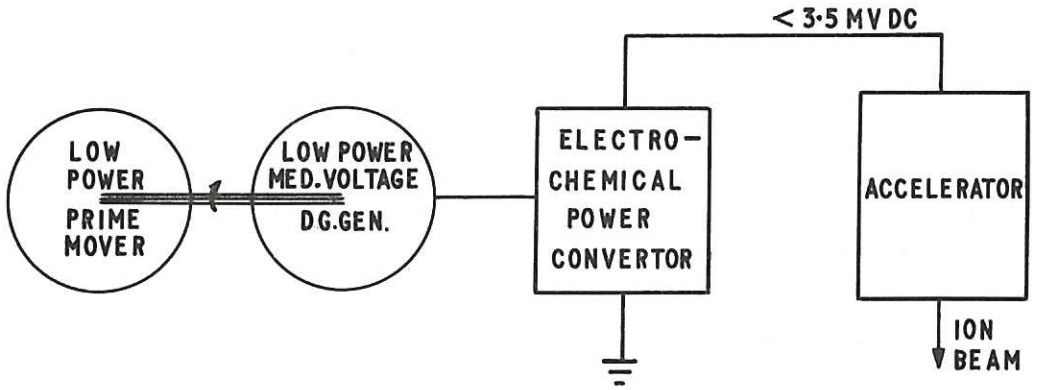

(b)

Electro-chemical converter with low power charger

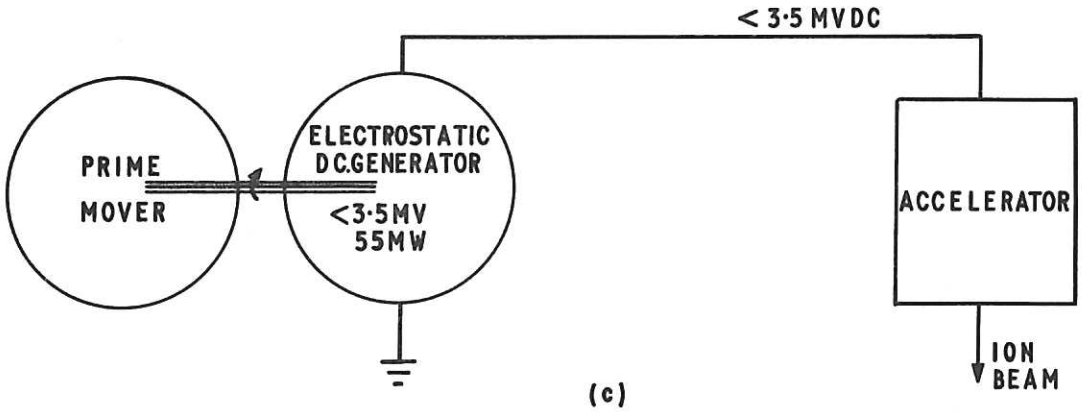

(c)

H.V.D.C. Generator directly coupled to prime mover & accelerator

Fig. A7.3 Required generator output characteristic.

CIM-R 112

systems are based is the three-phase full-wave (Graetz) bridge shown in Figure A7.4. Recently ASEA have put into operation a Graetz bridge rated at 30 MW at 150 kV[A7.6]. In this installation each valve unit comprises sixty 3kV (PIV) thyristors connected in series, giving an in-built reserve such that if a fault develops on one thyristor, the valve unit continues to operate.

For very high output voltage it is more economical to connect a number of bridges in cascade, each bridge being supplied by its own transformer (Figure A7.5).

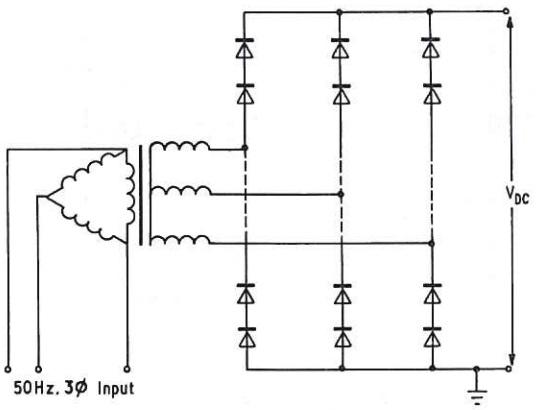

Fig. A7.4 Graetz Bridge Rectifier.

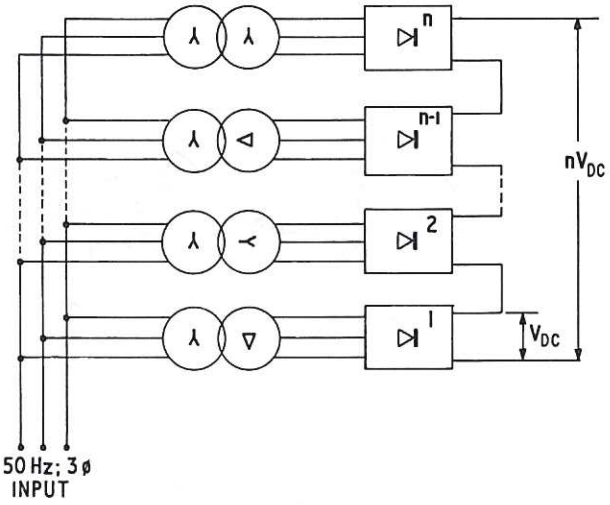

Fig. A7.5 n bridges in cascade.

CLM-R 112

The transformer supplying each bridge unit is phase-rotated with respect to its neighbours and in this way up to 24 pulse rectification can be obtained giving a relatively smooth (ripple voltage $\sim 0.25\%$) D.C. output without the use of a smoothing filter.

When extended towards the 3 MV regime this cascaded arrangement tends to become bulky and, consequently, costly. The transformers supplying each bridge must be insulated for their respective voltage levels and the insulation distances required become very large, but each transformer bridge unit is highly efficient ($\prec 99\%$), and for a very high continuous output power (1000 MW) where efficiency is important, this method compares favourably with all others.

Nevertheless, for an output voltage of 3 MV at 60 MW for a period of 1 minute the Insulating Core Transformer, using compact thyristor Graetz bridge rectifiers appears to be the most promising of all the methods under consideration.

The Insulating Core Transformer

This device was invented by R.J. Van de Graaff in the late 1950's to fill the needs of relatively high current, high voltage accelerators. It has been commercially successful at output voltages up to 2.5 MV D.C. and output currents up to 100 mA. The highest power ICT at present marketed (Figure A7.6), gives a maximum output of 60 kW (2 MV, 30 mA), with a full load voltage regulation of 25% and voltage ripple of 1.5% (peak to peak). There appears to be no fundamental reason preventing the method from being extrapolated to meet our requirements.

The schematic diagram (Figure A7.7) and simplified physical arrangements of the ICT (Figure A7.8) illustrate the general principles of the method.

The transformer secondary circuits are composed of modules which are individually supported on insulating decks. Each module comprises a three-phase secondary winding, a set of rectifiers, and any necessary control and protection components. These modules are mounted over insulated iron core legs and are electrically isolated at each level by a high grade insulating film. The construction provides a good magnetic flux path of low reluctance and high dielectric strength. Equipotential rings surrounding each of the stacked modules control the electric field throughout the volume of the transformer. The primary winding is wound around the three core legs at ground potential.

The transformer-rectifier assembly is housed in a steel vessel filled with sulphur hexafluoride at a pressure of about 60 p.s.i. Present models < 60 kW are cooled by forced gas convection and water cooled coils mounted in the vessel at ground potential. The transformer primary is supplied from a variable autotransformer with power factor correction capacitors.

At this stage of technological development the ICT three-phase full wave Graetz bridge rectifier promises to be the device most easy to develop for intermittently rated high power, high voltage applications.

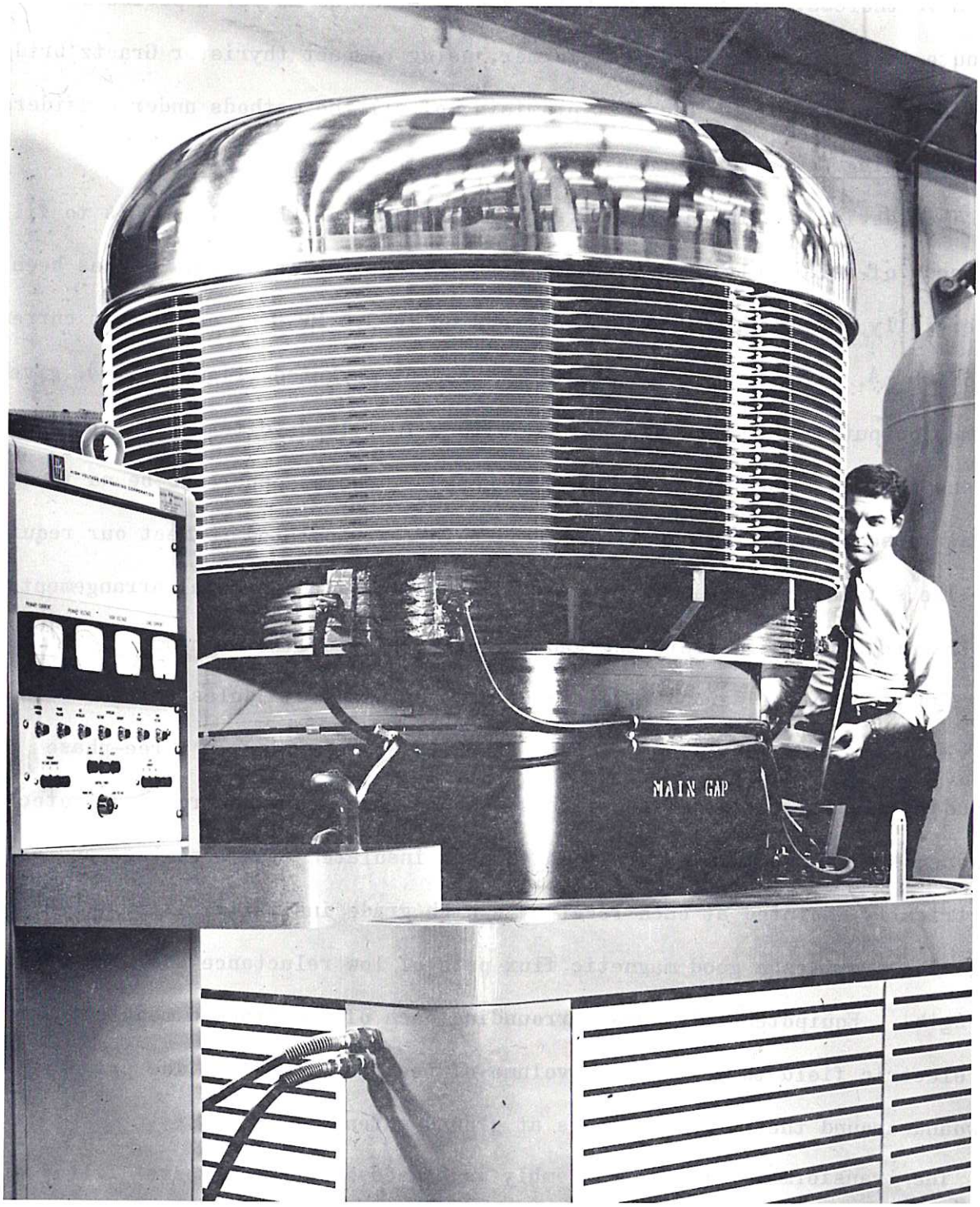

Fig. A7.6 Insulating core transformer (Reproduced by permission of High Voltage Power Corporation, Burlington, Mass. U.S.A.).

CLM-R 112

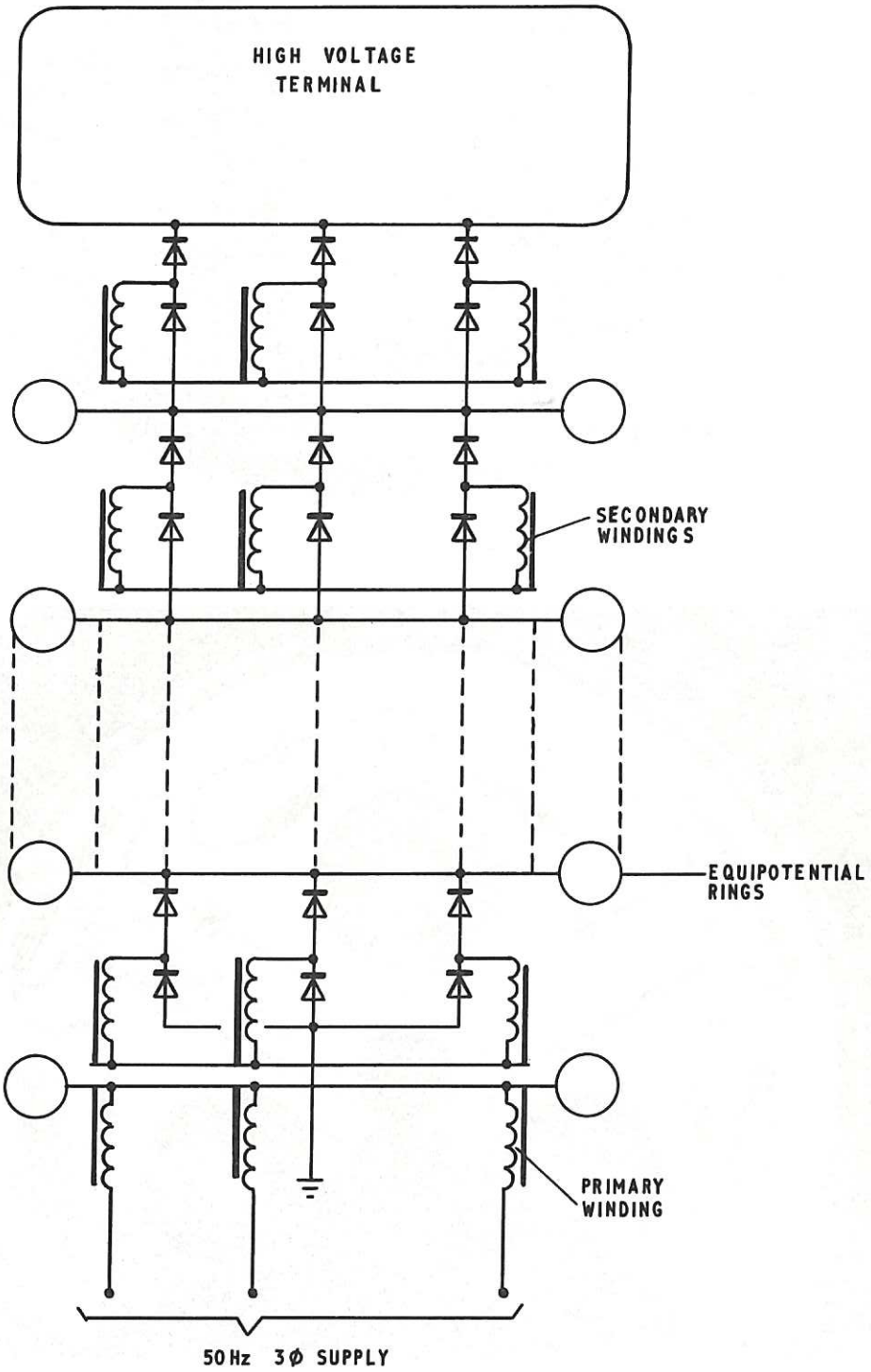

Fig. A7.7 Schematic diagram of I.C.T.

CLM-R 112

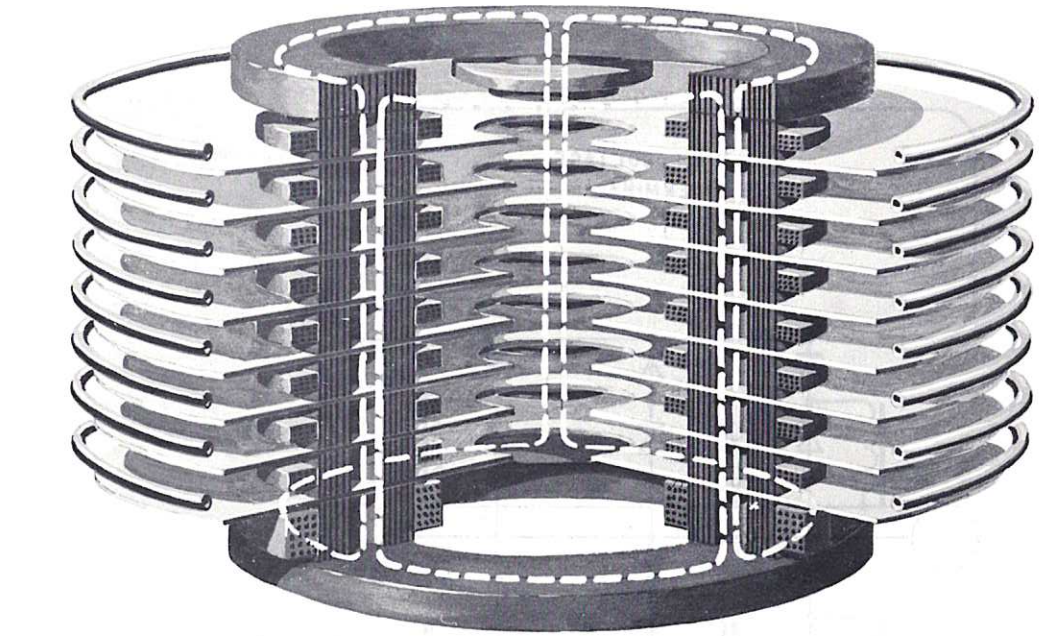

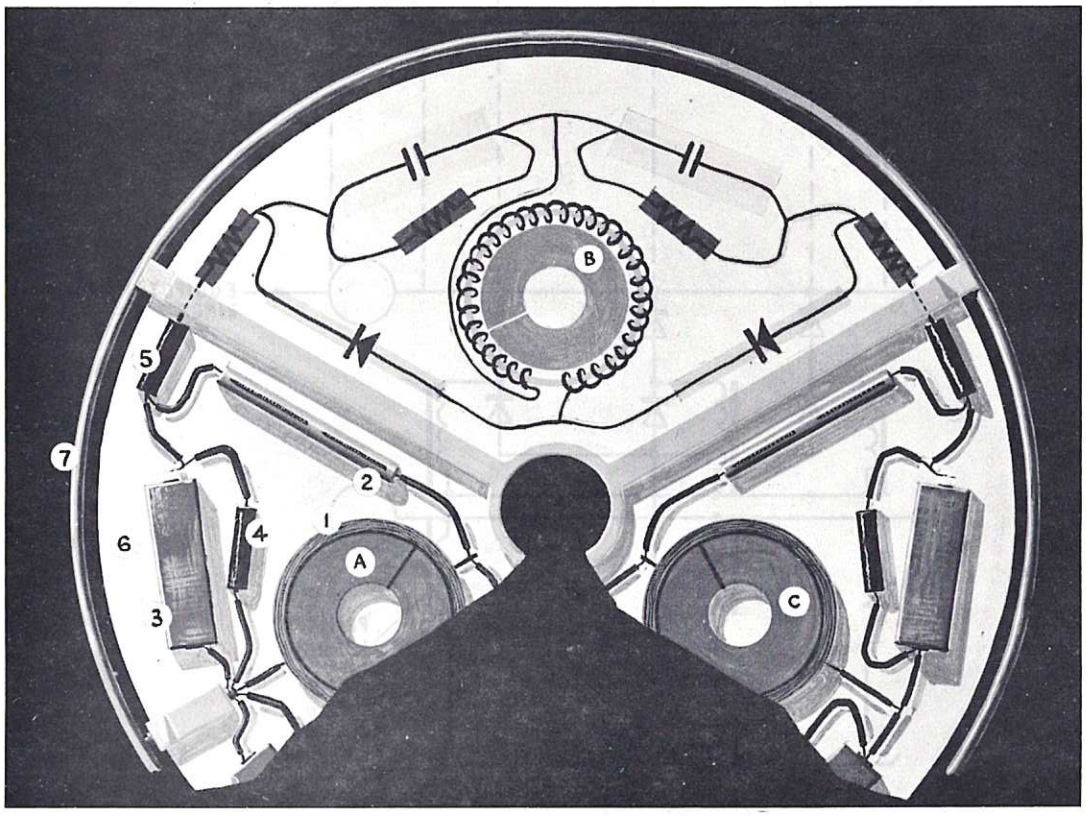

Fig. A7.8 Simplified physical arrangement of I.C.T. (Reproduced by permission of High Voltage Power Corporation, Burlington, Mass. (U.S.A.).

A,B,C	Three phase core sections	4	Bleeder Resistor
1	Secondary Windings	5	Series Resistor
2	Rectifiers	6	Deck Separator
3	Voltage Doubling Capacitors	7	Equipotential Ring

CLM-R 112

When compared with other possible methods it has the following advantages:

(i) The physical layout of the ICT assembly greatly simplifies the insulation problems associated with conventional transformer rectifier assemblies.

(ii) The ICT promises to be more compact and economic than all other methods.

(iii) Taking into account the present state of development of each of the possible competing methods the ICT compares very favourably in that it uses materials and components which do not differ essentially from the economically proven conventional transformer rectifier. Thus the amount and degree of technological development required to extend the ICT into the high power range should be much less than for the other methods under consideration.

(iv) For the reason given under (iii) the capital costs of an ICT should be comparable with those of a conventional transformer rectifier, i.e. $< £20$ per kW at an output power of 55 MW.

(v) The ICT intrinsically has a high leakage reactance which, in turn, gives rise to higher copper losses and lower efficiency than in the conventional transformer. However this feature is to some extent offset from our point of view in that its output volt-amp characteristic tends towards that shown in Figure A7.2.

A possible 3.5 MV 20A insulating core transformer rectifier arrangement as applied to an accelerator for neutral particle injection is outlined in Section 4.

Transformer-Rectifier-Capacitor Voltage Multipliers

A large number of commercially successful equipments of this type have been produced at voltages up to a few MV and output currents up to about 10 mA. They all derive from the original Cockroft Walton circuit and in practice they are limited to low output currents because they are dependent on energy storage by capacitors. Their voltage droop and output voltage ripple characteristics are determined by the size of the storage capacitors. One of the more suitable

circuits for higher output currents is the three-phase split bridge (Figure A7.9).

The D.C. output voltage of this circuit is given by:

$$V_{DC} = 2n\hat{E} - \frac{I}{3fC}\left[\frac{2n^3}{3} + \frac{n^2}{2} + \frac{n}{6}\right] \quad \ldots (A7.10)$$

where $\hat{E}$ is the peak value of the three-phase output voltage of the transformer

I is the D.C. load current

f is the supply frequency

n is number of stages = number of reservoir capacitors (C_R)

and $C = C_R = 2C_D$.

The second term in equation (A7.10) is the voltage drop due solely to the number of stages, size of capacitors and supply frequency employed. Ignoring voltage regulation due to other causes such as the internal impedance of the transformer, the physical size of capacitors required to meet our case can be roughly assessed by making the following assumptions:

Input voltage to multiplier (E) ... 105 kV

Operating frequency (f) ... 50 Hz

Number of stages (n) ..... 12 ,

Permissible voltage regulation at full load (20 A) ..... 12% .

Then typical values on open circuit would be

$$V'_{DC} = 2n\hat{E} = 3.56 \text{ MV}$$

and on full load

$$V_{DC} = 3.14 \text{ MV}$$

and minimum permissible $C = 400\mu F$ ... (A7.11)

and the peak stored energy in each reservoir capacitor (C_R) is

$$\mathcal{E} = \frac{1}{2} C_R \hat{E}^2 \approx 4.5 \text{ MJ}. \quad \ldots (A7.12)$$

Now maximum energy density so far achieved in practice by modern high voltage capacitors is about 1500 joules per cu. foot and the present price of energy storage by capacitor is about £0.5 per joule.

Methods dependent on capacitive energy storage at supply mains frequency are absurdly bulky and uneconomic. Clearly more favourable characteristics can be

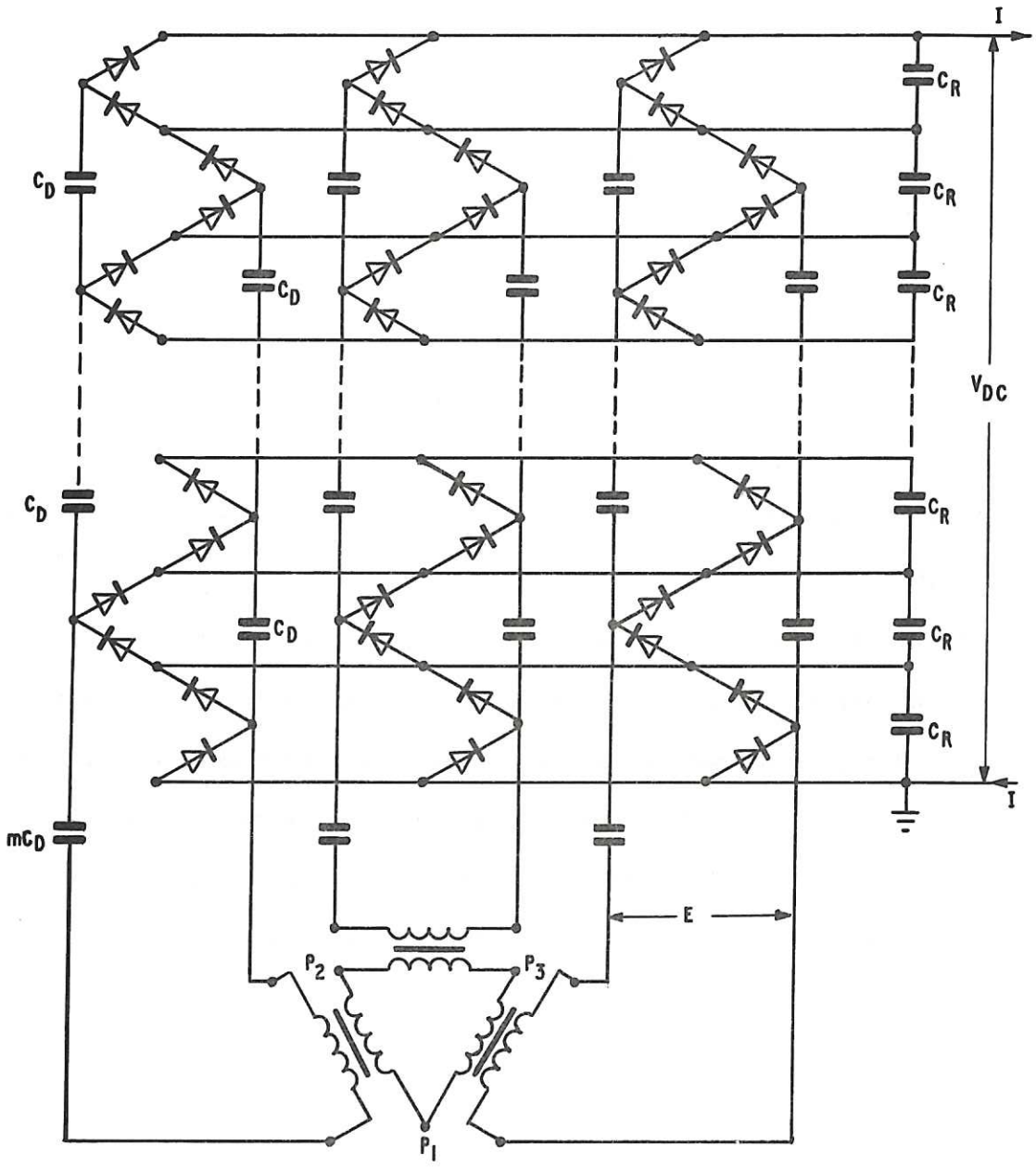

Fig. A7.9 Schematic diagram of 3 phase split bridge circuit.

CLM-R 112

obtained at higher operating frequencies but there are practical limitations. At frequencies above a few kHz the natural capacitances of practical corona shielded rectifier stacks begin to dominate the mode of operation. Also the upper limit of frequency at which present day thyristors operate satisfactorily is between 50 and 100 kHz. One of the most successful higher power voltage multipliers is the RF Dynamitron.

The RF (Dynamitron) Voltage Multiplier

This type of high voltage power supply is marketed by Radiation Dynamics Inc. Westbury, N.Y. Presently available models operate in the range 1.0 to 5.5 MV at currents between 25 mA and 3.5 mA. The maximum output power so far marketed has been 40 kW. Figure A7.10 is a schematic diagram of the Dynamitron high voltage generator. The H.T. rectifiers contained in the pressure vessel are hard vacuum valves. The Dynamitron is essentially a cascaded rectifier stack which is parallel fed through the inherent coupling capacitance between the corona rings of the stack and a pair of semi-cylindrical R.F. electrodes mounted just inside the pressure vessel wall. The operating frequency of present models is 112 kHz.

The tank circuit of the oscillator is formed by a gas insulated toroidal transformer and the total capacitance of the electrode system.

The oscillator is a tuned plate, untuned grid circuit. The grids of the oscillator valves are driven by a plate located between the R.F. electrode and the pressure vessel. The high voltage is controlled by varying the anode D.C. voltage by means of series pass tubes.

Present models operate at an efficiency of about 30% and it is unlikely that really high power Dynamitrons would be much more efficient.

Briefly, the advantages and the disadvantages of the system are summarised as follows:

Advantages: The equipment contained in the pressure vessel is extremely simple.

The stored energy of the system is low.

Disadvantages: Efficiency is low as compared with the ICT.

The radio interference produced would be troublesome to screen effectively from other necessary equipment and instrumentation.

The power amplifier required (150 MW output) represents a considerable extension of present day sizes.

The capital cost of such equipment is likely to be considerably in excess of £15/kW which appears to be likely for the ICT.

We shall therefore conclude that at this stage the Dynamitron cannot be considered as a serious competitor, although in principle a 3 MV 20 A Dynamitron could be made. Design equations for Dynamitrons are given by Thompson and Cleland (A7.7).

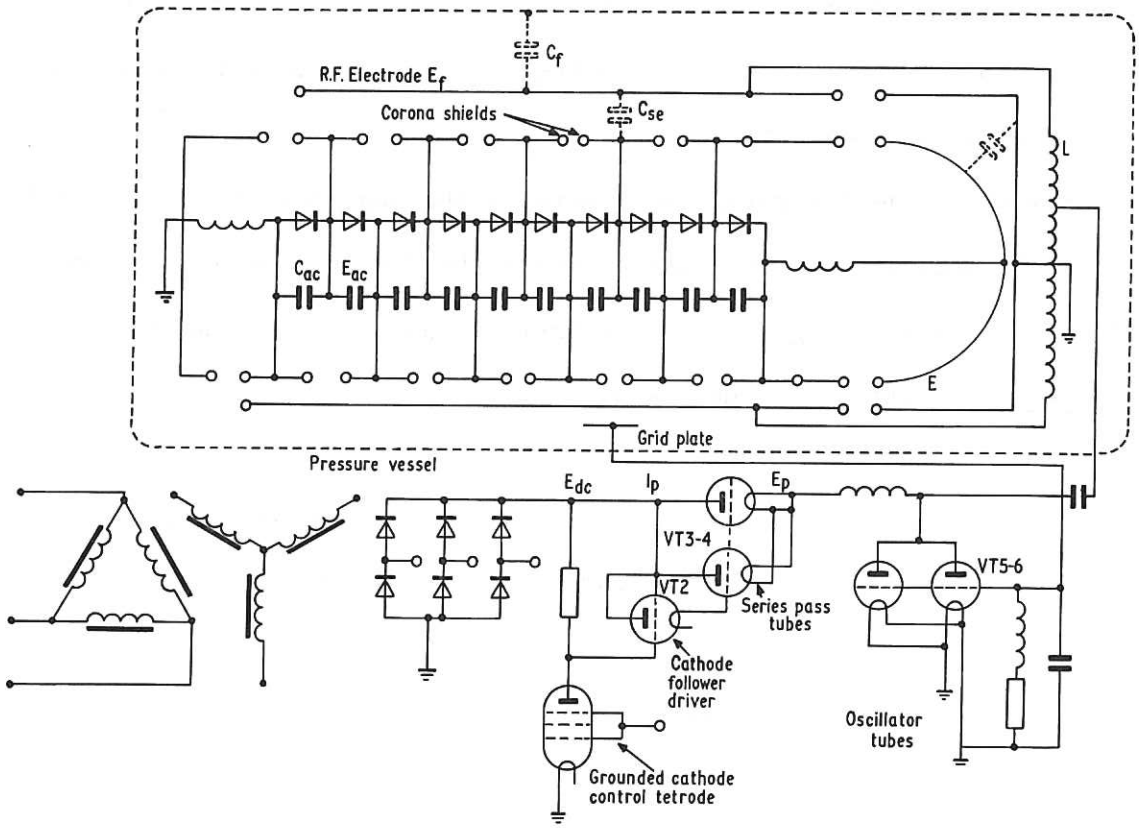

Fig. A7.10 Schematic diagram of Dynamitron
(Radiation Dynamics Inc., Westbury, Long Island, N.Y.)

CLM-R 112

Group B - Electrochemical Methods (Figure A7.3(b))

The secondary storage battery typifies this group. It is fundamentally a D.C. device with high energy to volume ratio ($\sim 10^6$ joules per cu. ft.) and low capital cost (£5-£10 per kW). Commercially fully established in low voltage regimes it cannot be dismissed lightly and if the specification of 55 MW for 1 minute is strictly applied with a pulse repetition rate of say once per hour or longer this method might prove economical. However, the terms of reference imply that the method chosen should, in principle, be essentially CW and capable of design extension to continuous rating. The most serious disadvantage of this method is due to the lack of D.C. high voltage switches, and problems of safety and protection become almost insuperable at voltages above about 10 kV. The overall efficiency of an arrangement such as Figure A7.3(b), taking into account charging and discharging cycles, is not more than about 50% when using conventional secondary cells. Also the attendant maintenance costs are likely to be prohibitive.

Because of the foregoing disadvantages the application of electrochemical methods to high voltage generation awaits the development of a cheap, compact and safe DC high voltage circuit breaker and an efficient secondary cell.

Group C - Electrostatic Generators

There are two general classes:

(i) Those of substantially fixed capacitance which use charge transporters, such as belts, discs, cylinders, dust, liquids, or metallic elements.

(ii) Those which use the variation of capacitance to pump charge from one level, change its potential, and cyclically transfer it to a higher potential level.

All generators in class (i) are rotating machines suitable for direct drive by a prime mover, arranged as in Figure A7.3(c), they are all essentially direct current rather than voltage generators. That is to say, their intrinsic

output characteristics are such that their output power falls to zero, as in Figure A7.2, when they are short circuited.

Class (ii) are all essentially A.C. generators; for the production of D.C. they must be used in conjunction with additional rectifiers in just the same way as the transformer-rectifier arrangement which has already been developed to a high power level. So that, without looking more closely into their characteristics we discard them in favour of transformer-rectifiers.

Returning to Class (i), gas, dust and liquid machines do not appear to be likely to reach commercial viability in the foreseeable future, only the Van de Graaff type using solid insulant transporters have so far been successful. Their ability to transport charge is dependent upon the electrical and mechanical strength of the transporter and on the electrical strength of the environmental gas. The most compact machines of this type have been marketed by SAMES, Grenoble. These are drum machines using conventional materials operating in 20 atmospheres of hydrogen, they attain a power density of 20 kW per m^2 of rotor surface area. Using similar materials an insulant disc machine having a rotor surface area of about 3000 square metres could produce an output of 55 MW. Such a machine can be envisaged with a rotor of about 12m diameter and 10 m long,comprising say forty insulant discs surrounded and interleaved by a multipole charging and collection system of equipotential elements. Because the power output of this type of machine is dependent upon the surface area of the rotor it is bound to be much more bulky and expensive than the electromagnetic machine, the power output of which depends upon the volume of its active parts.

4. Summary

Of all the relatively conventional methods considered here, the transformer rectifier stands out at this time as the most suitable generation device in the 3 MV high power regime. If continuously rated high power ($\sim$1000 MW) 3 MV supplies are required, (for use with Mirror Reactors) within the next decade, it is unlikely that they would differ in principle from high voltage power convertors used in present day H.V. D.C. transmission systems. Both

R & D and capital costs associated with the extension of such systems into the 3 MV regime are likely to be considerably greater than those required for intermittently rated 3 MV systems. But because efficiency is of paramount importance in high power continuous systems, it is unlikely that other methods will be found, during the next decade, which will compete favourably with the cascaded bridge (efficiency 98%) arrangement of Figure A7.5. On this score alone, toroidal reactors seem to be more practicable than mirror reactors.

In the case of our present specification with an intermittent output of 3 MV, 55 MW, where efficiency is of secondary consideration, then the insulating core transformer is the most promising device. Present ICT's achieve an efficiency of about 70%, and due to their compactness, when intermittently rated, it should be possible to achieve capital costs comparable with those of Figure A7.1.

Thus it is envisaged that each 7000 MW (th) toroidal reactor would require ten injectors, each of which would be supplied by a 3.5 MV 55 MW ICT (1 minute rated).

Each ICT would be housed in its own pressure vessel and connected through a branch pipe to its accelerator, contained in a separate vessel. Since each ICT requires an input of ~60 MVA we can assume that an independent and reliable source of 600 MVA at 50 Hz must be provided. This could be provided by three fossil-fuelled turbo-alternators (two on duty and one on standby) each rated at 300 MVA. These three machines being used for dual functions, namely as prime movers during the reactor ignition period and subsequently for outgoing generation during peak demand periods.

At this stage, rough calculations indicate that the specification in Section 3.1, p.A7-10 could be met by an ICT of about 20 ft. diameter and 30 ft. height. Each ICT would be similar in principle to the HV PC model ICT 2000-30 shown in Figure A7.6 but would incorporate some additional features. For example, an additional secondary winding could be fitted on the core at the 3.5 MV level to supply the ion source power units which could be housed in the

HT terminal of the ICT. These power units being connected to the accelerator ion source via a 3.5 MV bus bar system passing through the branch pipe between the two pressure vessels. Each module of the ICT would probably include an additional low power transformer winding and thyristor bridge for control purposes. These control thyristors being operated by light beams from ground potential would control the output of the power thyristors in each module. The complete assembly could be made very compact by oil immersing the H.T. stack which would be provided with vertical oilways throughout. The H.T. terminal and bus bar regions need not be oil immersed but simply surrounded by pressurised sulphur hexafluoride. The output of each ICT would be voltage controlled and current limited according to the demands of its accelerator.

With this general picture in mind it is possible to arrive at a rough estimate of the capital costs of the high voltage generation and distribution system required for the ignition of a 7000 MW (th) toroidal reactor, ignited by neutral particle injection.

Assuming that the capital costs of the ICT, when in large scale production, would not be significantly greater than present day HV DC transmission system convertors; and that thyristors have been developed to the point at which they are fully competitive with mercury arc rectifiers, then the likely capital costs at 1970 prices would be roughly as follows:

	£M
Ten 55 MW ICT's (on duty) at £15 per kW	8.25
Two " " " (on stand by/maintenance) at £15 per kW..	1.65
AC switch gear distribution and PF correction	1.1
Total costs of 3.5 MV system:	£M 11.0

Note: Costs of three independent turbo alternators are not included because they also serve as peak demand generators.

Of course, in the first instance, a prototype 55 MW ICT would have to bear the necessary development costs and we should expect it to cost several times as much as production models.

Obviously a much more thorough study of methods and prices will be needed and it is worth noting the following firms with long experience in the production and marketing of high voltage equipment:

Firm	Present Capability
AEI-GEC Limited (Manchester-Stafford)	H.V. Transformer Rectifiers
HVEC and HVPC (Burlington, Mass.)	HV Equipment < 10 MV Insulating Core Transformers up to 2.5 MV at present
Radiation Dynamics (Westbury N.Y.)	Dynamitrons up to 5 MV
SAMES, Grenoble	Electrostatic drum machines up to ~ 1 MV
Haefely (Basle)	HV Equipment up to 3 MV

As the injector research programme goes forward a compatible generator design should emerge and appropriate generator development and trials work should be run concurrently. Even at this stage it might not be too soon to get a reaction from some of the above firms when confronted with the specification in Section 3, page A7-10.

REFERENCES

(A7.1) McDaniel, E.W. Collision phenomena in ionized gases (New York, Wiley, 1964) pp 186-188.

(A7.2) Barnett, C.F., and others. Atomic and molecular collision cross sections of interest in controlled thermonuclear research. Oak Ridge National Laboratory report ORNL 3113, revised 1965.

(A7.3) Julian, F.A., and Allen, W.D. Colloques Internationalaux du Centre National de la Recherche Scientifique, 1960, pp 179-207.

(A7.4) Miller, D.J. Proceedings of the Conference on high-voltage D.C. transmission, Manchester, September 1966. (London, IEE, 1966, Conference Publication no. 22), pp 66-69.

(A7.5) Sweetman, D.R. Culham Laboratory, unpublished work, 1970.

(A7.6) New Scientist, vol.46, no. 703, 28 May 1970, p 429.

(A7.7) Cleland, M.R. and Thompson, C.C. IEEE,Trans. Nucl. Sc., vol. NE-16, no. 3, June 1969, pp 124-127.

Available from

HER MAJESTY'S STATIONERY OFFICE

49 High Holborn, London, W.C.1
13a Castle Street, Edinburgh 2
109 St. Mary Street, Cardiff CF1 1JW
Brazennose Street, Manchester M60 8AS
50 Fairfax Street, Bristol BS1 3DE
258 Broad Street, Birmingham 1
7-11 Linenhall Street, Belfast BT2 8AY

or through any bookseller.